Coupling and Controllability in Optimal Design and Control

by

Diane L. Peters

A dissertation submitted in partial fulfillment
of the requirements for the degree of
Doctor of Philosophy
(Mechanical Engineering)
in The University of Michigan
2010

Doctoral Committee:

Professor Panos Y. Papalambros, Co-Chair
Professor A. Galip Ulsoy, Co-Chair
Professor Jing Sun
Associate Professor Katsuo Kurabayashi

Dedicated to my late, beloved American Eskimo Dog, Igloo; he started with me on this journey, but couldn't be here to celebrate the completion.

ACKNOWLEDGEMENTS

When I first told my family and friends that I was going to quit my job and go back to school for a Ph.D., I wasn't sure what kind of reaction I would get. I was prepared for everything from wholehearted support to questions about my sanity. What I received was universal support, approbation, and enthusiasm (even from those who did, in fact, question my sanity). My family and friends stood behind me every step of the way, even those who weren't quite sure what I was doing or why I wanted to do it. My thanks go out to my parents, Thomas and Margaret Peters, who put up with my books and laptop coming to every holiday gathering for the past four years and listening to me talk about what I'm doing, and to my siblings, Catherine, Patrick, Michael, and Jennifer, for their patience. Special thanks to my best friend, Anne Lucietto, her husband Richard Scheffrahn, and their daughter Elisabeth. Their encouragement has been a lifeline to me when things were tough, and they have shared in my joy when things went well. Anne has heard more than she probably ever wanted to know about my research, and yet has been able to share my enthusiasm for neat technical stuff. Jo Lynn Sedgewick has been a good sounding board for mathematical issues who was willing to discuss Taylor series, matrix algebra, or differential geometry, as well as serving as my 'Maple Guru'. Other friends from my pre-University of Michigan life who have provided moral support are Donn Dengel, Mary Mueller, Deanna Heffron, Wendy Landwehr, Sue Biancheri, Tony Puntuzs, and Karen Preston Wozniak.

As I planned to go back to school and worked to choose a university, there were a number of people who provided advice, help, and support of various types. I'd like to thank Professors Steven Skaar and Michael Stanisic at the University of Notre Dame, who gave

me their time and the benefit of their experience, and wrote letters of recommendation for schools and fellowships. Thanks also to Mike Dunn, a former boss of mine from Western Printing Machinery (WPM), who wrote recommendation letters, and to Kent Troxel, my last boss at WPM, who signed off on all those vacation requests as I visited various schools. I'm also grateful to the company as a whole, for throwing me a terrific send-off party with good food, gifts, and good wishes as I went on to a new phase of life. I also had the support of my colleagues at Oakton Community College, where I taught as adjunct faculty. In particular, my thanks to Joe Cirone, who wrote recommendation letters for me.

As I joined the University of Michigan community, I gained colleagues who have at various times served as friends, mentors, sounding boards, a workout partner, a co-author, and a carpool. In particular, I'd like to mention Tahira Reid, Bart Frischnecht, Steven Hoffenson, Michael Alexander, Kwang Jae Lee, Abigail Mechtenberg, Sun Yi, Rachel Bis, Shifang Li, Yongseob Lin, Shanna Daly, Kukhyun Ahn, John and Katie Whitefoot, Yi Ren, Jarod Kelley, Erin MacDonald, Andreas Malikopoulos, James Allison, and everyone connected with the Optimal Design Laboratory. Within the larger Ann Arbor community, I've been privileged to meet some really terrific people, who have served at times as a cheering section and at other times as a source of balance and perspective. I'd particularly like to acknowledge my fellow volunteers at the Humane Society of Huron Valley (HSHV), who have often asked me how my work was coming along as we walked dogs. The dogs at HSHV have always been good listeners, as have my own dogs - my late American Eskimo, Igloo, and Kari and Sydney, who have heard countless presentations before I practiced them on humans.

As I approached the end of my time at the University of Michigan, I spent two months in the summer of 2009 interning at the Tank Army Research and Development Center (TARDEC). This was an interesting experience due to the efforts of several people. I'd like to thank Dave Gorsich, Geri Neal, Greg Hudas, and Mark Brudnak in particular for their time and efforts while I was there.

While the encouragement of the people in my life has been vital, financial support is also a necessity, and I've been fortunate to benefit from several sources of funding. My thanks go out to the Rackham Graduate School, for the Rackham Merit Fellowship; the National Science Foundation, for funding my advisors' grant; the Automotive Research Center; and the Teresan Scholarship Fund, which paid for my first year's textbooks.

And, finally, these acknowledgements wouldn't be complete without mentioning my advisors and committee. My advisors, Dr. Papalambros and Dr. Ulsoy, have taught me a tremendous amount about my research and about academic life. My thanks also to Dr. Kurabayashi and Dr. Sun, who have served on my committee. Without their guidance, this dissertation would never have been started, much less completed.

TABLE OF CONTENTS

DEDICATION ii

ACKNOWLEDGEMENTS iii

LIST OF FIGURES ix

LIST OF TABLES xi

LIST OF APPENDICES xii

CHAPTER

I. Introduction 1

1.1 Summary 1
1.2 Motivation 2
1.3 Definition and Quantification of Coupling 3
1.3.1 Bi-Directional and Uni-Directional Coupling 4
1.3.2 Measures of Coupling 4
1.4 Examples of Coupled Systems 9
1.4.1 Structural Systems with Active Control 9
1.4.2 Robotics and Mechatronics 10
1.4.3 MEMS 11
1.5 Optimization Methods for Coupled Systems 12
1.5.1 Sequential Optimization 12
1.5.2 Iterative Optimization 15
1.5.3 Simultaneous Optimization 15
1.5.4 Partitioned Optimization 16
1.5.5 Nested Optimization 16
1.6 Use of Controllability in System Design 17
1.7 Original Contributions 17
1.8 Dissertation Outline 20

II. Relationships Between Coupling Measures 21

2.1 Introduction . . . 21
2.2 Relations between Coupling Measures . . . 21
2.2.1 Coupling Vector, Γ_v, and Sensitivity of the Control Objective . . . 22
2.2.2 Coupling Vector, Γ_v, and Coupling Matrix, Γ_m . . . 23
2.2.3 Coupling Vector, Γ_v, and Normalized Sensitivities . . . 25
2.3 Illustrative Example: Positioning Gantry . . . 26
2.3.1 Uncoupled System Optimization . . . 28
2.3.2 Coupled System Optimization . . . 31
2.4 Choice of Coupling Metric . . . 34
2.5 Physical Significance of Coupling Vector . . . 34
2.6 Extensions of Coupling Vector, Γ_v . . . 35
2.6.1 Extension of Coupling Vector to Non-Linear Objective Combination . . . 36
2.6.2 Extension of Coupling Vector to Bi-Directional Coupling 38
2.7 Summary . . . 39

III. Relationship Between Coupling and Controllability . . . 40

3.1 Introduction . . . 40
3.2 Metrics Used for Coupling and Controllability . . . 41
3.3 Relationships Between Γ_v and W_c . . . 43
3.3.1 Case I: Control Effort as Objective . . . 44
3.3.2 Case II: Time as Objective . . . 48
3.3.3 Case III: Linear Quadratic Regulator (LQR) . . . 51
3.4 Physical Demonstration: Positioning Gantry . . . 56
3.4.1 Description of Apparatus . . . 56
3.4.2 Demonstration Procedure . . . 58
3.4.3 Results of Demonstration . . . 60
3.5 Summary . . . 62

IV. Design for Ease of Control Using Control Proxy Functions . . . 64

4.1 Introduction . . . 64
4.2 Characteristics of Effective Control Proxy Functions (CPFs) . . . 66
4.2.1 Characterization of a Perfect CPF . . . 67
4.2.2 Quantification of the 'Closeness' of a CPF Point to the Pareto Frontier . . . 70
4.2.3 Monotonicity of Controller Objective and CPF . . . 71
4.2.4 Locations of Unconstrained Minima of f_c and χ . . . 73
4.3 Control Proxy Functions for Specific Co-Design Problem Formulations . . . 76
4.3.1 Natural Frequency as a Control Proxy Function . . . 76

4.3.2 Control Proxy Functions Based on the Controllability Grammian . . . 82
4.4 Summary . . . 88

V. Application of the CPF Method . . . 90

5.1 Introduction . . . 90
5.2 Overview of Design Process Using a CPF . . . 91
5.3 MEMS Actuator and Controller Case Study . . . 97
5.4 Co-Design of MEMS Actuator for Steady-State Displacement and Settling Time . . . 101
5.4.1 Optimization Using Natural Frequency . . . 107
5.4.2 Optimization Using Controllability Grammian . . . 110
5.5 Co-Design of MEMS Actuator for Final Displacement and Control Effort . . . 111
5.6 Summary . . . 116

VI. Summary, Conclusions and Future Work . . . 118

6.1 Summary . . . 118
6.2 Conclusions . . . 118
6.2.1 Derivation of Relationships Between Coupling Measures and Extension of Coupling Vector to Bi-Directional Coupling . . . 119
6.2.2 Derivation of Relationships Between Coupling and Controllability for Several Important Classical Control Problems . . . 119
6.2.3 Development of a Modified Sequential Method Using a Control Proxy Function (CPF) for Cases of Uni-directional Coupling . . . 120
6.2.4 Categorization of Problems According to Nature of Coupling and Appropriate Solution Methods . . . 121
6.2.5 Application of New Method to Case Studies . . . 122
6.3 Future Work . . . 122
6.3.1 Further Investigation of Decoupling Conditions . . . 122
6.3.2 Further Development of Control Proxy Function (CPF) Method . . . 123
6.3.3 Consideration of Observability . . . 124
6.3.4 Application of the CPF Method to Additional Case Studies . . . 124

APPENDICES . . . 125

BIBLIOGRAPHY . . . 149

LIST OF FIGURES

Figure

1.1 Subsystem Configuration (after [*Bloebaum* (1995)]) 7

1.2 Solution Methods for Coupled Systems (after [*Fathy* (2003)]) 13

2.1 Subsystem Structure for Simplified System 24

2.2 Configuration of Positioning Gantry 26

2.3 Schematic of System Controller 27

2.4 Pareto Points for Coupled System Optimization 33

3.1 Pareto Frontier for Positioning Gantry Example of Case I 49

3.2 Pareto Frontier for Positioning Gantry Example of Case II 52

3.3 Apparatus for Physical Demonstration of Gantry Example (Item 1: QET motor assembly, Item 2: mounting plate, Item 3: linear rail, Item 4: angle bracket, Item 5: extension spring, Item 6: fixed mounting bracket, Item 7: pulley) 57

3.4 Control Screen for QET-DCMCT Software 59

3.5 Apparatus with Modified Spring Configuration 60

3.6 Voltage for Single and Dual Spring Configurations 61

3.7 Position Response for Single and Dual Spring Configurations 62

4.1 Control Proxy Function Problem Formulation 65

4.2 Comparison of Simultaneous and CPF Solutions for $\mathbf{\Gamma}_v \parallel \nabla\chi$ 69

4.3 Comparison of angle ξ and distance ε 71

4.4 Comparison of Simultaneous and CPF Solutions for Appropriate Monotonicity 73

4.5 Comparison of Simultaneous and CPF Solutions for Inappropriate Monotonicity 74

4.6 Comparison of Simultaneous and CPF Solutions for Two Choices of CPF 75

5.1 Choice of Solution Method for Co-Design Problems 93

5.2 MEMS Actuator Configuration 98

5.3 Hinge Actuation 98

5.4 Micro-Hinge Structure 99

5.5 Plan View of Silicon Shuttle 100

5.6 Control Architecture and System Dynamics 100

5.7 Comparison of CPF Points and Simultaneous Optimization Points for Frequency-Based CPF 109

5.8 Comparison of CPF Points and Simultaneous Optimization Points for Controllability-Based CPF 112

5.9 CPF Points for Optimization of MEMS Actuator 116

5.10 Comparison of CPF Points for Optimization with χ_1 and χ_2 117

A.1 Gradients at Points A and B 129

A.2 Pareto-Optimal Point B and CPF Points A and C 133

A.3 Unconstrained Minima of f_c and χ 138

LIST OF TABLES

Table

2.1 Parameters for Optimization of Uncoupled System 29

2.2 Results of Optimization of Uncoupled System 30

2.3 Parameters for Optimization of Coupled System 32

2.4 Results of Optimization of Coupled System 33

3.1 Parameters for Optimization of Gantry Using LQR Control 56

3.2 Results of Optimization of Gantry Using LQR Control 56

4.1 Comparison of Minima of Objective Functions and Control Proxy Functions 75

5.1 Control Proxy Functions (CPFs) and Conditions for Use (See Eqs. (4.38), (4.35), (4.44), (4.45), (4.43), (3.4), and (3.5) for the definitions of $\boldsymbol{B}$, b, ω_c, ζ_c, ζ_n, $\boldsymbol{W}_c\left(t_f\right)$, and $\boldsymbol{W}_c^{\infty}$, respectively.) 94

5.2 Parameter Values for MEMS Actuator 103

5.3 Original Design of MEMS Actuator [*Tung and Kurabayashi* (2005)] . . . 104

5.4 Sequential Optimization Results Using Natural Frequency 108

5.5 CPF Optimization Results Using χ_1 115

LIST OF APPENDICES

Appendix

A. Proofs for Theorems 4.1 – 4.4 126

B. Derivation of Artifact and Control Objective and Constraints for MEMS Actuator 142

CHAPTER I

Introduction

1.1 Summary

Many of the new products and systems being designed today require the design of both a physical system, or artifact, and a controller. A significant number of such systems exhibit coupling between the artifact and its controller, i.e., the performance of the artifact itself may depend upon the controller, and the performance of the controller may depend on the physical configuration of the device. In designing the complete system via optimization, this coupling between the product and its controller can be critical for achieving the best system performance. Previous research has shown that, when coupling is present, optimal system design presents special challenges. In particular, failure to address coupling appropriately results in sub-optimal systems.

This chapter introduces the motivation for the dissertation research work in Section 1.2. The concept of coupling is defined, and existing measures used to quantify coupling are explained in Section 1.3. Examples of coupled systems are then given in Section 1.4, and optimization methods in the existing literature are discussed in Section 1.5. The use of controllability in system design is summarized in Section 1.6. Section 1.7 lists the dissertation's original contributions to the literature. The chapter concludes in Section 1.8 with an outline of the contents of the dissertation.

1.2 Motivation

New technologies and 'smart' products have the potential to improve life dramatically and to transform our understanding of the world. New technologies at the smallest scale promise to radically change people's lives. Nanotechnology and biological microelectrical mechanical systems (bioMEMS) carry the potential to allow people with a wide variety of medical conditions, such as epilepsy, diabetes, and high cholesterol, to monitor and control their health with minimal intrusion into their ability to live a normal life. Hearing aids, pacemakers, and many other devices can be drastically improved, allowing our aging population to remain active and productive. Scientific instruments utilizing these technologies in the hands of talented researchers will facilitate new discoveries.

On a larger scale, smart systems address challenges in our society's needs for energy and transportation. Smart electrical grids, intelligent hybrid cars, and smart appliances can improve the reliability of our infrastructures, reduce wasted energy, and limit our impact on the environment. Achieving these revolutions, however, requires a change in engineering design practices. All of these applications require the design of both an artifact and a controller, and it can be reasonably asserted that optimal designs of artifact and controller are required in order to realize the full benefit of these technologies. The problem of designing both the artifact and its controller for such smart products will be referred to here as the *co-design problem*. Coupling between the artifact and controller has been demonstrated to be critical in the proper co-design of many systems. The existence of such coupling seems to indicate that a simultaneous problem formulation is preferable to a sequential one in order to achieve a system-optimal design. However, the simultaneous formulation presents challenges. Computationally, it is a larger problem and is more difficult to solve. Even if the problem is tractable, though, formulating it requires multiple areas of expertise. It is unlikely that a single person, or even a single group within an organization, would possess all of the necessary expertise. Multiple groups need to be involved in the design of a typical artifact. Thus, separation of the two problems, design and control, and solution

in some sequential or iterative manner is very appealing in engineering practice. Various methods have been proposed to address these design problems, but none is totally satisfactory. Therefore, a new approach is needed. By formulating a method of co-design that considers coupling in a sequential design method, practical design of artifacts for control can be improved, resulting in better designs and bringing about advances in knowledge and quality of life.

1.3 Definition and Quantification of Coupling

Prior to discussing the solution of coupled design and control, or co-design, problems, it is necessary to define exactly what constitutes a co-design problem, and what is meant by coupling. A co-design problem will be defined as an optimization problem in which both a controlled system, called the artifact, and a controller are to be optimized. The artifact objective function, denoted as f_a, is to be minimized subject to a set of inequality and equality constraints, denoted as $\boldsymbol{g}_a$ and $\boldsymbol{h}_a$, respectively.

$$\min f_a(\boldsymbol{d}_a, \boldsymbol{d}_c) \tag{1.1}$$

$$\text{subject to} \quad \boldsymbol{g}_a(\boldsymbol{d}_a, \boldsymbol{d}_c) \leq \boldsymbol{0} \tag{1.2}$$

$$\boldsymbol{h}_a(\boldsymbol{d}_a, \boldsymbol{d}_c) = \boldsymbol{0} \tag{1.3}$$

Likewise, the control objective function, denoted as f_c, is to be minimized subject to inequality and equality constraints, $\boldsymbol{g}_c$ and $\boldsymbol{h}_c$.

$$\min f_c(\boldsymbol{d}_a, \boldsymbol{d}_c) \tag{1.4}$$

$$\text{subject to} \quad \boldsymbol{g}_c(\boldsymbol{d}_a, \boldsymbol{d}_c) \leq \boldsymbol{0} \tag{1.5}$$

$$\boldsymbol{h}_c(\boldsymbol{d}_a, \boldsymbol{d}_c) = \boldsymbol{0} \tag{1.6}$$

In the most general problem formulation, all of the functions f_a, $\boldsymbol{g}_a$, $\boldsymbol{h}_a$, f_c, $\boldsymbol{g}_c$ and $\boldsymbol{h}_c$ may be functions of both $\boldsymbol{d}_a$ and $\boldsymbol{d}_c$, where $\boldsymbol{d}_a$ is the vector of artifact design variables and $\boldsymbol{d}_c$ is the vector of control design variables. Coupling is said to exist if the solution of the bi-objective co-design problem given by Eqs. (1.19) - (1.23)) is a Pareto set, rather than a single point solution. This can occur if any of the artifact objective function or constraints are functions of $\boldsymbol{d}_c$, or if any of the control objective or constraint functions depend on $\boldsymbol{d}_a$.

1.3.1 Bi-Directional and Uni-Directional Coupling

As previously stated, in the most general case, all of the objective and constraint functions may depend on both $\boldsymbol{d}_a$ and $\boldsymbol{d}_c$. In this case, coupling is described as *bi-directional*. However, there exists a large class of problems in which none of the artifact objective function and constraints are functions of $\boldsymbol{d}_c$, i.e., $f_a = f_a(\boldsymbol{d}_a)$, $\boldsymbol{g}_a = \boldsymbol{g}_a(\boldsymbol{d}_a)$, and $\boldsymbol{h}_a = \boldsymbol{h}_a(\boldsymbol{d}_a)$. These problems are said to exhibit *uni-directional coupling*. Of course, if the artifact objective function and constraints are functions only of $\boldsymbol{d}_a$ and the controller objective function and constraints are functions only of $\boldsymbol{d}_c$, then the problem does not exhibit coupling at all, and is said to be *uncoupled*. There are special cases in which a problem can become uncoupled despite the appearance of the artifact design variables $\boldsymbol{d}_a$ in the control objective function and constraints, and this shall be discussed later in this dissertation.

1.3.2 Measures of Coupling

If coupling does exist, then it is useful to know whether it is 'strong' or 'weak'. If coupling is weak, then it may be possible to neglect it. In contrast, if coupling is strong, then neglecting it will result in solutions that are far from optimality. Coupling has been measured by the presence or absence of interaction, or coupling, variables, but this measure does not indicate how strong the dependence on those coupling variables might be [*Reyer* (2000)]. One might define a system to be more strongly coupled if it exhibits a greater number of coupling variables, but this is not necessarily a useful definition if the func-

tional dependence on those coupling variables is weak. Several researchers have presented measures of coupling that account for the sensitivity of objective functions to the coupling variables, and these measures shall be discussed briefly.

Sensitivity of the Control Objective

Haftka and co-workers considered structural problems with uni-directional coupling and proposed to characterize coupled systems by two types of sensitivity [*Haftka et al.* (1986)]. The first type of sensitivity, used as a measure of the robustness of the design, was computed as the sensitivities of the control objective and constraints to the artifact design variables at the nominal optimum design, i.e., the sensitivities $\frac{\partial f_c}{\partial \boldsymbol{d}_a}(\boldsymbol{d}_a^*, \boldsymbol{d}_c^*)$ and $\frac{\partial \boldsymbol{g}_c}{\partial \boldsymbol{d}_a}(\boldsymbol{d}_a^*, \boldsymbol{d}_c^*)$. The second type of sensitivity measures the change in the optimum control as the structure is modified:

$$\frac{\partial f_c^*}{\partial \boldsymbol{d}_a} = \frac{\partial f_c}{\partial \boldsymbol{d}_a} - \sum_{j=1}^{m} \mu_j \frac{\partial g_{c_j}}{\partial \boldsymbol{d}_a} \tag{1.7}$$

where the number of active control constraints is equal to the number of artifact design variables, $\boldsymbol{\mu}$ is the vector of Lagrange multipliers, m is the size of the constraint vector $\boldsymbol{g}_c$, and j is its component index [*Haftka et al.* (1986)]. The sensitivity of the control design variables to the artifact design variables was also computed. For the linear structural applications considered,

$$\frac{\partial \boldsymbol{d}_c^*}{\partial \boldsymbol{d}_a} = -\left(N^T\right)^{-1} \frac{\partial \boldsymbol{g}_c}{\partial \boldsymbol{d}_a} \tag{1.8}$$

where the matrix $N = \frac{\partial \boldsymbol{g}_c}{\partial \boldsymbol{d}_c}$ [*Haftka et al.* (1986)].

Coupling Vector

Fathy and co-workers quantified the strength of coupling in the case of uni-directional coupling, assuming a particular co-design problem structure, and considered the special circumstances in which it vanishes [*Fathy et al.* (2004)]. In this work, it was assumed that the system objective function was defined as a linear combination of the artifact and control

objective functions, i.e.,

$$\min_{\boldsymbol{d}_a,\boldsymbol{d}_c} \quad f = w_a f_a(\boldsymbol{d}_a) + w_c f_c(\boldsymbol{d}_a,\boldsymbol{d}_c) \tag{1.9}$$

$$\text{subject to} \quad \boldsymbol{g}_a(\boldsymbol{d}_a) \leq \boldsymbol{0} \tag{1.10}$$

$$\boldsymbol{h}_a(\boldsymbol{d}_a) = \boldsymbol{0} \tag{1.11}$$

$$\boldsymbol{g}_c(\boldsymbol{d}_a,\boldsymbol{d}_c) \leq \boldsymbol{0} \tag{1.12}$$

$$\boldsymbol{h}_c(\boldsymbol{d}_a,\boldsymbol{d}_c) \leq \boldsymbol{0} \tag{1.13}$$

The coupling measure is a vector quantity given by

$$\boldsymbol{\Gamma}_v = \frac{w_c}{w_a}\left(\frac{\partial f_c}{\partial \boldsymbol{d}_a} + \frac{\partial f_c}{\partial \boldsymbol{d}_c}\frac{d\boldsymbol{d}_c}{d\boldsymbol{d}_a}\right) \tag{1.14}$$

where w_a and w_c are the weights assigned to the artifact and control objectives, respectively, with $w_a + w_c = 1$. The Euclidean norm of this vector, evaluated at the system optimal solution, was used to characterize the overall coupling strength for a system. In general, this will be a non-zero value, indicating that the system is coupled. The special cases in which a system decouples are termed *objective decoupling* and *constraint decoupling*. In the case of objective decoupling, the coupling vector is zero. In constraint decoupling, the coupling vector is non-zero, but active constraints prevent the system from achieving a zero coupling vector. This may occur in regions of the Pareto frontier where constraint activity changes, or where redundant constraints are satisfied [*Frischknecht et al.* (2009)].

Local Normalized Sensitivities

One definition of coupling strength is a matrix of local normalized sensitivities [*Bloebaum* (1995)]. Given two sub-systems *SSA* and *SSB*, the design variables in these sub-systems are denoted as $\boldsymbol{XA}$ and $\boldsymbol{XB}$, respectively, as shown in Fig. 1.1. Each system has an output, denoted as *YA* and *YB*, which is passed to the other. The matrix of sensitivities is

then computed as [*Bloebaum* (1995)]

$$\begin{bmatrix} \frac{\partial YA}{\partial \boldsymbol{XA}} & 0 \\ 0 & \frac{\partial YB}{\partial \boldsymbol{XB}} \end{bmatrix} = \begin{bmatrix} 1 & -\frac{\partial YA}{\partial YB} \\ -\frac{\partial YB}{\partial YA} & 1 \end{bmatrix} \begin{bmatrix} \frac{dYA}{d\boldsymbol{XA}} & \frac{dYA}{d\boldsymbol{XB}} \\ \frac{dYB}{d\boldsymbol{XA}} & \frac{dYB}{d\boldsymbol{XB}} \end{bmatrix} \tag{1.15}$$

which are then scaled using the relations

$$\frac{\partial YA'}{\partial YB} = \frac{YB}{YA}\frac{\partial YA}{\partial YB} \tag{1.16}$$

$$\frac{\partial YB'}{\partial YA} = \frac{YA}{YB}\frac{\partial YB}{\partial YA} \tag{1.17}$$

where A', B' are the scaled outputs.

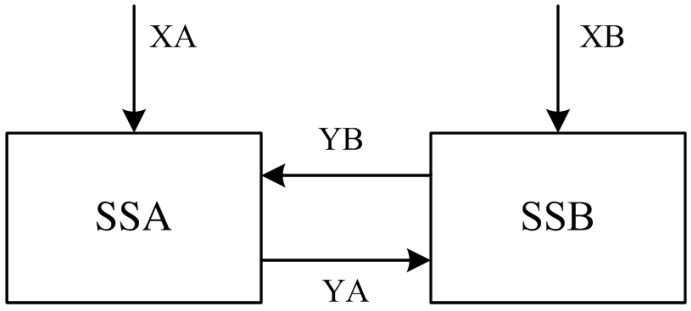

Figure 1.1: Subsystem Configuration (after [*Bloebaum* (1995)])

Note that, while the equations are presented here for only two sub-systems, this coupling metric can be used in systems with more than two sub-systems. Furthermore, it is applicable to problems with bi-directional coupling.

Coupling Matrix

Another metric used to quantify coupling is a matrix developed by Alyaqout and co-workers, which incorporates optimality conditions into the global sensitivity equations

[*Alyaqout et al.* (2005)]. This matrix takes the form of

$$\boldsymbol{\Gamma}_m = \begin{bmatrix} \frac{\partial F}{\partial f_1}\frac{\partial f_1}{\partial \boldsymbol{y}_{11}} \\ \vdots \\ \frac{\partial F}{\partial f_N}\frac{\partial f_N}{\partial \boldsymbol{y}_{1N}} \\ \vdots \\ \frac{\partial F}{\partial f_1}\frac{\partial f_1}{\partial \boldsymbol{y}_{N1}} \\ \vdots \\ \frac{\partial F}{\partial f_N}\frac{\partial f_N}{\partial \boldsymbol{y}_{NN}} \end{bmatrix}^T \begin{bmatrix} \frac{d\hat{\boldsymbol{y}}_{11}}{d\boldsymbol{x}_1} & \frac{d\hat{\boldsymbol{y}}_{11}}{d\boldsymbol{x}_2} & \cdots & \frac{d\hat{\boldsymbol{y}}_{11}}{d\boldsymbol{x}_N} \\ \vdots & & & \vdots \\ \frac{d\hat{\boldsymbol{y}}_{1N}}{d\boldsymbol{x}_1} & \ddots & & \frac{d\hat{\boldsymbol{y}}_{1N}}{d\boldsymbol{x}_N} \\ \vdots & & & \vdots \\ \frac{d\hat{\boldsymbol{y}}_{N1}}{d\boldsymbol{x}_1} & & \ddots & \vdots \\ \vdots & & & \vdots \\ \frac{d\hat{\boldsymbol{y}}_{NN}}{d\boldsymbol{x}_1} & \cdots & \cdots & \frac{d\hat{\boldsymbol{y}}_{NN}}{d\boldsymbol{x}_N} \end{bmatrix} + \begin{bmatrix} \sum_{j=1}^N \frac{\partial F}{\partial \boldsymbol{x}_j}\frac{d\hat{\boldsymbol{x}}_j}{d\boldsymbol{x}_1} \\ \vdots \\ \sum_{j=1}^N \frac{\partial F}{\partial \boldsymbol{x}_j}\frac{d\hat{\boldsymbol{x}}_j}{d\boldsymbol{x}_N} \end{bmatrix}^T + \begin{bmatrix} \sum_{p=1}^N \sum_{j=1}^N \left(\frac{\partial F}{\partial f_p}\frac{\partial f_p}{\partial \boldsymbol{x}_j}\frac{d\hat{\boldsymbol{x}}_j}{d\boldsymbol{x}_1}\right) \\ \vdots \\ \sum_{p=1}^N \sum_{j=1}^N \left(\frac{\partial F}{\partial f_p}\frac{\partial f_p}{\partial \boldsymbol{x}_j}\frac{d\hat{\boldsymbol{x}}_j}{d\boldsymbol{x}_N}\right) \end{bmatrix}^T . \tag{1.18}$$

where N is the number of sub-systems present indexed as $j = 1,\ldots,N$, F is the overall system objective, y_{jp} are coupling variables, f_p are the individual system objective functions indexed as $p = 1,\ldots,N$, $\boldsymbol{x}_j$ are the variables in the total problem, $\hat{\boldsymbol{x}}_j$ are local copies of $\boldsymbol{x}_j$, and $\hat{\boldsymbol{y}}_{jp}$ are local copies of y_{jp} [*Alyaqout* (2006), *Alyaqout et al.* (2005)]. An uncoupled system would be characterized, in this case, by a zero matrix. It is useful to note that this formulation is extremely general; not only can it be used in the case of bi-directional coupling, but it can be used with multiple sub-systems. Thus, it is applicable to design problems more general than co-design. The functional form of F is not specified. Therefore, $\boldsymbol{\Gamma}_m$ is not limited to a simple linear combination of sub-system objectives. Furthermore, this measure allows both 'global' and 'local' copies of variables, and lends itself to more complex decomposition strategies.

1.4 Examples of Coupled Systems

The literature on coupled systems is extremely rich, and presents examples from diverse areas such as aeronautical structures, machine tools, automotive engineering, micro-electrical mechanical systems (MEMS), mechanisms, and chemical processing [e.g., *Kajiwara and Haftka* (2000), *Chen and Cheng* (2006), *Fathy et al.* (2003), *Carley et al.* (2001), *Tilbury and Kota* (1999), *Wan et al.* (2002), *Shabde and Hoo* (2008)]. Several broad areas shall be discussed here. These areas are structural systems, robotics and mechatronics, and MEMS.

1.4.1 Structural Systems with Active Control

Some of the first systems in which coupling was studied were in the field of aerospace engineering. A typical example of this would be an aerospace structure subject to active control. There may be a high cost associated with weight, particularly for a structure that is to be flown or placed in orbit [*Hale et al.* (1985)]. Thus, specifications for these structures typically emphasize minimum weight, which results in a more flexible structure that can be more difficult to control. It has, therefore, been recognized by many researchers that a sequential optimization, in which the structure itself is first optimized and then the optimal controller is designed for that structure, may not produce an optimal system. The structure may be very light, but it could require an unacceptably large control effort. Heavy control actuators may be necessary in order to meet other specifications such as displacements, buckling, vibration, and stress [*Khot and Abhyankar* (1993), *Maghami et al.* (1996), *Messac* (1998)].

Experimental and analytical studies have been carried out, demonstrating the potential for both detrimental and advantageous interactions between a structure and its controller (e.g., *Haftka et al.* (1986), *Rao and Pan* (1990)). The problem of simultaneous design of a structure and its controller is made easier by the linear models typically used for the structure. However, it still presents significant challenges, as discussed by numerous researchers

[*Ou and Kikuchi* (1996), *Kosut et al.* (1990), *Milman et al.* (1991), *Sobieszczanski-Sobieski and Haftka* (1997)]. Some of the issues addressed in the literature are the effect of coupling on the stability of the control system, the large number of modes of vibration present, and a variety of techniques that can be used to design a 'controllable' structure [*Haftka* (1990), *Onoda and Watanabe* (1989)]. These techniques include locating the open-loop eigenvalues in 'desirable' areas of the complex plane and the use of the controllability Grammian matrix, which shall be discussed further in Section 1.6, to place actuators.

1.4.2 Robotics and Mechatronics

In contrast to the structural co-design problem, robotic systems are typically non-linear. Furthermore, while a structure is intended to have fixed relationships between its components, the components of a robotic system are expected to move relative to one another. However, like structural systems, robots often exhibit coupling between the physical robot and its controller [e.g., *Ravichandran et al.* (2006), *Zhu et al.* (2001), *Zhang et al.* (1999)]. In a typical robotics application, an end-effector must track a particular path or achieve a specified final position, possibly with specified velocity [*Li et al.* (1999)]. The robot may be either an open kinematic chain, as in [*Ravichandran et al.* (2006), *Zhu et al.* (2001)] or a closed kinematic chain [*Zhang et al.* (1999)]. Typical objectives for the artifact design are minimizing weight or minimizing deflection. Controller objectives may be minimizing tracking errors for a particular trajectory, overshoot, or settling time [*Ouyang et al.* (2002)]. In these problems, speed and accuracy are in conflict; mechanisms with lower inertia are more flexible, resulting in a fast response but lower accuracy, while a higher inertia will produce a stiffer mechanism that is more accurate but results in lower speeds [*Li et al.* (1999), *Zhu et al.* (2001)]. Many applications, however, require both high speed and high accuracy, and therefore design of these systems must consider the coupling between the artifact and control objectives [*Park and Asada* (1992)]. The robotics co-design problem may also be complicated by the expectation that the robot will perform multiple tasks with

different specifications.

Robotics may be considered to be part of the field of mechatronics, an area which has grown out of the union of mechanical and electrical systems. By its very nature, it requires multidisciplinary optimization [*Isermann* (1996a), *Isermann* (1996b), *Youcef-Toumi* (1996)]. Since it covers a wide range of applications, it is not possible to specify typical objectives for artifact and control design. There is a number of case studies in the literature, showing that, in at least some cases, the artifact and control designs are coupled. These cases include machine tools, automotive suspensions, and elevators [*Chen and Cheng* (2005), *Fathy et al.* (2003), *Fathy et al.* (2002)].

Because of the non-linear nature of many of these problems, techniques that have been successfully used in structural applications are not generally applicable. In addition, the specifications and constraints are typically different than those in structural co-design problems. In the design of aerospace structures, the size of actuators is typically subject to restrictive limits. In robotics and mechatronics, the actuators are still limited in size, but accuracy is weighted more heavily in the overall system performance. Many of the methods used for co-design in robotics and mechatronics are based on either experimentation, as in [*Pil and Asada* (1996)], or on heuristics, as in [*Li et al.* (2001)].

1.4.3 MEMS

Yet another area in which the artifact and control design problems can be coupled is the field of microelectrical mechanical systems (MEMS). MEMS devices are typically made of silicon, or a silicon-based polymer such as polydimethyl siloxane (PDMS), with their mechanical and electrical components integrated as they are created on a silicon wafer. These devices may be used in applications such as positioning of mirrors in optical switches, magnetic storage devices, acceleration sensors, and gyroscopes, to name a few [*Chu et al.* (2005), *Carley et al.* (2001), *Oldham et al.* (2005), *Wolfram et al.* (2005), *Park and Horowitz* (2003)]. The MEMS device typically must be designed to have a certain

range of motion for an actuator or sensing range for a sensor, with a controller designed to give a fast response and high accuracy. These objectives are often conflicting. In addition, MEMS devices may experience an instability problem known as pull-in. In this condition, for higher voltages, there is no stable position for the device. The voltage at which this occurs is a function of the physical configuration of the device, and therefore couples the artifact design and control design problems. This phenomenon has been a subject of concern in many devices, including comb drives [*Legtenberg et al.* (1996)] and microbeams [*Abdalla et al.* (2005)].

1.5 Optimization Methods for Coupled Systems

While some systems are weakly coupled or uncoupled, many systems do exhibit strong coupling. In particular, it has been shown that both uncertainty in system parameters and more demanding performance requirements are associated with strongly coupled systems [*Youcef-Toumi* (1996)]. Similarly, uncertainty and increased performance requirements are associated with coupling in the related problem of modeling and controller design [*Brusher et al.* (1997a), *Brusher et al.* (1997b)]. The demonstrated existence of coupled systems, and their prevalence, quite naturally leads to the question of how to design such systems most effectively. A number of strategies have been developed, both sequential and simultaneous, as shown in Fig. 1.2 [*Fathy* (2003)].

1.5.1 Sequential Optimization

The sequential approach is the traditional practical means of optimizing co-design problems. In the simplest sequential strategy, the artifact is first optimized. In the case of uni-directional coupling, the controller architecture is completely ignored. If bi-directional coupling exists, then the control design variables are assumed to take on certain values, which are parameters in the initial optimization. Once this design is complete, the artifact design variables are treated as parameters in the design of the controller. This approach

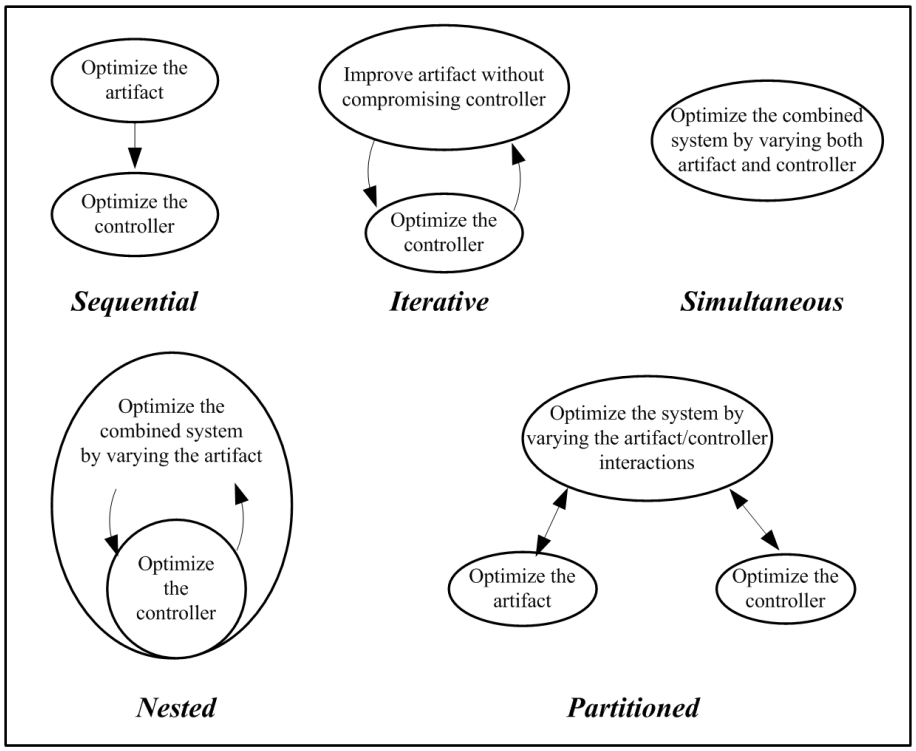

Figure 1.2: Solution Methods for Coupled Systems (after [*Fathy* (2003)])

works well in many cases. However, it will only find the system optimum when coupling does not exist. When uni-directional coupling is present, the solution found will be optimal for the artifact objective, f_a, but not for the control objective, f_c. In fact, it may prove to be impossible to find a feasible solution for the controller design. In the case of bi-directional coupling, the solution found may not be optimal for either objective function. This method of solution does not provide the designer with any information on the nature of tradeoffs present between the artifact and controller objectives, and thus even in the case of uni-directional coupling, where the solution lies at an endpoint of the Pareto frontier, the designer is unable to consider the merits of different designs on the Pareto frontier.

Because of the disadvantages of a simple sequential optimization, a modified sequential formulation has been utilized for a number of systems. This strategy includes one or more constraints on the artifact design that are intended to predispose the resultant design to effective control and ensure that a feasible control design will exist. The most commonly

used constraint is based on open-loop eigenvalues. In the design of the artifact, the system's open-loop eigenvalues are required to fall into a certain region of the complex plane. This method is typically used in structural applications, and in certain cases it can be quite effective. The combined artifact and control problem can be formulated to use this type of approach to avoid areas of high sensitivity and move the eigenvalues into acceptable regions when the structure is designed, thus predisposing the structure to effective control [*Bodden and Junkins* (1985)]. These methods are not always applicable, however, and they can also present some difficulties. The problem can become of very high dimensionality due to the large number of structural vibration modes and is often non-linear [*Bodden and Junkins* (1985)]. Some difficulties with this approach were overcome by Yee and Tsuei, who developed a more efficient method of effectively locating the eigenvalues [*Yee and Tsuei* (1991)]. This method, however, locates the open-loop eigenvalues, while the system behavior is controlled by the closed-loop eigenvalues. The literature has shown that in some cases, the locations of the closed-loop eigenvalues will not fall into acceptable regions when this approach is used [*Belvin and Park* (1990), *Eastep et al.* (1987)]. At this point, there is no sequential method of design that effectively locates closed-loop eigenvalues.

As previously stated, methods of design that may be effective for structural applications, such as the location of open-loop eigenvalues, are typically not applicable to non-linear problems such as robotics and mechatronics, and researchers have developed methods with these types of problems in mind. One method of modifying the design problem in order to account for coupling, specifically intended for mechatronic applications, is described in [*Li et al.* (2001)]. It emphasizes finding a simple dynamic model of the system of interest and the selection of parameters in the artifact design problem in order to facilitate control. Since mechatronic applications have not typically been given any kind of a standard formulation, there is a great deal of variety in the design problems that could arise, and the method described is quite general in nature.

1.5.2 Iterative Optimization

In this approach, the system is repeatedly solved, first for the artifact design, then for the controller design. The solution from each iteration becomes the starting point for the new iteration [*Grigoriadis and Skelton* (1998)]. One advantage of this approach is that it maintains the smaller sub-problems of the sequential optimization. It does converge to a solution in some cases, but not in others, and it cannot be guaranteed to converge to an optimal solution [*Reyer* (2000)].

1.5.3 Simultaneous Optimization

In simultaneous optimization, an overall system objective is defined as a function of the individual sub-system objective functions, f_a and f_c. Typically, this is a linear combination. However, due to the inherent limitations of this type of system objective, such as the inability to find points on a non-convex Pareto frontier, other formulations may be used [*Athan* (1994), *Athan and Papalambros* (1996), *Das and Dennis* (1997)]. The constraints and design variables for the simultaneous problem are the union of the individual constraints and variables for the individual sub-problems. Thus, the problem is formulated as in Eqs. (1.19) - (1.23).

$$\min_{\boldsymbol{d}_a,\boldsymbol{d}_c} \quad f = f\left(f_a\left(\boldsymbol{d}_a,\boldsymbol{d}_c\right), f_c\left(\boldsymbol{d}_a,\boldsymbol{d}_c\right)\right) \tag{1.19}$$

$$\text{subject to} \quad \boldsymbol{g}_a\left(\boldsymbol{d}_a,\boldsymbol{d}_c\right) \leq \boldsymbol{0} \tag{1.20}$$

$$\boldsymbol{g}_c\left(\boldsymbol{d}_a,\boldsymbol{d}_c\right) \leq \boldsymbol{0} \tag{1.21}$$

$$\boldsymbol{h}_a\left(\boldsymbol{d}_a,\boldsymbol{d}_c\right) = \boldsymbol{0} \tag{1.22}$$

$$\boldsymbol{h}_c\left(\boldsymbol{d}_a,\boldsymbol{d}_c\right) = \boldsymbol{0} \tag{1.23}$$

This approach has the advantage that, if a solution is found, it will be system optimal. However, this approach has some disadvantages. It may be operationally inconvenient, since the problem requires two disparate objectives from different disciplines to be formulated and

combined. The problem cannot be solved until both the artifact and control objectives have been formulated, so it requires the choice of controller architecture to be made early in the design process, prior to the final design of the artifact. The simultaneous problem is also computationally intensive due to its larger size, and may be non-convex, even if the individual objectives f_a and f_c are convex [*Balling and Sobieszczanski-Sobieski* (1996)].

1.5.4 Partitioned Optimization

In partitioned optimization strategies, a large problem is broken up into sub-problems. These sub-problems are then solved, with some form of coordination to ensure that the various sub-problems are consistent with one another. This type of strategy is frequently used in the multidisciplinary optimization field, and a number of different methods have been developed to implement this type of strategy for optimization problems that exhibit coupling, including Analytical Target Cascading [e.g., *Allison et al.* (2005)]. In the context of co-design problems, separate sub-problems are maintained for the artifact and the controller, with a master problem governing the interactions between the two. The system is then optimized by coordinating the optimization of the artifact, controller, and interactions. Reyer advocated this type of strategy as a way to accommodate the coupled nature of co-design problems, while still taking advantage of particular techniques developed for specific disciplines [*Reyer* (2000)]. For the problem considered by Reyer, in which the control optimization problem was formulated as an optimal gains problem, it was shown that system-level optimality was guaranteed. It is important to note that this approach is able to solve co-design problems with bi-directional coupling.

1.5.5 Nested Optimization

In the nested (or bilevel) approach, the combined system is first optimized by varying only the artifact design variables. Next, the controller is optimized, and then the process repeats. Again, the results of each iteration become the starting point for the next iteration.

It has been shown that, in the case of uni-directional coupling, this approach will yield system-optimal solutions [*Fathy* (2003)], but in bi-directional coupling it may not [*Reyer* (2000)].

1.6 Use of Controllability in System Design

As discussed in Sections 1.4.1 and 1.5.1, open-loop eigenvalues have been used as a measure of a system's 'ease of control'. In addition to these efforts, other control characteristics have been used in system design, particularly to locate actuators and sensors [*Roh and Park* (1997), *Lim and Gawronski* (1993), *Junkins and Kim* (1993)]. In these efforts, researchers have considered how to link the concepts of controllability and observability to the output of a physical system [e.g., *Muller and Weber* (1972), *Brown* (1966)]. Muller and Weber examined this issue in detail, considering several candidates for physically meaningful metrics based on the inverse of the controllability Grammian matrix, $\boldsymbol{W}_c^{-1}\left(t_f\right)$, where t_f is the final time of the interval of interest. Their candidates were the maximum eigenvalue of $\boldsymbol{W}_c^{-1}\left(t_f\right)$, the trace of $\boldsymbol{W}_c^{-1}\left(t_f\right)$, and the determinant of $\boldsymbol{W}_c^{-1}\left(t_f\right)$. Their analysis indicated that any of these three measures could be used to formulate some 'measure of quality' of a time-varying system [*Muller and Weber* (1972)]. Furthermore, they showed that optimization of a system using such a measure can produce a system that is amenable to control. This dissertation will make use of this concept in the development of the Control Proxy Function (CPF) problem formulation in Chapter IV, with several CPFs based on the controllability Grammian matrix, which is further discussed in Section 3.2.

1.7 Original Contributions

This chapter introduced the co-design problem, described the ways in which coupling can be measured in this type of problem, and presented some examples from the literature demonstrating the existence of coupling. It also presented a brief survey of the optimiza-

tion methods available to solve the co-design problem. Despite the depth and breadth of previous work in this area, there are still important unanswered questions and issues that have not yet been resolved. This dissertation answers some of these questions. Specifically, it makes the following original contributions:

1. Derivation of relationships between coupling measures, with the extension of the coupling vector to bi-directional cases

   The existence of multiple coupling measures quite naturally raises the question of how they might relate to one another. Since these various measures allegedly are measuring the same thing, one might expect that there will be some relationship between them. This dissertation shows that there are indeed relationships between different coupling measures. Furthermore, in the case of one coupling measure, the coupling vector Γ_v, it is possible to extend the range of application of the measure, from uni-directional coupling only to also include bi-directional coupling, and this is also presented.

2. Derivation of relationships between coupling and controllability for several important classical control problems

   One weakness of the currently used coupling measures is the need to evaluate them at an optimal solution. In other words, the co-design problem must first be solved before the strength of the coupling can be determined with certainty. However, knowing the strength of the coupling prior to attempting a solution would be desirable, since that information could be used in the selection of a method of solution. In several important classical control problems, it is possible to obtain an expression for the coupling vector, Γ_v, that is independent of the controller architecture. Thus, it is possible to study the coupling prior to solving the co-design problem. There are several conditions under which coupling can be shown to vanish, prior to the problem solution, and these conditions are discussed.

3. Development of a modified sequential method using a Control Proxy Function (CPF) for cases of uni-directional coupling

   As discussed in Section 1.5.1, there have been a number of attempts to design a system for 'ease of control'. This dissertation introduces a particular formulation of the co-design problem, using a Control Proxy Function (CPF), to predispose the artifact to ease of control. Guidelines are given for the choice of an effective CPF, a condition to guarantee Pareto optimality is presented, and a measure of the quality of the CPF solution is derived. It is important to note that this quality measure, which indicates the 'distance' from Pareto optimality, can be evaluated without any information about the true Pareto frontier.

4. Categorization of problems according to the nature of coupling and appropriate solution methods

   As discussed in Section 1.5, there is a variety of solution methods available. Choice of an appropriate method is critical in the efficient and effective solution of a co-design problem. Guidelines are presented for the categorization of co-design problems based on the existence and nature of the coupling (bi-directional, uni-directional, or uncoupled), and appropriate solution methods are indicated for each case. These guidelines include the evaluation of whether the new CPF method is suitable for a given problem, and if it is, what type of CPF should be selected.

5. Application of new method to case studies

   A co-design problem is formulated using a MEMS actuator, and solved with the new CPF method. Two different problem formulations are presented, and it is shown that in each case, an appropriate CPF can be chosen which yields Pareto optimal results.

1.8 Dissertation Outline

The following chapters describe the above contributions in further detail. Chapter II shows the relationships between the coupling vector, $\boldsymbol{\Gamma}_v$, and each of the other coupling metrics presented in Section 1.3.2. It also shows the relationship between $\boldsymbol{\Gamma}_v$ and the slope of the Pareto frontier, and extends the range of applicability of $\boldsymbol{\Gamma}_v$ to problems in which the system objective function is a non-linear combination of f_a and f_c, and to problems that exhibit bi-directional coupling. Chapter III presents the relationships between coupling, as measured by $\boldsymbol{\Gamma}_v$, and the controllability Grammian matrix, $\boldsymbol{W}_c$. The relationship between $\boldsymbol{\Gamma}_v$ and $\boldsymbol{W}_c\left(t_f\right)$ is derived for two classical control problems, that of minimizing control effort and that of minimizing time subject to a constraint on control effort. In addition, a relationship between $\boldsymbol{\Gamma}_v$ and the steady-state controllability Grammian, $\boldsymbol{W}_c^{\infty}$, is derived for Linear Quadratic Regulator (LQR) control. In Chapter IV, the Control Proxy Function (CPF) method is formulated for problems with uni-directional coupling. The characteristics of an effective CPF are given, and a metric is provided for the evaluation of a CPF. The given conditions are then used to derive several CPFs that are effective for specific problem formulations. In Chapter V, a method is presented for the evaluation of co-design problems to determine the nature of coupling and to choose an appropriate solution method. This method is then demonstrated through the solution of two co-design problems for a MEMS actuator. The thesis concludes in Chapter VI with a summary, concluding remarks, and discussion of future work.

The appendices provide additional details on the proofs of certain theorems (Appendix A) and the optimization model formulation used in Chapter V (Appendix B).

CHAPTER II

Relationships Between Coupling Measures

2.1 Introduction

As discussed in Section 1.3.2, there are several measures of coupling proposed in the literature. This raises questions about whether these metrics are measuring the same quantity, how they may be related, and how to choose among them in a given problem. In this chapter, it will be shown that various measures of coupling are related. However, they are not equivalent, and they are not necessarily commensurate. This will be illustrated with a simple example. One of these measures, the coupling vector $\mathbf{\Gamma}_v$, is specifically chosen for use in this work. Its physical interpretation shall be addressed, and extensions to its range of applicability will be derived.

2.2 Relations between Coupling Measures

In this section, relationships will be derived between the coupling vector, $\mathbf{\Gamma}_v$, and each of three other coupling measures. These three coupling vectors are the sensitivity of the control objective, normalized sensitivities, and the coupling matrix, $\mathbf{\Gamma}_m$. It will be shown that the coupling vector and the sensitivity of the control objective are commensurate, while the coupling vector is not commensurate with either the normalized sensitivities or the coupling matrix, $\mathbf{\Gamma}_m$.

2.2.1 Coupling Vector, Γ_v, and Sensitivity of the Control Objective

Consider a co-design problem with uni-directional coupling that takes the form of Eqs. (2.1) - (2.3).

$$\min_{\boldsymbol{d}_a,\boldsymbol{d}_c} \quad f_a(\boldsymbol{d}_a) + \frac{w_c}{w_a} f_c(\boldsymbol{d}_a,\boldsymbol{d}_c) \tag{2.1}$$

$$\text{subject to} \quad \boldsymbol{g}_a(\boldsymbol{d}_a) \leq \boldsymbol{0} \tag{2.2}$$

$$\frac{w_c}{w_a}\boldsymbol{g}_c(\boldsymbol{d}_a,\boldsymbol{d}_c) \leq \boldsymbol{0} \tag{2.3}$$

The Karush-Kuhn-Tucker (KKT) conditions [*Papalambros and Wilde* (2000), *Kuhn and Tucker* (1950)] may be written as

$$\left[\begin{array}{cc} \dfrac{\partial f_a}{\partial \boldsymbol{d}_a} + \dfrac{w_c}{w_a}\dfrac{\partial f_c}{\partial \boldsymbol{d}_a} & \dfrac{w_c}{w_a}\dfrac{\partial f_c}{\partial \boldsymbol{d}_c} \end{array}\right] - \left[\begin{array}{cc} \boldsymbol{\mu}_1 & \boldsymbol{\mu}_2 \end{array}\right] \left[\begin{array}{cc} \dfrac{\partial \boldsymbol{g}_a}{\partial \boldsymbol{d}_a} & \boldsymbol{0} \\ \dfrac{w_c}{w_a}\dfrac{\partial \boldsymbol{g}_c}{\partial \boldsymbol{d}_a} & \dfrac{w_c}{w_a}\dfrac{\partial \boldsymbol{g}_c}{\partial \boldsymbol{d}_c} \end{array}\right] = \boldsymbol{0} \tag{2.4}$$

The vector $\boldsymbol{\Gamma}_v$ was defined in [*Fathy* (2003)] as the difference between the KKT conditions for a coupled and uncoupled system, and is found to be

$$\boldsymbol{\Gamma}_v = \frac{w_c}{w_a}\left(\frac{\partial f_c}{\partial \boldsymbol{d}_a} - \boldsymbol{\mu}_2 \frac{\partial \boldsymbol{g}_c}{\partial \boldsymbol{d}_a}\right) \tag{2.5}$$

evaluated at the system optimum, which can then be written in terms of the sensitivity metric introduced in Section 1.3.2 as

$$\boldsymbol{\Gamma}_v = \frac{w_c}{w_a}\frac{\partial f_c^*}{\partial \boldsymbol{d}_a}. \tag{2.6}$$

Therefore, $\boldsymbol{\Gamma}_v$ will be parallel to $\dfrac{\partial f_c^*}{\partial \boldsymbol{d}_a}$. These two measures will be consistent in determining whether or not a system is coupled, and in determining which of two systems is more strongly coupled.

2.2.2 Coupling Vector, Γ_v, and Coupling Matrix, Γ_m

As noted in Section 1.3.2, the coupling vector $\boldsymbol{\Gamma}_v$ and coupling matrix $\boldsymbol{\Gamma}_m$ do not have the same range of applicability. Therefore, in order to examine the relationship between the two coupling measures, certain assumptions are necessary.

1. The system has two objective functions, one for the artifact and one for the controller.
2. Coupling is unidirectional.
3. The overall objective function is a weighted sum of the individual objectives.
4. There are no local copies of variables.

The system in question, then, can be represented by the diagram given in Fig. 2.1.

From assumptions 1–4, the following substitutions can be made in Eq. (1.18):

$$\begin{aligned} N &= 2 \\ f_1 &= f_a \\ f_2 &= f_c \\ \hat{\boldsymbol{x}}_1 &= \boldsymbol{x}_1 = \mathbf{0} \\ \hat{\boldsymbol{x}}_2 &= \boldsymbol{x}_2 = \boldsymbol{d}_c \\ \hat{\boldsymbol{y}}_{12} &= \boldsymbol{y}_{12} = \boldsymbol{d}_a \\ \hat{\boldsymbol{y}}_{21} &= \boldsymbol{y}_{21} = \boldsymbol{d}_a \\ \hat{\boldsymbol{y}}_{11} &= \boldsymbol{y}_{11} = \mathbf{0} \\ \hat{\boldsymbol{y}}_{22} &= \boldsymbol{y}_{22} = \mathbf{0} \end{aligned}$$

These substitutions give a simplified coupling matrix

$$\boldsymbol{\Gamma}_m = \begin{bmatrix} \mathbf{0} \\ w_a \dfrac{\partial f_a}{\partial \boldsymbol{d}_a}\dfrac{d\boldsymbol{d}_a}{d\boldsymbol{d}_c} + w_c \dfrac{\partial f_c}{\partial \boldsymbol{d}_a}\dfrac{d\boldsymbol{d}_a}{d\boldsymbol{d}_c} + w_c \dfrac{\partial f_c}{\partial \boldsymbol{d}_c} \end{bmatrix}^T . \tag{2.7}$$

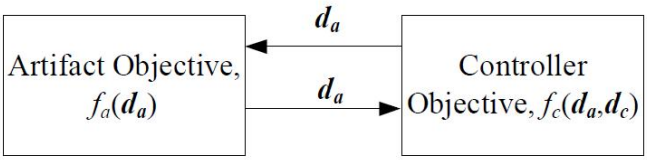

Figure 2.1: Subsystem Structure for Simplified System

It is then possible to relate $\mathbf{\Gamma}_v$ and $\mathbf{\Gamma}_m$:

$$\mathbf{\Gamma}_m = \begin{bmatrix} \mathbf{0} \\ w_a \left(\dfrac{df_a}{d\boldsymbol{d}_c} + \left(\mathbf{\Gamma}_v - \dfrac{w_c}{w_a} \dfrac{\partial f_c}{\partial \boldsymbol{d}_c} \dfrac{d\boldsymbol{d}_c}{d\boldsymbol{d}_a} \right) \dfrac{d\boldsymbol{d}_a}{d\boldsymbol{d}_c} + \dfrac{w_c}{w_a} \dfrac{\partial f_c}{\partial \boldsymbol{d}_c} \right) \end{bmatrix}^T . \tag{2.8}$$

If the problem is unconstrained, then Eq.(2.8) simplifies to

$$\mathbf{\Gamma}_m = \begin{bmatrix} 0 \\ w_a \dfrac{df_a}{d\boldsymbol{d}_c} + w_a \mathbf{\Gamma}_v \dfrac{d\boldsymbol{d}_a}{d\boldsymbol{d}_c} \end{bmatrix}^T . \tag{2.9}$$

The derivative $\frac{d\boldsymbol{d}_a}{d\boldsymbol{d}_c}$ can be calculated either analytically, from the KKT conditions, or numerically.

The following observations can then be made:

1. $\mathbf{\Gamma}_m$ captures information about the interactions between variables in each sub-problem that is not contained within $\mathbf{\Gamma}_v$. This is consistent with the differing origins of the metrics. Since $\mathbf{\Gamma}_m$ was derived from the GSEs, it can be expected to contain information about the sensitivity of one variable to another within the same sub-system.

2. In a problem with active constraints, it is possible for $\mathbf{\Gamma}_m$ to be non-zero when $\mathbf{\Gamma}_v = \mathbf{0}$. This would indicate that relations between the design variables in a sub-system are highly significant, and the solution will be sensitive to small changes in the variables.

3. In both a constrained and an unconstrained problem, it is possible for $\mathbf{\Gamma}_m$ and $\mathbf{\Gamma}_v$ to

disagree on when a system is more strongly coupled. This will happen in the case of high sensitivity in the relations between the variables.

4. For the case where constraints are active, but there is only one artifact design variable and one controller design variable, Eq.(2.8) simplifies to Eq.(2.9), just as it does for the unconstrained case. This reflects the fact that there are no possible interactions between variables within a sub-system. The same situation will occur when all active constraints consist of simple bounds.

5. If an unconstrained system is uncoupled, then $f_a = f_a(\boldsymbol{d}_a)$ and $f_c = f_c(\boldsymbol{d}_c)$. In this case, $\dfrac{df_a}{d\boldsymbol{d}_c} = 0$ since, by definition of an uncoupled system, the artifact objective function f_a does not depend on the controller variables $\boldsymbol{d}_c$. Also, $\boldsymbol{\Gamma}_v = \mathbf{0}$, since the equations representing the KKT conditions will be identical for both sequential and simultaneous solutions of the system. This results in $\boldsymbol{\Gamma}_m = \mathbf{0}$, and therefore the two criteria will be consistent in having zero value for uncoupled problems.

2.2.3 Coupling Vector, $\boldsymbol{\Gamma}_v$, and Normalized Sensitivities

In evaluating the application of normalized sensitivities

$$\begin{bmatrix} \dfrac{\partial f_a}{\partial \boldsymbol{d}_a} & \mathbf{0} \\ \mathbf{0} & \dfrac{\partial f_c}{\partial \boldsymbol{d}_c} \end{bmatrix} = \begin{bmatrix} 1 & -\dfrac{\partial f_a}{\partial f_c} \\ -\dfrac{\partial f_c}{\partial f_a} & 1 \end{bmatrix} \begin{bmatrix} \dfrac{df_a}{d\boldsymbol{d}_a} & \dfrac{df_a}{d\boldsymbol{d}_c} \\ \dfrac{df_c}{d\boldsymbol{d}_a} & \dfrac{df_c}{d\boldsymbol{d}_c} \end{bmatrix} \tag{2.10}$$

The coupling vector, $\boldsymbol{\Gamma}_v$, can be expressed as

$$\boldsymbol{\Gamma}_v = \frac{w_c}{w_a} \frac{df_c^*}{d\boldsymbol{d}_a} \tag{2.11}$$

and thus Eq. (2.10) can be seen to contain $\mathbf{\Gamma}_v$, as shown below.

$$\begin{bmatrix} \dfrac{\partial f_a}{\partial \boldsymbol{d}_a} & \mathbf{0} \\ \mathbf{0} & \dfrac{\partial f_c}{\partial \boldsymbol{d}_c} \end{bmatrix} = \begin{bmatrix} 1 & -\dfrac{\partial f_a}{\partial f_c} \\ -\dfrac{\partial f_c}{\partial f_a} & 1 \end{bmatrix} \begin{bmatrix} \dfrac{df_a}{d\boldsymbol{d}_a} & \dfrac{df_a}{d\boldsymbol{d}_c} \\ \dfrac{w_a}{w_c}\mathbf{\Gamma}_v & \dfrac{df_c}{d\boldsymbol{d}_c} \end{bmatrix} \tag{2.12}$$

These metrics are not commensurate, since the normalized sensitivities contain terms that do not appear in $\mathbf{\Gamma}_v$.

2.3 Illustrative Example: Positioning Gantry

In this section, the coupling vector and coupling matrix are applied to a simple system, and it is shown that they agree on the presence of coupling in some cases and disagree in others. The system shown here shall be used also as an illustrative example in Chapter III.

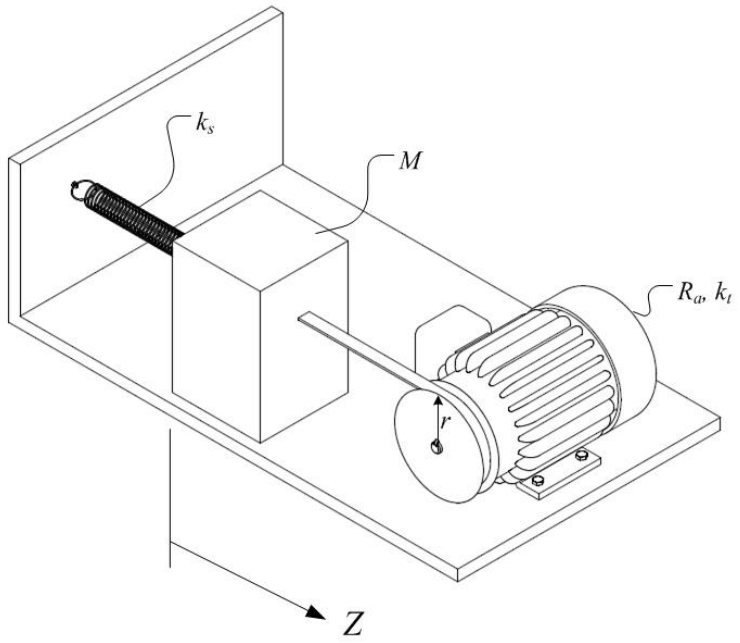

Figure 2.2: Configuration of Positioning Gantry

Consider a simple model of a positioning gantry, as shown in Fig. 2.2. In this system, a mass M is connected to a fixed surface by a linear spring with constant k_s. A flexible

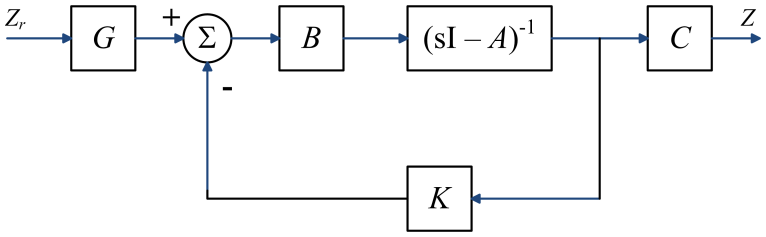

Figure 2.3: Schematic of System Controller

inelastic belt is connected to the mass and wraps around a pulley with radius r, which is mounted on a DC motor with armature resistance R_a and motor constant k_t. It is assumed that the rotor inertia of the motor and the inertia of the pulley are negligible. The motor will be actuated by a voltage signal. The displacement of the mass from its original position is Z. The system can be modeled by the following equations:

$$\dot{\boldsymbol{x}} = \boldsymbol{A}\boldsymbol{x} + \boldsymbol{B}u \tag{2.13}$$

$$Z = \boldsymbol{C}\boldsymbol{x} \tag{2.14}$$

$$\boldsymbol{x} = \begin{bmatrix} Z \\ \dot{Z} \end{bmatrix} \tag{2.15}$$

$$\boldsymbol{A} = \begin{bmatrix} 0 & 1 \\ -\frac{k}{m} & -\frac{b}{m} \end{bmatrix} \tag{2.16}$$

$$\boldsymbol{B} = \begin{bmatrix} 0 \\ \frac{1}{m} \end{bmatrix} \tag{2.17}$$

$$\boldsymbol{C} = \begin{bmatrix} 1 & 0 \end{bmatrix} \tag{2.18}$$

where u is the voltage, V, and the terms m, b, and k are given by

$$m = \frac{MrR_a}{k_t} \tag{2.19}$$

$$b = \frac{k_t}{r} \tag{2.20}$$

$$k = \frac{k_s r R_a}{k_t} \tag{2.21}$$

A state-feedback controller with a precompensator G and gains $\boldsymbol{K} = [K_1\ K_2]$ is applied to the system, as shown in Fig. 2.3. This system will be optimized twice. The artifact objective function f_a will remain the same, but the artifact design variables $\boldsymbol{d}_a$ and artifact constraint g_1 will be changed to produce both an uncoupled and a coupled optimization problem. The artifact objective is to maximize the steady-state displacement of the mass, Z_{ss}. The controller objective function f_c, controller design variables $\boldsymbol{d}_c$, and controller constraint g_2 take the same form in both formulations. The controller objective is to minimize a combination of the maximum voltage V_{max} and the settling time t_s. The relative importance of V_{max} and t_s are specified by weighting parameters.

2.3.1 Uncoupled System Optimization

The system optimization formulation is:

$$\min_{r,k_t,K_1,K_2,G} \quad w_a f_a + w_c f_c \tag{2.22}$$

$$\text{subject to} \quad g_1 = c_1 + \left(\frac{k_t V_{ss}}{rR_a} - c_2\right)^{\frac{1}{2}} - r \leq 0 \tag{2.23}$$

$$g_2 = M_p - M_{p,all} \leq 0 \tag{2.24}$$

$$h_1 = Z_{ss} - Z_r = 0 \tag{2.25}$$

Table 2.1: Parameters for Optimization of Uncoupled System

Parameter	Value
M	2.00 kg
k_s	0.75 N/mm
R_a	10.00 kΩ
V_{ss}	10.00 V
$M_{p,all}$	5%
c_1	2.50
c_2	4.00
a_1	15.00
a_2	0.25

The individual objectives f_a and f_c are given by

$$f_a = -Z_{ss} = -\frac{k_t V_{ss}}{r R_a k_s} \tag{2.26}$$

$$f_c = a_1 V_{max} + a_2 t_s \tag{2.27}$$

where Z_{ss} is derived by setting $\dot{\boldsymbol{x}} = 0$ in Eq. (2.13). and the position overshoot M_p is given by

$$M_p = \mathrm{e}^{-\pi\varsigma/\sqrt{1-\varsigma^2}} \tag{2.28}$$

$$\varsigma = \frac{b + K_2}{2\sqrt{m\,(k + K_1)}} \tag{2.29}$$

where V_{ss} is the steady-state voltage applied to the motor, V_{max} is the maximum applied voltage, t_s is the 1% settling time, $M_{p,all}$ is the limit imposed on the overshoot, and Z_r is the reference signal entering the controller. The artifact weight w_a and the controller weight w_c have strictly positive values between 0 and 1. The constraint g_1 is formulated to ensure that the pulley radius r is appropriate for the thickness of belt required for the forces present.

The constraints were determined to be active by monotonicity analysis and were used to eliminate the variables k_t, G, and K_1, which creates a problem where Eq. (2.9) is applicable. Using the values shown in Table 2.1, the optimum solution and both coupling metrics were

Table 2.2: Results of Optimization of Uncoupled System

Quantity	Value
$\boldsymbol{d}_a = \begin{bmatrix} r \\ k_t \end{bmatrix}$	$\begin{bmatrix} 2.50 \text{ cm} \\ 10.00 \text{ N-m/A} \end{bmatrix}$
$\boldsymbol{d}_c = \begin{bmatrix} K_1 \\ K_2 \\ G \end{bmatrix}$	$\begin{bmatrix} 0.72 \\ 1.23 \\ 2.59 \end{bmatrix}$
Z_{ss}	5.33 cm
t_s	8.79 s
V_{max}	13.83 V

calculated. The optimal values of the design variables and of Z_{ss}, V_{max}, and t_s are given in Table 2.2. For all values of w_a and w_c in the specified range, $\Gamma_v = 0$ and $\boldsymbol{\Gamma}_m = [0\ 0]$, and, therefore, both measures were consistent in indicating that the system is uncoupled. These coupling measures are also consistent with the results of the system optimization itself; identical results were found for both sequential optimization and for simultaneous optimization with various combinations of weights.

This co-design problem can be solved without eliminating constraints, however. Consider the case where the variables k_t and K_1 are retained, but the variable G is eliminated by substitution. In this case, the coupling vector, $\boldsymbol{\Gamma}_v$, is given by the relation

$$\boldsymbol{\Gamma}_v = \frac{w_c}{w_a}\left(\begin{bmatrix} \dfrac{\partial f_c}{\partial r} \\ \dfrac{\partial f_c}{\partial k_t} \end{bmatrix}^T + \begin{bmatrix} \dfrac{\partial f_c}{\partial K_1} \\ \dfrac{\partial f_c}{\partial K_2} \end{bmatrix}^T \begin{bmatrix} \dfrac{\partial K_1}{\partial r} & \dfrac{\partial K_1}{\partial k_t} \\ \dfrac{\partial K_2}{\partial r} & \dfrac{\partial K_2}{\partial k_t} \end{bmatrix} \right) \tag{2.30}$$

The problem is still uncoupled, as determined by $\boldsymbol{\Gamma}_v$; at the solution,

$$\boldsymbol{\Gamma}_v = \begin{bmatrix} 0 & 0 \end{bmatrix}. \tag{2.31}$$

However, the problem is not uncoupled when the coupling matrix, $\boldsymbol{\Gamma}_m$, is used. For this

form of the problem,

$$\mathbf{\Gamma}_m = \begin{bmatrix} \mathbf{0} \\ w_a \begin{bmatrix} \frac{\partial f_a}{\partial r} \\ \frac{\partial f_a}{\partial k_t} \end{bmatrix}^T \begin{bmatrix} \frac{\partial r}{\partial K_1} & \frac{\partial r}{\partial K_2} \\ \frac{\partial k_t}{\partial K_1} & \frac{\partial k_t}{\partial K_2} \end{bmatrix} + w_c \left(\begin{bmatrix} \frac{\partial f_c}{\partial r} \\ \frac{\partial f_c}{\partial k_t} \end{bmatrix}^T \begin{bmatrix} \frac{\partial r}{\partial K_1} & \frac{\partial r}{\partial K_2} \\ \frac{\partial k_t}{\partial K_1} & \frac{\partial k_t}{\partial K_2} \end{bmatrix} + \begin{bmatrix} \frac{\partial f_c}{\partial K_1} \\ \frac{\partial f_c}{\partial K_2} \end{bmatrix}^T \right) \end{bmatrix}. \tag{2.32}$$

For the weights $w_a = 0.5$, $w_c = 0.5$, the matrix $\mathbf{\Gamma}_m$ is computed as

$$\mathbf{\Gamma}_m = \begin{bmatrix} 0 & 0 \\ -0.162 & -0.183 \end{bmatrix} \tag{2.33}$$

Note, then, that if constraints are active, $\mathbf{\Gamma}_v$ and $\mathbf{\Gamma}_m$ may disagree on whether or not a problem is coupled. Furthermore, $\mathbf{\Gamma}_m$ can indicate that the same problem is either coupled or uncoupled, depending on the formulation of that problem. This indicates that, if parametric uncertainty in the constraints is neglected, the problem will be uncoupled; however, $\mathbf{\Gamma}_m$ is capable of capturing information on the parametric uncertainty of the constraints, and this uncertainty will affect the control objective of the co-design problem [*Alyaqout* (2006)].

2.3.2 Coupled System Optimization

Now, consider a different formulation of the system optimization. In this case, the design variables are k_s, R_a, G, K_1, and K_2, the objective functions and constraints g_2 and h_1 are unchanged, but constraint g_1 is changed. The new constraint g_1 is formulated to ensure that the spring is sized appropriately for the loads present.

Table 2.3: Parameters for Optimization of Coupled System

Parameter	Value
M	2.00 kg
k_t	10.00 N-m/A
r	2.50 cm
V_{ss}	10.00 V
$M_{p,all}$	5%
c_3	1.50
c_4	1.00
a_1	15.00
a_2	0.20

$$\min_{k_s,R_a,K_1,K_2,G} \quad w_a f_a + w_c f_c \tag{2.34}$$

$$\text{subject to} \quad g_1 = \left(\frac{V_{ss}k_t}{rR_a} + c_4\right)^{1.5} - c_3 - k_s \leq 0 \tag{2.35}$$

$$g_2 = M_p - M_{p,all} \leq 0 \tag{2.36}$$

$$h_1 = Z_{ss} - Zr = 0 \tag{2.37}$$

where f_a and f_c are given by Eq.(2.26) and (2.27), respectively.

Again, monotonicity analysis was used to determine that all constraints were active, and therefore used to eliminate the variables k_s, G, and K_1 and produce an unconstrained system. Again, this creates a problem in which Eq. (2.9) is applicable. The problem was solved for the parameters in Table 2.3 and several sets of weights. Results for two sets of weights are given in Table 2.4. The first set given corresponds to point "A" and the second set of weights to point "B" in Fig. 2.4.

In this case, both coupling measures are non-zero. This agrees with the results of the system optimization; assigning different weights to the objectives f_a and f_c in the simultaneous system solution yields different results. The sequential problem cannot be solved in this case without additional constraints, since it is unbounded.

Table 2.4: Results of Optimization of Coupled System

	Value for Given Weights	
Quantity	Point A $w_a = 0.4$, $w_c = 0.6$	Point B $w_a = 0.7$, $w_c = 0.3$
$\boldsymbol{d}_a = \begin{bmatrix} R_a \\ k_s \end{bmatrix}$	$\begin{bmatrix} 28.60\ \text{k}\Omega \\ 2.21\ \text{N/mm} \end{bmatrix}$	$\begin{bmatrix} 38.75\ \text{k}\Omega \\ 1.40\ \text{N/mm} \end{bmatrix}$
$\boldsymbol{d}_c = \begin{bmatrix} K_1 \\ K_2 \\ G \end{bmatrix}$	$\begin{bmatrix} -1.43 \\ 15.81 \\ 14.40 \end{bmatrix}$	$\begin{bmatrix} -2.15 \\ 16.50 \\ 11.38 \end{bmatrix}$
Z_{ss}	0.63 cm	0.74 cm
t_s	6.64 s	8.70 s
V_{max}	10.26 V	10.27 V
Γ_v	0.058	0.113
$\boldsymbol{\Gamma}_m$	$\begin{bmatrix} 0 \\ 0.0039 \end{bmatrix}^T$	$\begin{bmatrix} 0 \\ -0.0033 \end{bmatrix}^T$

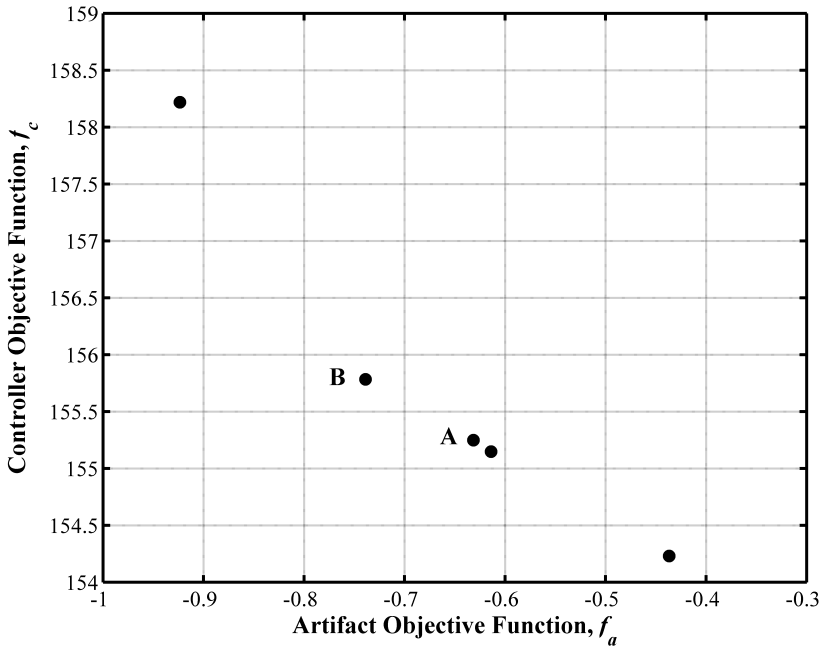

Figure 2.4: Pareto Points for Coupled System Optimization

Note that, while both coupling metrics agree that the system is coupled, they do not agree on the coupling strength. The value of $\boldsymbol{\Gamma}_v$ is positive for both points considered, but the non-zero component of $\boldsymbol{\Gamma}_m$ experiences a sign change between points A and B. The two measures are clearly not commensurate, even when they agree on the existence of coupling.

2.4 Choice of Coupling Metric

It has been shown that, of the four coupling metrics considered, only two of them are commensurate. The coupling vector, $\boldsymbol{\Gamma}_v$, is commensurate with the sensitivity of the control objective. However, the coupling vector is not commensurate with either the coupling matrix, $\boldsymbol{\Gamma}_m$, or with the normalized sensitivities. Therefore, it is necessary to consider which of these measures is most appropriate for this work. In this thesis, the coupling vector, $\boldsymbol{\Gamma}_v$, is chosen to represent coupling. This measure is judged to be most appropriate due to its simpler form and applicability to the problems of interest, i.e., co-design problems with uni-directional coupling.

2.5 Physical Significance of Coupling Vector

While the coupling vector, $\boldsymbol{\Gamma}_v$, is derived from the KKT conditions, it also has a physical interpretation as a component of the slope of the Pareto frontier for a co-design problem that exhibits uni-directional coupling. For the coupled co-design problem described here, it is possible to describe the relation between the optimum values of the two objectives as follows:

$$f_c^* = f(f_a^*) \tag{2.38}$$

By differentiating Eq. (2.38) and making appropriate substitutions, the slope of the Pareto frontier can be expressed as

$$\frac{df_c^*}{df_a^*} = \frac{w_a}{w_c}\boldsymbol{\Gamma}_v \frac{d\boldsymbol{d}_a}{df_a}^* . \tag{2.39}$$

The physical significance of the coupling vector $\boldsymbol{\Gamma}_v$, therefore, is that it contributes to the slope of the Pareto frontier, leading to the following observations:

1. If the coupling vector vanishes at one particular point, then the Pareto frontier will have zero slope at that point. If this point is not an end point of the Pareto frontier, then the curve will either be non-convex or discontinuous at this point.

2. It is possible for a non-zero coupling vector to be present at a point of zero slope. In this case, the coupling vector would be orthogonal to the derivative $\frac{d\boldsymbol{d}_a}{df_a}^*$.

3. Large changes in the direction of the coupling vector, while not definitive, may be a warning sign of a non-convex or discontinuous Pareto frontier, particularly when the derivative vector $\frac{d\boldsymbol{d}_a}{df_a}^*$ does not experience similar changes in its direction.

Information about the nature of the Pareto frontier can be useful. As noted in Section 1.5.3, if the Pareto frontier is determined to be non-convex, then a linear combination of objectives is not an effective formulation and another formulation, such as an exponential weighted criteria function [*Athan* (1994)], will be required. If the Pareto frontier is both convex and continuous, then it could be approximated by fitting a convex continuous curve to a relatively small number of points. This can be useful when the designer wishes to find points in a particular area of the Pareto frontier. Methods do exist for finding points in specific areas of the Pareto frontier, such as the normal-boundary intersection method to find the "knee" [*Das* (1999)]. However, the ability to approximate the curve is useful when another area of the Pareto frontier is considered to be desirable. Determination of the approximate curve has the potential to reduce the computational requirements to solve a problem.

2.6 Extensions of Coupling Vector, $\boldsymbol{\Gamma}_v$

As stated in Section 1.3, the coupling vector, $\boldsymbol{\Gamma}_v$, was derived based on certain assumptions. These assumptions impose limitations on the types of problems for which it is

applicable. Here, it will be shown that the scope of $\mathbf{\Gamma}_v$ may be extended in two ways. One extension, to problems in which the objective function is not a linear combination of f_a and f_c, will be directly relevant to this dissertation. The second extension, to problems with bi-directional coupling, will not be used for this work. However, it may be useful for later extension of this work to co-design problems with bi-directional coupling.

2.6.1 Extension of Coupling Vector to Non-Linear Objective Combination

Assume that a co-design problem is formulated as the sum of two functions, F_1 and F_2, as in Eqs. (2.40) - (2.44). The functions $F_1(f_a)$ and $F_2(f_c)$ are any functions that satisfy the conditions given in Eqs. (2.45) - (2.46).

$$\min_{\boldsymbol{d}_a, \boldsymbol{d}_c} \quad F = F_1(f_a(\boldsymbol{d}_a)) + F_2(f_c(\boldsymbol{d}_a, \boldsymbol{d}_c)) \tag{2.40}$$

$$\text{subject to} \quad \boldsymbol{g}_a(\boldsymbol{d}_a) \leq \mathbf{0} \tag{2.41}$$

$$\boldsymbol{h}_a(\boldsymbol{d}_a) = \mathbf{0} \tag{2.42}$$

$$\boldsymbol{g}_c(\boldsymbol{d}_a, \boldsymbol{d}_c) \leq \mathbf{0} \tag{2.43}$$

$$\boldsymbol{h}_c(\boldsymbol{d}_a, \boldsymbol{d}_c) = \mathbf{0} \tag{2.44}$$

$$\arg\min(F_1(f_a(\boldsymbol{d}_a))) = \arg\min(f_a(\boldsymbol{d}_a)) \tag{2.45}$$

$$\arg\min(F_2(f_c(\boldsymbol{d}_a, \boldsymbol{d}_c))) = \arg\min(f_c(\boldsymbol{d}_a, \boldsymbol{d}_c)) \tag{2.46}$$

Furthermore, assume that the control design variables, $\boldsymbol{d}_c$, can be expressed as a function of the artifact design variables, $\boldsymbol{d}_a$, i.e., $\boldsymbol{d}_c = \boldsymbol{d}_c(\boldsymbol{d}_a)$. Then, the KKT conditions can be

written as

$$\begin{bmatrix} \frac{\partial f_a}{\partial \boldsymbol{d}_a} + \frac{\frac{\partial F_2}{\partial f_c}}{\frac{\partial F_1}{\partial f_a}} \left(\frac{\partial f_c}{\partial \boldsymbol{d}_a} + \frac{\partial f_c}{\partial \boldsymbol{d}_c} \frac{\boldsymbol{d}_c}{\partial \boldsymbol{d}_a} \right) \\ \frac{\frac{\partial F_2}{\partial f_c}}{\frac{\partial F_1}{\partial f_a}} \frac{\partial f_c}{\partial \boldsymbol{d}_c} \end{bmatrix} + \boldsymbol{\lambda}^T \begin{bmatrix} \frac{\partial \boldsymbol{h}_a}{\partial \boldsymbol{d}_a} \\ \frac{\partial \boldsymbol{h}_c}{\partial \boldsymbol{d}_c} \end{bmatrix} + \boldsymbol{\mu}^T \begin{bmatrix} \frac{\partial \boldsymbol{g}_a}{\partial \boldsymbol{d}_a} \\ \frac{\partial \boldsymbol{g}_c}{\partial \boldsymbol{d}_c} \end{bmatrix} = \mathbf{0} \quad (2.47)$$

$$\boldsymbol{\mu}^T \begin{bmatrix} \boldsymbol{g}_a(\boldsymbol{d}_a) \\ \boldsymbol{g}_c(\boldsymbol{d}_a, \boldsymbol{d}_c) \end{bmatrix} = \mathbf{0} \quad (2.48)$$

$$\boldsymbol{\lambda} \neq \mathbf{0} \quad (2.49)$$

$$\boldsymbol{\mu} \geq \mathbf{0} \quad (2.50)$$

It is then possible to equate a generalized coupling vector, $\boldsymbol{\Gamma}'_v$, with the difference between the KKT conditions for the coupled and the uncoupled problem.

$$\boldsymbol{\Gamma}'_v = \frac{\partial F_2 / \partial f_c}{\partial F_a / \partial f_a} \left(\frac{\partial f_c}{\partial \boldsymbol{d}_a} + \frac{\partial f_c}{\partial \boldsymbol{d}_c} \frac{\partial \boldsymbol{d}_c}{\partial \boldsymbol{d}_a} \right) \quad (2.51)$$

Note that the vector $\boldsymbol{\Gamma}'_v$ is parallel to the vector $\boldsymbol{\Gamma}_v$. Therefore, any statement based on the direction of $\boldsymbol{\Gamma}_v$ will also apply to $\boldsymbol{\Gamma}'_v$. The original coupling vector $\boldsymbol{\Gamma}_v$ is a special case of $\boldsymbol{\Gamma}'_v$, where $F_1(f_a) = w_a f_a$ and $F_2(f_c) = w_c f_c$. Note that $\boldsymbol{\Gamma}'_v$ is not valid if a non-separable function of both f_a and f_c is considered.

As an example of a non-linear combination of f_a and f_c, consider the exponential weighted criteria formulation [*Athan* (1994)]. This formulation is given by

$$f = (e^{nw_a} - 1) e^{f_a} + (e^{nw_c} - 1) e^{f_c} \quad (2.52)$$

where n is a parameter, and w_a and w_c are the relative weights of f_a and f_c. For this formulation,

$$\boldsymbol{\Gamma}'_v = \frac{(e^{nw_c} - 1) e^{f_c}}{(e^{nw_a} - 1) e^{f_a}} \left(\frac{\partial f_c}{\partial \boldsymbol{d}_a} + \frac{\partial f_c}{\partial \boldsymbol{d}_c} \frac{\partial \boldsymbol{d}_c}{\partial \boldsymbol{d}_a} \right) \quad (2.53)$$

Since $\boldsymbol{\Gamma}_v' \parallel \boldsymbol{\Gamma}_v$, any derivations based on the direction of $\boldsymbol{\Gamma}_v$ will apply to problems in which the formulation in Eq. (2.52) is used.

2.6.2 Extension of Coupling Vector to Bi-Directional Coupling

As previously stated, the coupling vector $\boldsymbol{\Gamma}_v$ was derived based on the assumption of uni-directional coupling. While there are many systems which exhibit uni-directional coupling, bi-directional coupling is also common. Therefore, it is useful to extend the coupling vector to these cases. The extended coupling vector $\boldsymbol{\Gamma}_{vb}$ can be found by comparing the KKT conditions for the coupled and uncoupled cases. The system objective given as

$$\min_{\boldsymbol{d}_a,\boldsymbol{d}_c} f = w_a f_a(\boldsymbol{d}_a,\boldsymbol{d}_c) + w_c f_c(\boldsymbol{d}_a,\boldsymbol{d}_c) \tag{2.54}$$

can be re-written as

$$\min_{\boldsymbol{d}_a,\boldsymbol{d}_c} f = f_a(\boldsymbol{d}_a,\boldsymbol{d}_c) + \frac{w_c}{w_a} f_c(\boldsymbol{d}_a,\boldsymbol{d}_c), \tag{2.55}$$

subject to

$$\boldsymbol{g}(\boldsymbol{d}_a,\boldsymbol{d}_c) \leq \mathbf{0} \tag{2.56}$$

$$\boldsymbol{h}(\boldsymbol{d}_a,\boldsymbol{d}_c) = \mathbf{0}. \tag{2.57}$$

The solution will be system-optimal if $\boldsymbol{d}_a^*$ minimizes not f_a but $f_a + \frac{w_c}{w_a} f_c$; likewise, $\boldsymbol{d}_c^*$ must minimize not f_c but $f_a + \frac{w_c}{w_a} f_c$. The optimizers for the full problem, therefore, satisfy the relations

$$\frac{df_a}{d\boldsymbol{d}_a} + \boldsymbol{\mu}_a^T \frac{d\boldsymbol{g}_a}{d\boldsymbol{d}_a} + \boldsymbol{\lambda}_a^T \frac{d\boldsymbol{h}_a}{d\boldsymbol{d}_a} + \frac{w_c}{w_a}\frac{df_c^*}{d\boldsymbol{d}_a} = \mathbf{0} \tag{2.58}$$

$$\frac{df_c}{d\boldsymbol{d}_c} + \boldsymbol{\mu}_c^T \frac{d\boldsymbol{g}_c}{d\boldsymbol{d}_c} + \boldsymbol{\lambda}^T \frac{d\boldsymbol{h}_c}{d\boldsymbol{d}_c} + \frac{df_a^*}{d\boldsymbol{d}_c} = \mathbf{0} \tag{2.59}$$

For an uncoupled problem, the KKT stationarity condition is:

$$\frac{df_a}{d\boldsymbol{d}_a} + \boldsymbol{\mu}_a^T \frac{d\boldsymbol{g}_a}{d\boldsymbol{d}_a} + \boldsymbol{\lambda}_a^T \frac{d\boldsymbol{h}_a}{d\boldsymbol{d}_a} = \mathbf{0} \tag{2.60}$$

$$\frac{df_c}{d\boldsymbol{d}_c} + \boldsymbol{\mu}_c^T \frac{d\boldsymbol{g}_c}{d\boldsymbol{d}_c} + \boldsymbol{\lambda}^T \frac{d\boldsymbol{h}_c}{d\boldsymbol{d}_c} = \mathbf{0} \tag{2.61}$$

The difference between Eqs. (2.58 - 2.59) and (2.60 - 2.61) quantifies the coupling for the bi-directional problem. Using the chain rule, this leads to the following bi-directional coupling vector $\boldsymbol{\Gamma}_{vb}$:

$$\boldsymbol{\Gamma}_{vb} = \left[\begin{array}{cc} \frac{w_c}{w_a}\left(\frac{\partial f_c}{\partial \boldsymbol{d}_a} + \frac{\partial f_c}{\partial \boldsymbol{d}_c}\frac{d\boldsymbol{d}_c}{d\boldsymbol{d}_a}\right) & \frac{\partial f_a}{\partial \boldsymbol{d}_c} + \frac{\partial f_a}{\partial \boldsymbol{d}_a}\frac{d\boldsymbol{d}_a}{d\boldsymbol{d}_c} \end{array} \right], \tag{2.62}$$

where the constraints containing both $\boldsymbol{d}_a$ and $\boldsymbol{d}_c$ provide the relation between $\boldsymbol{d}_a$ and $\boldsymbol{d}_c$. Note that the uni-directional coupling vector in Eq. (1.14) appears within Eq. (2.62), which can be re-written as

$$\boldsymbol{\Gamma}_{vb} = \left[\begin{array}{cc} \boldsymbol{\Gamma}_v & \frac{\partial f_a}{\partial \boldsymbol{d}_c} + \frac{\partial f_a}{\partial \boldsymbol{d}_a}\frac{d\boldsymbol{d}_a}{d\boldsymbol{d}_c} \end{array} \right]. \tag{2.63}$$

As with the uni-directional coupling vector $\boldsymbol{\Gamma}_v$, the strength of the coupling can be quantified by evaluating the vector norm $\|\boldsymbol{\Gamma}_{vb}\|_2$.

2.7 Summary

In this chapter, four coupling measures have been compared, and relationships between them have been derived. It has been shown that only two measures are commensurate with each other. For two of these metrics, the coupling vector, $\boldsymbol{\Gamma}_v$, and the coupling matrix, $\boldsymbol{\Gamma}_m$, the differences in their description of coupling in a given problem were illustrated through an example. The coupling vector, $\boldsymbol{\Gamma}_v$, was chosen as the metric to be used in this thesis, and its physical interpretation was examined. Its range of applicability was also studied, and two extensions were derived. In Chapter III, relationships will be derived between the coupling vector, $\boldsymbol{\Gamma}_v$, and the controllability Grammian matrix of a system.

CHAPTER III

Relationship Between Coupling and Controllability

3.1 Introduction

As discussed in Chapter I, knowledge of coupling is important in choosing an appropriate method of solution for a particular co-design problem. Although the solutions found via simultaneous optimization are system-optimal, this approach is computationally intensive, organizationally challenging, and precludes the use of many specialized techniques developed for optimization in specific disciplines [*Balling and Sobieszczanski-Sobieski* (1996)]. A sequential approach, while simpler and easier to solve, does not typically find the system optimum. It would, therefore, be useful to identify and quantify coupling prior to choosing a solution method for the problem. However, as discussed in Chapter II, existing methods used to determine coupling require knowledge of the system solution. Therefore, coupling cannot be calculated until the problem has been solved. In this chapter it is shown that for some problem formulations, representing important classical control problems, coupling can be determined *a priori* using the controllability Grammian, which offers a significant advantage in choosing appropriate methods of solution.

3.2 Metrics Used for Coupling and Controllability

Several metrics have been developed for quantification of coupling, as discussed in Chapter II. The coupling vector, $\boldsymbol{\Gamma}_v$, will be used in this work. This metric is preferred for co-design problems with uni-directional coupling for its relatively simple form and suitability to the problem being considered [*Peters et al.* (2009)]. The coupling vector, which is given by Eq. (1.14), must be evaluated at the optimal solution to Eqs. (1.9) - (1.13). Consequently, the coupling cannot be determined *a priori*, i.e., before the simultaneous co-design problem in Eqs. (1.9)-(1.13) is solved.

There is a variety of ways to determine controllability. One metric which is particularly useful is the controllability Grammian matrix. A characteristic of the controllability Grammian which makes it useful in this work is that it can be used to calculate the optimal controller performance based only on the dynamics of the uncontrolled system, i.e., independently of the controller architecture chosen.

For a linear system expressed in the form

$$\dot{\boldsymbol{x}} = \boldsymbol{A}\boldsymbol{x} + \boldsymbol{B}u \tag{3.1}$$

$$y = \boldsymbol{C}\boldsymbol{x} \tag{3.2}$$

the controllability Grammian is the matrix

$$\boldsymbol{W}_c\left(t_f\right) = \int_0^{t_f} \boldsymbol{\Phi}\left(\tau\right)\boldsymbol{B}\left(\tau\right)\boldsymbol{B}\left(\tau\right)^T\boldsymbol{\Phi}^T\left(\tau\right)d\tau \tag{3.3}$$

where $\boldsymbol{\Phi}\left(\tau\right)$ is the state transition matrix [*Skogestad and Postlethwaite* (2005)]. If the matrices $\boldsymbol{A}$ and $\boldsymbol{B}$ are time-invariant, then $\boldsymbol{W}_c\left(t_f\right)$ is given by

$$\boldsymbol{W}_c\left(t_f\right) = \int_0^{t_f} e^{\boldsymbol{A}\tau}\boldsymbol{B}\boldsymbol{B}^T e^{\boldsymbol{A}^T\tau}d\tau \tag{3.4}$$

In the case where the final time $t_f \to \infty$, the steady-state controllability Grammian, $\boldsymbol{W}_c^{\infty}$, can also be found by solving the Lyapunov equation

$$\boldsymbol{A}\boldsymbol{W}_c^{\infty} + \boldsymbol{W}_c^{\infty}\boldsymbol{A}^T = -\boldsymbol{B}\boldsymbol{B}^T. \tag{3.5}$$

The controllability Grammian is often used to determine simply whether or not a system is controllable; if it is singular, the system is not controllable. However, it can also be used to determine the minimum control effort required to move a system from the origin to a final state $\boldsymbol{x}_f$ at some final time t_f. Consequently, it can provide a measure of how easy or difficult a system is to control. The minimum possible value of the control effort is given by [*Skogestad and Postlethwaite* (2005)]:

$$E^* = \boldsymbol{x}_f^T \boldsymbol{W}_c \left(t_f\right)^{-1} \boldsymbol{x}_f. \tag{3.6}$$

Note that E^* is independent of the controller and thus is a function only of $\boldsymbol{d}_a$. The control effort, E, is given by

$$E = \int_0^{t_f} \left(u\left(t\right)\right)^2 dt. \tag{3.7}$$

Since $u\left(t\right)$ is a function of both the artifact and the controller, E is a function of $\boldsymbol{d}_a$ and $\boldsymbol{d}_c$. Thus, the control effort can be related to the controllability Grammian by

$$E\left(\boldsymbol{d}_a, \boldsymbol{d}_c\right) \geq E^*\left(\boldsymbol{d}_a\right) \tag{3.8}$$

and $E^*\left(\boldsymbol{d}_a\right)$ is a *lower bounding function* for the control effort, $E\left(\boldsymbol{d}_a, \boldsymbol{d}_c\right)$ [*Papalambros and Wilde* (2000)].

It is important to note that this minimum control effort in Eq. (3.6) is independent of the control architecture; it depends only on the dynamics of the uncontrolled system, i.e., $\boldsymbol{A}$ and $\boldsymbol{B}$, the final state $\boldsymbol{x}_f$, and the final time t_f. The optimal controller performance

depends on the controllability Grammian, which is independent of the control architecture and variables. Thus, in cases where the controller objective, $f_c(\boldsymbol{d}_a, \boldsymbol{d}_c)$, or the active controller constraints, $\boldsymbol{h}_c(\boldsymbol{d}_a, \boldsymbol{d}_c)$ and $\boldsymbol{g}_c(\boldsymbol{d}_a, \boldsymbol{d}_c)$, are based on control effort, the Grammian can be used to determine coupling *a priori*. Three such situations will be presented here.

3.3 Relationships Between $\boldsymbol{\Gamma}_v$ and $\boldsymbol{W}_c$

Here, a relationship is developed between $\boldsymbol{\Gamma}_v$ and $\boldsymbol{W}_c$ for some engineering problems of interest. Consider three types of objectives representing several classical control problems. In the first case, representing the case of fixed terminal time, energy is of primary interest, and the problem is formulated to minimize control effort [*Bryson and Ho* (1975)]. In the second case, the speed of response is of importance; a constraint is placed on control effort, but the control objective is to minimize the response time. This is representative of the class of unspecified terminal time problems [*Bryson and Ho* (1975)]. In the third case, the control problem is formulated as a classical Linear Quadratic Regulator (LQR) problem, in which a weighted combination of control effort and the system state errors is minimized.

All of the cases considered here have the following characteristics:

1. The system exhibits uni-directional coupling, as in (1.9) - (1.13), and the matrices $\boldsymbol{A}$ and $\boldsymbol{B}$ may be functions of the artifact design variables $\boldsymbol{d}_a$.

2. The objective function for the optimization is a weighted sum of the two individual objectives, where the weights w_a and w_c are strictly positive.

3. The system can be modeled in state-space form as linear and time-invariant.

4. The artifact objective function, $f_a(\boldsymbol{d}_a)$, and constraints, $\boldsymbol{h}_a(\boldsymbol{d}_a)$ and $\boldsymbol{g}_a(\boldsymbol{d}_a)$, are arbitrary functions of $\boldsymbol{d}_a$.

3.3.1 Case I: Control Effort as Objective

In Case I, the primary concern in controller design is energy. The system is to be moved from the origin to a state $\boldsymbol{x}_f$ at time t_f, where t_f is a parameter. In the most general case, the final state $\boldsymbol{x}_f$ may be a function of $\boldsymbol{d}_a$. The control objective function to accomplish this is selected as the control effort required to move the system from the origin to a state $\boldsymbol{x}_f$ at some specified time t_f.

$$f_c = \int_0^{t_f} u(t)^2 dt \tag{3.9}$$

Using (3.6) and (3.9), the controller objective function f_c will satisfy the relation

$$f_c \geq \boldsymbol{x}_f^T \boldsymbol{W}_c \left(t_f\right)^{-1} \boldsymbol{x}_f \tag{3.10}$$

where the equality applies if an optimal controller that minimizes control effort is chosen. The coupling vector is computed from (1.14) as follows:

$$\boldsymbol{\Gamma}_v = \frac{w_c}{w_a} \frac{\partial}{\partial \boldsymbol{d}_a} \left(\boldsymbol{x}_f^T \boldsymbol{W}_c \left(t_f\right)^{-1} \boldsymbol{x}_f \right) \tag{3.11}$$

$$\boldsymbol{\Gamma}_v = \frac{w_c}{w_a} \begin{bmatrix} \boldsymbol{x}_f^T \dfrac{\partial \boldsymbol{W}_c \left(t_f\right)^{-1}}{\partial d_{a_1}} \boldsymbol{x}_f + 2\boldsymbol{x}_f^T \boldsymbol{W}_c \left(t_f\right)^{-1} \dfrac{\partial \boldsymbol{x}_f}{\partial d_{a_1}} \\ \boldsymbol{x}_f^T \dfrac{\partial \boldsymbol{W}_c \left(t_f\right)^{-1}}{\partial d_{a_2}} \boldsymbol{x}_f + 2\boldsymbol{x}_f^T \boldsymbol{W}_c \left(t_f\right)^{-1} \dfrac{\partial \boldsymbol{x}_f}{\partial d_{a_2}} \\ \vdots \\ \boldsymbol{x}_f^T \dfrac{\partial \boldsymbol{W}_c \left(t_f\right)^{-1}}{\partial d_{a_n}} \boldsymbol{x}_f + 2\boldsymbol{x}_f^T \boldsymbol{W}_c \left(t_f\right)^{-1} \dfrac{\partial \boldsymbol{x}_f}{\partial d_{a_n}} \end{bmatrix}^T \tag{3.12}$$

where $\boldsymbol{d}_a$ is indexed as $i = 1, \ldots, n$ and n is the number of artifact design variables. Given a particular system, then, it is possible to express the coupling in terms of the artifact design variables $\boldsymbol{d}_a$, constants, and parameters in the problem. Given the known values of constants and parameters, and the range of allowable values for $\boldsymbol{d}_a$, it is possible to

determine whether coupling will exist, and whether it will be weak or strong. If the i^{th} term in the coupling vector vanishes, then it is known that the i^{th} artifact design variable will not participate in the coupling. If all terms in the coupling vector vanish, then the problem is known to be uncoupled. A particular coupling term will vanish under one of two conditions:

1. The vectors $\boldsymbol{x}_f$ and $\left(2\boldsymbol{W}_c\left(t_f\right)^{-1}\dfrac{\partial \boldsymbol{x}_f}{\partial d_{a_i}}+\dfrac{\partial \boldsymbol{W}_c\left(t_f\right)^{-1}}{\partial d_{a_i}}\boldsymbol{x}_f\right)$ are orthogonal.
2. $\dfrac{\partial \boldsymbol{x}_f}{\partial d_{a_i}}=-\dfrac{1}{2}\boldsymbol{W}_c\left(t_f\right)\dfrac{\partial \boldsymbol{W}_c\left(t_f\right)^{-1}}{\partial d_{a_i}}\boldsymbol{x}_f.$

The second condition can occur when the variables $\boldsymbol{d}_a$ result in changes in the control effort that counteract the effects of the changes in $\boldsymbol{x}_f$. As an example, a change in $\boldsymbol{d}_a$ might simultaneously cause an increase in $\boldsymbol{x}_f$ and an increase in mechanical advantage. The improvement in mechanical advantage would balance the increase in the final state, resulting in constant control effort for the optimal controller.

Within the class of problems denoted here as Case I, there are two sub-classes that are of interest.

Case Ia: Final State as a Parameter: If the final state $\boldsymbol{x}_f$ is a specified parameter, then the expression given in (3.12) can be simplified to

$$\boldsymbol{\Gamma}_v=\frac{w_c}{w_a}\begin{bmatrix}\boldsymbol{x}_f^T\dfrac{\partial \boldsymbol{W}_c\left(t_f\right)^{-1}}{\partial d_{a_1}}\boldsymbol{x}_f\\ \boldsymbol{x}_f^T\dfrac{\partial \boldsymbol{W}_c\left(t_f\right)^{-1}}{\partial d_{a_2}}\boldsymbol{x}_f\\ \vdots\\ \boldsymbol{x}_f^T\dfrac{\partial \boldsymbol{W}_c\left(t_f\right)^{-1}}{\partial d_{a_n}}\boldsymbol{x}_f\end{bmatrix}^T \tag{3.13}$$

If $\boldsymbol{W}_c$ is not a function of $\boldsymbol{d}_a$, then $\dfrac{\partial \boldsymbol{W}_c\left(t_f\right)^{-1}}{\partial \boldsymbol{d}_a}=\boldsymbol{0}$ for any value of $\boldsymbol{d}_a$. In this case, each of the components in this relation will vanish. Therefore, $\boldsymbol{\Gamma}_v=\boldsymbol{0}$, and the system is uncoupled. Note, however, that while this is a sufficient condition for decoupling, it is

not necessary and sufficient. It is still possible for the system to decouple if $\frac{\partial \boldsymbol{W}_c^{-1}}{\partial \boldsymbol{d}_a} \neq \mathbf{0}$. Specific values of $\boldsymbol{x}_f$ may cause particular terms to drop out of the final result, or the vector $\frac{\partial \boldsymbol{W}_c^{-1}}{\partial \boldsymbol{d}_a}\boldsymbol{x}_f$ may be orthogonal to $\boldsymbol{x}_f$.

Case Ib: Constant Controllability Grammian: Assume that the controllability Grammian $\boldsymbol{W}_c$ is not dependent on $\boldsymbol{d}_a$. This may occur when the variables $\boldsymbol{d}_a$ represent conversions from one form of energy to another, which will not change the total effort required to control the system. Then, the coupling vector $\boldsymbol{\Gamma}_v$ can be expressed as

$$\boldsymbol{\Gamma}_v = \frac{w_c}{w_a} \begin{bmatrix} 2\boldsymbol{x}_f^T \boldsymbol{W}_c\left(t_f\right)^{-1} \dfrac{\partial \boldsymbol{x}_f}{\partial d_{a_1}} \\ 2\boldsymbol{x}_f^T \boldsymbol{W}_c\left(t_f\right)^{-1} \dfrac{\partial \boldsymbol{x}_f}{\partial d_{a_2}} \\ \vdots \\ 2\boldsymbol{x}_f^T \boldsymbol{W}_c\left(t_f\right)^{-1} \dfrac{\partial \boldsymbol{x}_f}{\partial d_{a_n}} \end{bmatrix}^T \tag{3.14}$$

In this case, a term in the coupling vector will vanish in either of two conditions. The first condition, $\frac{\partial \boldsymbol{x}_f}{\partial d_{a_i}} = 0$, represents the case where neither $\boldsymbol{x}_f$ nor $\boldsymbol{W}_c\left(t_f\right)$ is a function of $\boldsymbol{d}_a$, and thus E^* is independent of $\boldsymbol{d}_a$. In the second condition, the vectors $\frac{\partial \boldsymbol{x}_f}{\partial d_{a_i}}$ and $\boldsymbol{W}_c\left(t_f\right)^{-1}\boldsymbol{x}_f$ are orthogonal.

Positioning Gantry Example: For the positioning gantry described in Chapter II, the following objectives and constraints are selected:

$$\min_{k_t, r} \quad f_a = -Z_f\left(k_t, r\right) \tag{3.15}$$

$$\text{subject to simple bounds} \quad 2.5 \leq r \leq 7.5 \tag{3.16}$$

$$5 \leq k_t \leq 20 \tag{3.17}$$

where the final displacement Z_f represents the peak displacement, with a 10% overshoot over the steady-state displacement, Z_{ss}. The equation for the steady-state displacement, Z_{ss},

is derived in Chapter II. Thus,

$$Z_f = 1.1 Z_{ss} = \frac{1.1 u_{ss} k_t}{r R_a k_s} \tag{3.18}$$

The final state, $\boldsymbol{x}_f$, is therefore given by

$$\boldsymbol{x}_f = \begin{bmatrix} Z_f \\ 0 \end{bmatrix}. \tag{3.19}$$

It is desired to minimize the control effort required to move the system to this position at a specified time, $t_f = 0.5s$, and thus the controller objective is

$$\min_{K_1,K_2,G} f_c = \int_0^{t_f} \left(u\left(t\right)\right)^2 dt. \tag{3.20}$$

This optimization problem fits the description for a Case I problem. The controllability Grammian $\boldsymbol{W}_c\left(t_f\right)$ of this system is given by

$$\boldsymbol{W}_c\left(t_f\right) = \begin{bmatrix} W_{c_{11}}\left(t_f\right) & W_{c_{12}}\left(t_f\right) \\ W_{c_{21}}\left(t_f\right) & W_{c_{22}}\left(t_f\right) \end{bmatrix} \tag{3.21}$$

where the individual terms are as follows:

$$\begin{aligned} W_{c_{11}}\left(t_f\right) =& \frac{1}{2bk} - \frac{2me^{-\frac{b}{m}t_f}}{b\left(4mk-b^2\right)} + \frac{e^{-\frac{b}{m}t_f}}{2k\sqrt{4mk-b^2}} \sin\left(\sqrt{4mk-b^2}\frac{t_f}{m}\right) \\ &+ \frac{e^{-\frac{b}{m}t_f}}{2k\left(4mk-b^2\right)} \cos\left(\sqrt{4mk-b^2}\frac{t_f}{m}\right) \end{aligned} \tag{3.22}$$

$$W_{c_{12}}\left(t_f\right) = \frac{e^{-\frac{b}{m}t_f}}{4mk-b^2}\left(1-\cos\left(\sqrt{4mk-b^2}\frac{t_f}{m}\right)\right) \tag{3.23}$$

$$W_{c_{21}}\left(t_f\right) = \frac{e^{-\frac{b}{m}t_f}}{4mk-b^2}\left(1-\cos\left(\sqrt{4mk-b^2}\frac{t_f}{m}\right)\right) \tag{3.24}$$

$$\begin{aligned} W_{c_{22}}\left(t_f\right) =& \frac{1}{2bm} - \frac{4ke^{-\frac{b}{m}t_f}}{b\left(4mk-b^2\right)} + \frac{e^{-\frac{b}{m}t_f}}{m\left(4mk-b^2\right)^{3/2}}\sin\left(\frac{t_f}{m}\sqrt{4mk-b^2}\right) \\ & - \frac{be^{-\frac{b}{m}t_f}}{m\left(4mk-b^2\right)}\cos\left(\frac{t_f}{m}\sqrt{4mk-b^2}\right) \end{aligned} \tag{3.25}$$

Expressions for m, b, and k are given by Eqs. (2.19) - (2.21). Using these expressions, it can be shown that $\boldsymbol{W}_c\left(t_f\right)$ is a function of r and k_t, as is $\boldsymbol{x}_f$. Taking derivatives of both $\boldsymbol{x}_f$ and $\boldsymbol{W}_c\left(t_f\right)$ with respect to $\boldsymbol{d}_a$, it can be shown that there are no feasible values of r and k_t for which $\boldsymbol{\Gamma}_v = \boldsymbol{0}$. Therefore, it is concluded that the problem will be coupled, and an appropriate solution method for a coupled problem should be chosen. When the simultaneous co-design problem is solved, it is indeed seen to be coupled, with the expected tradeoff between the objectives shown in Fig. 3.1.

3.3.2 Case II: Time as Objective

In Case II problems, the primary concern is the speed with which the system responds; or, alternatively, the final time at which the system reaches the state $\boldsymbol{x}_f$ is to be minimized. Control effort is constrained to be less than some maximum value, E_{max}, where E_{max} is a parameter. The controller objective function and constraint are as follows:

$$\min_{\boldsymbol{d}_a,\boldsymbol{d}_c} \quad f_c = t_f \tag{3.26}$$

$$\text{subject to} \quad \boldsymbol{g}_c\left(\boldsymbol{d}_a,\boldsymbol{d}_c\right) = \int_0^{t_f} u(t)^2 dt - E_{max} \leq 0 \tag{3.27}$$

It can be assumed that the constraint will be active, since a linear system could have an arbitrarily small response time if infinite control effort were available. Assuming that the

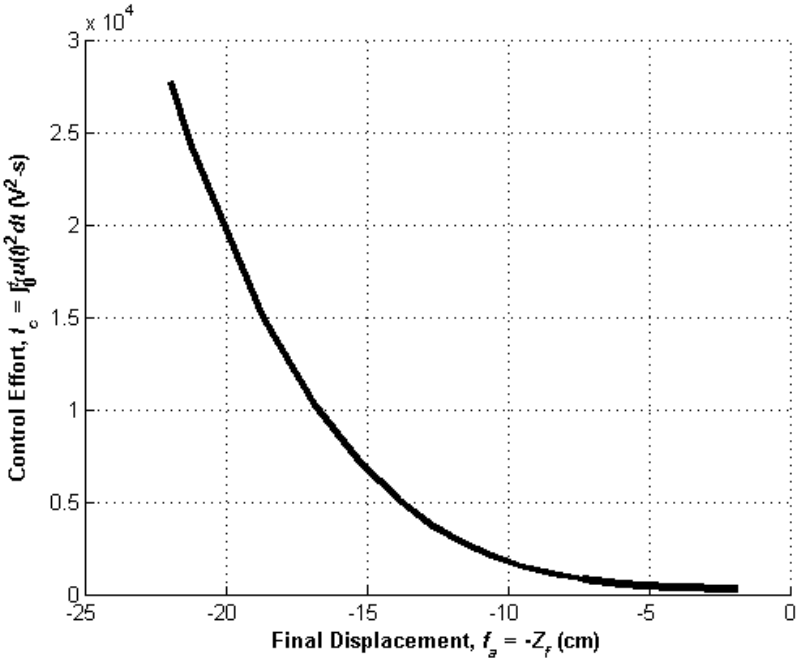

Figure 3.1: Pareto Frontier for Positioning Gantry Example of Case I

constraint is active and that an optimal controller is chosen,

$$\boldsymbol{x}_f^T \boldsymbol{W}_c \left(t_f\right)^{-1} \boldsymbol{x}_f = E_{max}. \tag{3.28}$$

Taking derivatives of (3.28) and solving for $\dfrac{\partial t_f}{\partial d_{a_i}}$,

$$\frac{\partial t_f}{\partial d_{a_i}} = -\frac{2\boldsymbol{x}_f^T \boldsymbol{W}_c \left(t_f\right)^{-1} \dfrac{\partial \boldsymbol{x}_f}{\partial d_{a_i}} + \boldsymbol{x}_f^T \dfrac{\partial \boldsymbol{W}_c \left(t_f\right)^{-1}}{\partial d_{a_i}} \boldsymbol{x}_f}{2\boldsymbol{x}_f^T \boldsymbol{W}_c \left(t_f\right)^{-1} \dfrac{\partial \boldsymbol{x}_f}{\partial t_f} + \boldsymbol{x}_f^T \dfrac{\partial \boldsymbol{W}_c \left(t_f\right)^{-1}}{\partial t_f} \boldsymbol{x}_f} \tag{3.29}$$

the coupling can be expressed as

$$\boldsymbol{\Gamma}_v = -\frac{w_c}{w_a T}\begin{bmatrix} 2\boldsymbol{x}_f^T \boldsymbol{W}_c\left(t_f\right)^{-1}\dfrac{\partial \boldsymbol{x}_f}{\partial d_{a_1}} + \boldsymbol{x}_f^T \dfrac{\partial \boldsymbol{W}_c\left(t_f\right)^{-1}}{\partial d_{a_1}}\boldsymbol{x}_f \\ 2\boldsymbol{x}_f^T \boldsymbol{W}_c\left(t_f\right)^{-1}\dfrac{\partial \boldsymbol{x}_f}{\partial d_{a_2}} + \boldsymbol{x}_f^T \dfrac{\partial \boldsymbol{W}_c\left(t_f\right)^{-1}}{\partial d_{a_2}}\boldsymbol{x}_f \\ \vdots \\ 2\boldsymbol{x}_f^T \boldsymbol{W}_c\left(t_f\right)^{-1}\dfrac{\partial \boldsymbol{x}_f}{\partial d_{a_n}} + \boldsymbol{x}_f^T \dfrac{\partial \boldsymbol{W}_c\left(t_f\right)^{-1}}{\partial d_{a_n}}\boldsymbol{x}_f \end{bmatrix}^T \tag{3.30}$$

where $T = 2\boldsymbol{x}_f^T \boldsymbol{W}_c\left(t_f\right)^{-1}\dfrac{\partial \boldsymbol{x}_f}{\partial t_f} + \boldsymbol{x}_f^T \dfrac{\partial \boldsymbol{W}_c\left(t_f\right)^{-1}}{\partial t_f}\boldsymbol{x}_f$.

Note that the coupling vector is parallel to that seen for Case I, and the conditions for decoupling in this problem are mathematically identical. This indicates that the physical conditions under which the problems decouple are also the same. As in Case I, therefore, one situation which would result in decoupling is that in which changes in $\boldsymbol{d}_a$ produce both a greater displacement $\boldsymbol{x}_f$ of the system and a more efficient use of the available control effort. Within this class of problems, there are two sub-classes of interest, similar to those discussed for Case I.

Case IIa: Final State as a Parameter: If the final state $\boldsymbol{x}_f$ is a parameter, then the coupling simplifies to

$$\boldsymbol{\Gamma}_v = -\frac{w_c}{w_a\left(\boldsymbol{x}_f^T \dfrac{\partial \boldsymbol{W}_c\left(t_f\right)^{-1}}{\partial t_f}\boldsymbol{x}_f\right)}\begin{bmatrix} \boldsymbol{x}_f^T \dfrac{\partial \boldsymbol{W}_c\left(t_f\right)^{-1}}{\partial d_{a_1}}\boldsymbol{x}_f \\ \boldsymbol{x}_f^T \dfrac{\partial \boldsymbol{W}_c\left(t_f\right)^{-1}}{\partial d_{a_2}}\boldsymbol{x}_f \\ \vdots \\ \boldsymbol{x}_f^T \dfrac{\partial \boldsymbol{W}_c\left(t_f\right)^{-1}}{\partial d_{a_n}}\boldsymbol{x}_f \end{bmatrix}^T \tag{3.31}$$

and the coupling vector is parallel to that seen in Case Ia, with identical conditions for decoupling.

Constant Controllability Grammian: Assume that the controllability Grammian matrix

$\boldsymbol{W}_c\left(t_f\right)$ is not dependent on $\boldsymbol{d}_a$. As in Case I, this can happen when $\boldsymbol{d}_a$ represents the conversion of energy with no loss. Then, the coupling vector $\boldsymbol{\Gamma}_v$ can be expressed as

$$\boldsymbol{\Gamma}_v = -\frac{w_c}{w_a\left(\boldsymbol{x}_f^T\boldsymbol{W}_c\left(t_f\right)^{-1}\dfrac{\partial \boldsymbol{x}_f}{\partial t_f}\right)}\begin{bmatrix} \boldsymbol{x}_f^T\boldsymbol{W}_c\left(t_f\right)^{-1}\dfrac{\partial \boldsymbol{x}_f}{\partial d_{a_1}} \\ \boldsymbol{x}_f^T\boldsymbol{W}_c\left(t_f\right)^{-1}\dfrac{\partial \boldsymbol{x}_f}{\partial d_{a_2}} \\ \vdots \\ \boldsymbol{x}_f^T\boldsymbol{W}_c\left(t_f\right)^{-1}\dfrac{\partial \boldsymbol{x}_f}{\partial d_{a_n}} \end{bmatrix}^T \tag{3.32}$$

and, in this case, the coupling vector is parallel to that seen in Case Ib, with identical conditions for decoupling.

Positioning Gantry Example: Assume, in this case, that the artifact design objective and constraints are as given in Eqs. (3.15) - (3.17). The controller design objective and constraints are as follows:

$$\min_{K_1,K_2,G} f_c = t_f \tag{3.33}$$

subject to

$$g_1\left(K_1,K_2,G\right) = \int_0^{t_f}\left(u\left(t\right)\right)^2 dt - E_{max} \leq 0 \tag{3.34}$$

Monotonicity analysis indicates that the constraint g_1 will be active, and therefore this problem meets the conditions established for Case II. The controllability Grammian is given by Eqs. (3.21)-(3.25). In this case, the coupling is again non-zero for every allowed value of r and k_t. When the problem is solved, the anticipated tradeoff between f_a and f_c is evident, as shown in Fig. 3.2.

3.3.3 Case III: Linear Quadratic Regulator (LQR)

The infinite-time LQR problem is designed to find the optimal control signal $\boldsymbol{u}\left(t\right)$ to transition a system from an initial state $\boldsymbol{x}_0 = \boldsymbol{x}\left(0\right)$ to the zero state. The optimal control

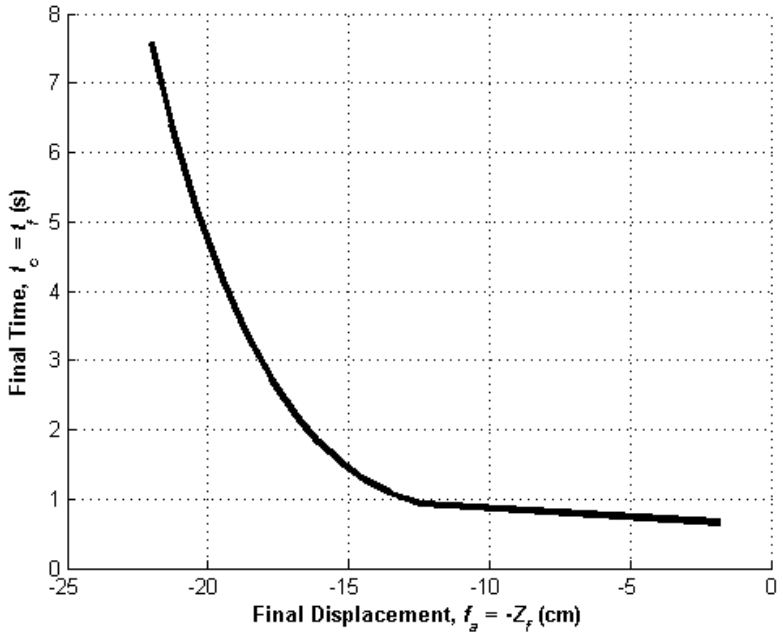

Figure 3.2: Pareto Frontier for Positioning Gantry Example of Case II

signal is defined as the one which minimizes the cost function

$$J = \int_0^\infty \left(\boldsymbol{x}(t)^T \boldsymbol{Q} \boldsymbol{x}(t) + \boldsymbol{u}(t)^T \boldsymbol{R} \boldsymbol{u}(t) \right) dt. \tag{3.35}$$

It is well-established that the optimal solution is [*Skogestad and Postlethwaite* (2005)]:

$$\boldsymbol{u}(t) = -\boldsymbol{K} \boldsymbol{x}(t) \tag{3.36}$$

$$\boldsymbol{K} = \boldsymbol{R}^{-1} \boldsymbol{B}^T \boldsymbol{X} \tag{3.37}$$

with the precompensator G, shown in Fig. 2.3, vanishing due to the reference state being defined as the zero state. The matrix $\boldsymbol{X}$ is the positive semi-definite solution of the algebraic Riccati equation

$$\boldsymbol{A}^T \boldsymbol{X} + \boldsymbol{X} \boldsymbol{A} - \boldsymbol{X} \boldsymbol{B} \boldsymbol{R}^{-1} \boldsymbol{B}^T \boldsymbol{X} + \boldsymbol{Q} = 0 \tag{3.38}$$

and the optimal value of J is given by the equation

$$J^* = \boldsymbol{x}_0^T \boldsymbol{X} \boldsymbol{x}_0. \tag{3.39}$$

If the system is controllable, then it has also been proven that there exists a reduced equivalent transformation of the system, and the symmetric matrix $\boldsymbol{X}$ satisfies the Lyapunov equation [*Ionescu et al.* (1999)]:

$$\boldsymbol{A}^T \boldsymbol{X} + \boldsymbol{X} \boldsymbol{A} + \boldsymbol{Q} = \boldsymbol{0} \tag{3.40}$$

In the most general case, where $\boldsymbol{Q}$ can be selected as any positive semidefinite matrix, there is no explicit relation between J^* and $\boldsymbol{W}_c^\infty$, and thus no explicit relation between $\boldsymbol{\Gamma}_v$ and $\boldsymbol{W}_c^\infty$. However, if the matrix $\boldsymbol{Q}$ is selected as

$$\boldsymbol{Q} = \gamma \boldsymbol{B} \boldsymbol{B}^T, \tag{3.41}$$

as is common in loop-transfer recovery design [*Skogestad and Postlethwaite* (2005)], then by comparing Eq. (3.5) and (3.40), it can be shown that the matrix $\boldsymbol{X}$ can be expressed in terms of the controllability Grammian as [*Skogestad and Postlethwaite* (2005)]:

$$\boldsymbol{X} = \gamma \boldsymbol{A}^{-T} \boldsymbol{A} \boldsymbol{W}_c^\infty \tag{3.42}$$

and, therefore, the optimal performance is

$$J^* = \gamma \boldsymbol{x}_0^T \boldsymbol{A}^{-T} \boldsymbol{A} \boldsymbol{W}_c^\infty \boldsymbol{x}_0. \tag{3.43}$$

This allows the coupling to be derived as

$$\boldsymbol{\Gamma}_v = \gamma \frac{w_c}{w_a} \begin{bmatrix} \dfrac{\partial \left(\boldsymbol{x}_0^T \boldsymbol{A}^{-T} \boldsymbol{A} \boldsymbol{W}_c^{\infty} \boldsymbol{x}_0 \right)}{\partial d_{a_1}} \\ \dfrac{\partial \left(\boldsymbol{x}_0^T \boldsymbol{A}^{-T} \boldsymbol{A} \boldsymbol{W}_c^{\infty} \boldsymbol{x}_0 \right)}{\partial d_{a_2}} \\ \vdots \\ \dfrac{\partial \left(\boldsymbol{x}_0^T \boldsymbol{A}^{-T} \boldsymbol{A} \boldsymbol{W}_c^{\infty} \boldsymbol{x}_0 \right)}{\partial d_{a_n}} \end{bmatrix}^T \tag{3.44}$$

This expression for $\boldsymbol{\Gamma}_v$ is, again, a function only of the artifact design variables. It is important to note that this expression is only valid for the specific form of $\boldsymbol{Q}$ given by Eq. (3.41). For other forms of $\boldsymbol{Q}$, Eq. (3.42) is not valid. It is conjectured that more complex relations between $\boldsymbol{X}$ and $\boldsymbol{W}_c^{\infty}$ may be found for some other forms of $\boldsymbol{Q}$, and thus other relationships between coupling and controllability may hold for other cases of the LQR problem.

While Eq. (3.44) is a complex expression, in general, depending on the problem in question, it can simplify under certain circumstances. One particular situation is detailed below, in which it takes on a considerably simpler form.

Case IIIa: State $\boldsymbol{x}_0$ as a parameter and $\boldsymbol{A}$ independent of $\boldsymbol{d}_a$: If the forced response of a system is a function of $\boldsymbol{d}_a$ but the free response is not, then the $\boldsymbol{B}$ matrix will be a function of $\boldsymbol{d}_a$ but $\boldsymbol{A}$ will be independent of $\boldsymbol{d}_a$. If, in addition, the state $\boldsymbol{x}_0$ is a parameter, the coupling relation is given by

$$\boldsymbol{\Gamma}_v = \gamma \frac{w_c}{w_a} \begin{bmatrix} \boldsymbol{x}_0^T \boldsymbol{A}^{-T} \boldsymbol{A} \dfrac{\partial \boldsymbol{W}_c^{\infty}}{\partial d_{a_1}} \boldsymbol{x}_0 \\ \boldsymbol{x}_0^T \boldsymbol{A}^{-T} \boldsymbol{A} \dfrac{\partial \boldsymbol{W}_c^{\infty}}{\partial d_{a_2}} \boldsymbol{x}_0 \\ \vdots \\ \boldsymbol{x}_0^T \boldsymbol{A}^{-T} \boldsymbol{A} \dfrac{\partial \boldsymbol{W}_c^{\infty}}{\partial d_{a_n}} \boldsymbol{x}_0 \end{bmatrix}^T \tag{3.45}$$

Note that, in this case, there are several conditions in which decoupling will occur.

1. For all artifact design variables $\boldsymbol{d}_a$, the derivative $\dfrac{\partial \boldsymbol{W}_c^{\infty}}{\partial d_{a_i}} = \boldsymbol{0}$.

2. The matrix product $\boldsymbol{A}^{-T}\boldsymbol{A}\dfrac{\partial \boldsymbol{W}_c^{\infty}}{\partial d_{a_i}} = \boldsymbol{0}$ for all artifact design variables $\boldsymbol{d}_a$.

3. The vectors $\boldsymbol{x}_0$ and $\left(\boldsymbol{A}^{-T}\boldsymbol{A}\dfrac{\partial \boldsymbol{W}_c^{\infty}}{\partial d_{a_i}}\boldsymbol{x}_0\right)$ are orthogonal for all artifact design variables $\boldsymbol{d}_a$.

Positioning Gantry Example: Consider, again, the positioning gantry system shown in Chapter II. In this case, the artifact objective function is assumed to be the system's total weight. The weight depends on a number of system parameters, which shall be grouped into three constants for simplicity. The artifact objective then takes the form of

$$\min_{r,k_t} f_a = c_1 + c_2 k_t^{1.5} + c_3 r^2 \tag{3.46}$$

where $c_1 = 10$, $c_2 = 5$, and $c_3 = 0.1$, subject to the bounds given in Eqs. (3.16) - (3.17). Note that the pulley was assumed, in Section 2.3, to possess negligible rotational inertia; however, it is not assumed to be massless, and thus it appears in the calculation of system weight. The controller optimization problem is formulated as an LQR problem with controller objective $f_c = J$, where J is given by Eq. (3.35) with $\boldsymbol{x}_0 = \begin{bmatrix} 3.5 \\ 0 \end{bmatrix}$, $R = 1$, and $\boldsymbol{Q} = \begin{bmatrix} 0 & 0 \\ 0 & 1 \end{bmatrix}$. It can be shown that this choice of weighting matrix $\boldsymbol{Q}$ satisfies Eq. (3.41), with $\gamma = m^2$. Using Eq. (3.44), the coupling can be computed for this problem. In this case, the coupling can be shown to vanish for all values of r and k_t, indicating that the problem is uncoupled and that J^* is independent of these variables. Note that this is not a result that could be easily seen, though it can be explained physically; the variable r, the pulley diameter, represents a conversion of energy without loss, and the variable k_t, the motor torque constant, represents a tradeoff between the motor's speed and torque, which entails no loss of energy. When the co-design problem is solved for the values of parameters given

Table 3.1: Parameters for Optimization of Gantry Using LQR Control

Parameter	Value
R_a	2.0 kΩ
M	2.0 kg
k_s	2.0 N/mm
V_{ss}	10 V

Table 3.2: Results of Optimization of Gantry Using LQR Control

Quantity	Value
r	2.5 cm
k_t	5.0 N-m/A
K_1	-0.368
K_2	-7.696
G	0.132
f_a^*	66.53
f_c^*	5.78

in Table 3.1, no tradeoff is seen. For all values of w_a and w_c, the variables and objectives are found to have the values shown in Table 3.2.

3.4 Physical Demonstration: Positioning Gantry

The positioning gantry system described in Chapter II, and used to illustrate the concepts in this chapter and in Chapter II, was built and used for an experimental demonstration. The demonstration was designed to show that it is possible to predict, *a priori*, whether a problem will be coupled. In this section, the apparatus used for the demonstration will be described. The intention of the demonstration will be described, and results will be shown.

3.4.1 Description of Apparatus

The apparatus for the physical demonstration was constructed using a Quanser Engineering Trainer DC Motor Control Trainer (QET-DCMCT), as shown in Fig. 3.3. The

QET-DCMCT unit consists of a motor, encoder, associated electrical components, and software (item 1). A plate, item 2, was mounted to the QET-DCMCT unit. A linear rail, item 3 was mounted to the plate, and an angle bracket, item 4, was mounted to the block that mates with the rail. A spring, item 5, was attached at one end to item 4 and at the other end to a fixed bracket, item 6. A synchronous belt, item 8, was clamped to item 6 and driven by a pulley, item 7, which was mounted to the QET-DCMCT motor.

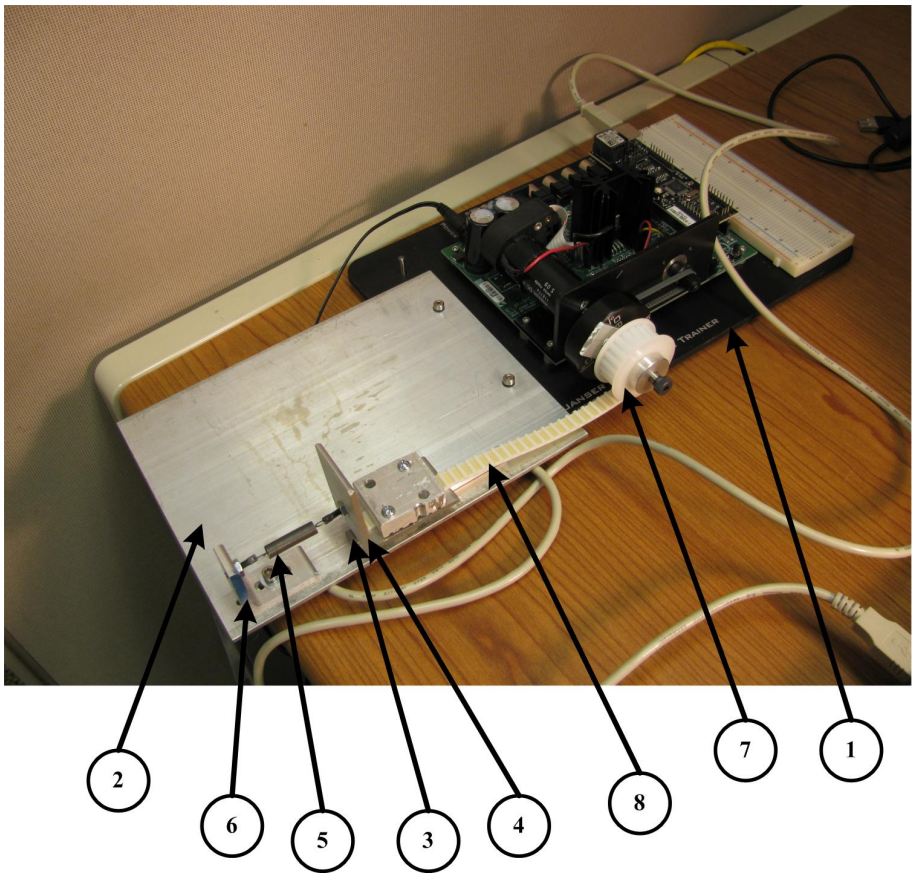

Figure 3.3: Apparatus for Physical Demonstration of Gantry Example (Item 1: QET motor assembly, Item 2: mounting plate, Item 3: linear rail, Item 4: angle bracket, Item 5: extension spring, Item 6: fixed mounting bracket, Item 7: pulley)

The spring corresponds to the spring with constant k_s shown in Fig. 2.2. The bracket and linear block correspond to the mass, M. The timing pulley corresponds to the pulley of radius r, and the QET-DCMCT unit corresponds to the motor with armature resistance R_a and torque constant k_t. It was assumed that the inertia of the pulley is negligible, and that

the friction between the block and rail is negligible.

The system was run by means of the supplied QET-DCMCT software. This software allows the user to specify the gains integral gain k_i, derivative gain k_d, and proportional gain k_p, as shown in Fig. 3.4. This controller is different from the controller shown in Fig. 2.3. The QET-DCMCT controller has integral control instead of a precompensator. The gain k_p is equivalent to the gain K_1, and k_d is equivalent to K_2. However, the controllability Grammian is still capable of predicting whether or not the system will be coupled, since it is independent of the control architecture.

3.4.2 Demonstration Procedure

This system corresponds to the positioning gantry shown in Fig. 2.2. As discussed in Sections 2.3.2 and 3.3, the co-design of this system will be a coupled problem for certain choices of artifact design variables. In particular, the spring constant, k_s, shall be studied for this demonstration. An optimization problem of the type described as Case I is formulated. It can be shown from Eq. (3.12) that this problem will be coupled. The results of this demonstration confirm this result.

The spring strength was varied by operating the system once with a single spring with $k_s = 0.81$ lbs/in, and a second time with two springs in series, as shown in Fig. 3.5. This has the effect of decreasing the spring constant by a factor of 2, to $k_s = 0.40$ lbs/in. The position command to the controller was a step input with a fixed terminal time for the system. The terminal time, t_f, was held constant at $t_f = 2.5$ sec.

The control objective function f_c, was the control effort, which was to be minimized. The final position of the system, Z_f, was a parameter with the value of $Z_f = 0.3$ in. The control objective, then, can be expressed as

$$\min_{k_p,k_d,k_i} f_c = E = \int_0^{t_f} (V(t))^2 \, dt \tag{3.47}$$

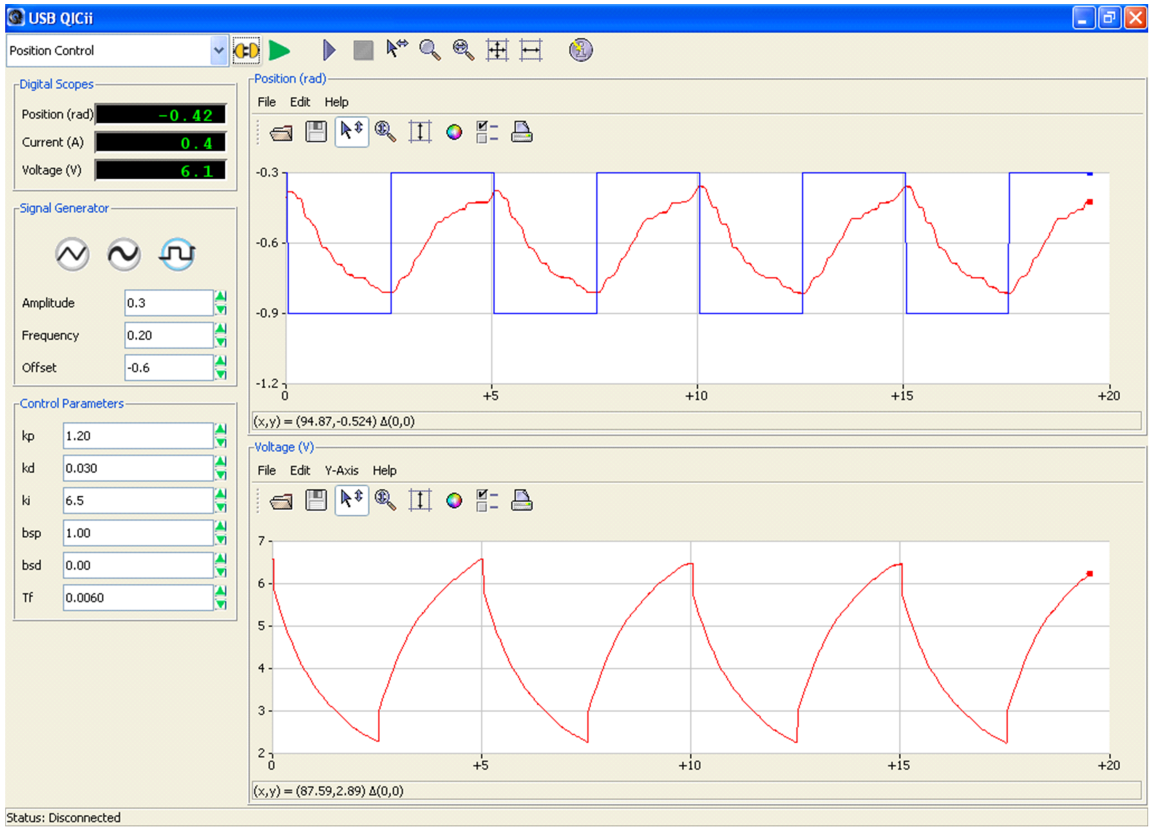

Figure 3.4: Control Screen for QET-DCMCT Software

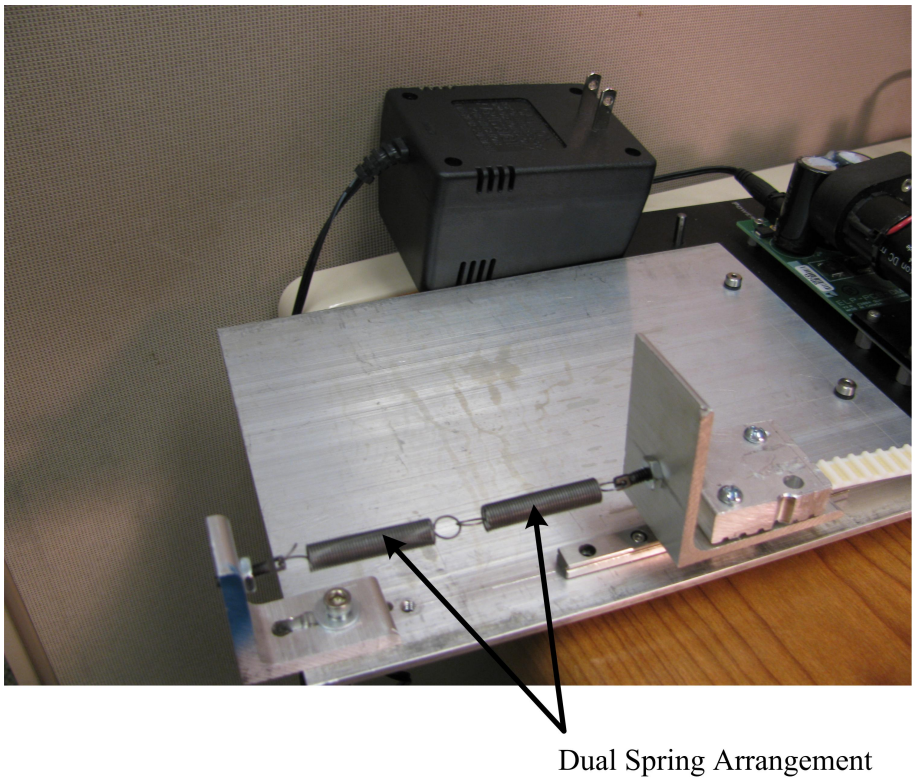

Figure 3.5: Apparatus with Modified Spring Configuration

where E is the control effort required to move the system to the desired final position.

If the system is uncoupled, then tuning the controller to different values of k_p, k_i, and k_d would yield the same minimum value of f_c for both spring configurations. If the system is coupled, however, then this will not be possible. When k_s is changed, then the minimum value of f_c would not be the same, regardless of how the gains were tuned. Since the controllability Grammian is a function of the spring constant k_s, it is expected that this system will exhibit coupling when the spring constant k_s is selected as a design variable.

3.4.3 Results of Demonstration

First, the system was operated with a single spring and the gains were manually tuned to be $k_p = 2.50$, $k_d = 0.060$, and $k_i = 9.0$. The control effort required was computed numerically and was found to be $E = 6.63\ \mathrm{V}^2 - \mathrm{s}$. Next, the system was operated with two

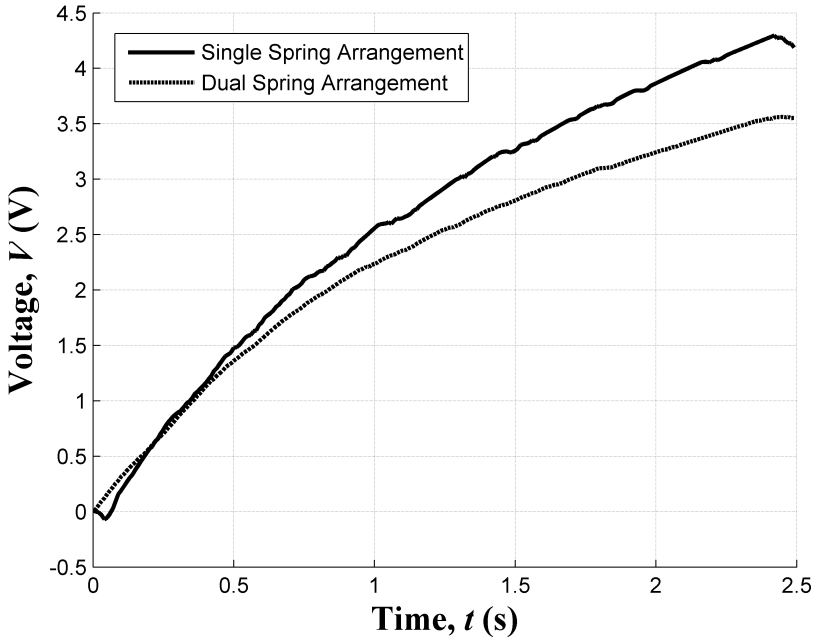

Figure 3.6: Voltage for Single and Dual Spring Configurations

springs, and the gains were tuned to minimize the control effort. The resulting gains were found to be $k_p = 1.20$, $k_d = 0.030$, and $k_i = 6.5$. The control effort required was computed numerically and was found to be $E = 5.74\ \mathrm{V}^2 - \mathrm{s}$. The voltage and position graphs for both configurations are given in Fig. 3.6 and 3.7, respectively.

Since the gains were tuned manually, no guarantee of optimality can be given. However, it can be seen from Fig. 3.7 that the position responses are very similar for both spring configurations, and thus the voltage required for each case can be compared on an equal basis. The control effort is the area under the curve; from Fig. 3.6, it can be seen that this area will be larger for the single spring configuration than for the dual spring configuration. Therefore, the control objective function, f_c, is a function of the spring constant, k_s. Thus, coupling is present, as predicted based on Eq. (3.12). It can thus be seen that the relationships presented between coupling and controllability are an effective tool in the analysis of a co-design problem prior to optimization.

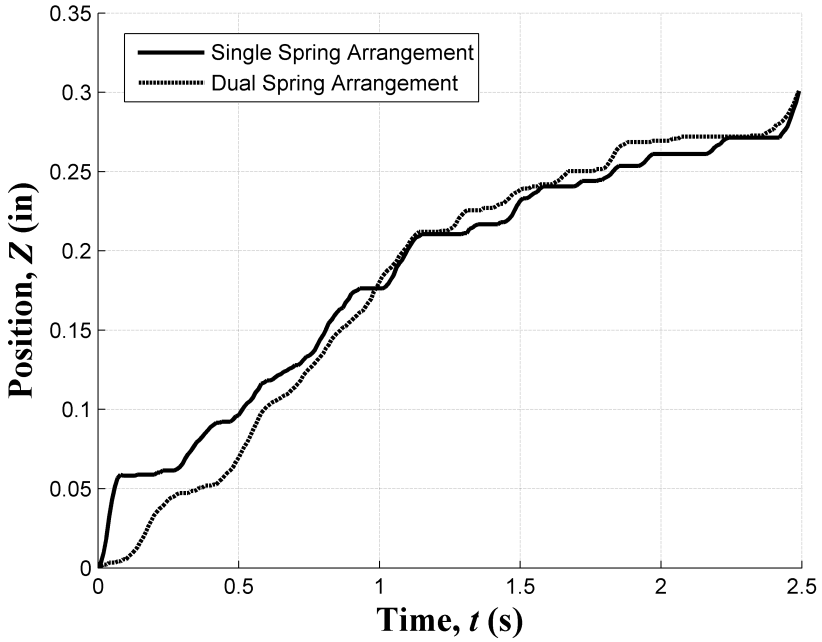

Figure 3.7: Position Response for Single and Dual Spring Configurations

3.5 Summary

As shown in this chapter, it is often possible to determine *a priori* whether or not a co-design problem exhibits coupling. If the control objective, $f_c(\boldsymbol{d}_a, \boldsymbol{d}_c)$, or the active controller constraints, $\boldsymbol{h}_c(\boldsymbol{d}_a, \boldsymbol{d}_c)$ or $\boldsymbol{g}_c(\boldsymbol{d}_a, \boldsymbol{d}_c)$, depend on control effort, then that objective or constraint can be related to the controllability Grammian matrix. This allows the coupling to be determined, without solving the co-design problem or even specifying the controller architecture, due to the relationship between the controllability Grammian and the optimal control performance. Three specific classical optimal control problem formulations were presented here; it is anticipated that other problem formulations can be found in which coupling can be similarly related to controllability. The experiment conducted on the gantry example showed that these relationships can be used to predict whether or not a co-design problem will be coupled.

If the problem is uncoupled, then a sequential strategy can be used and will find the

system optimal solution. If the problem is coupled, then an appropriate solution strategy can be chosen. A variety of solution strategies for coupled problems have been proposed, as discussed in Chapter I. A new strategy for co-design problems with uni-directional coupling will be proposed in the following chapter, utilizing the concept of a Control Proxy Function. The relations between coupling and controllability developed in this chapter will also be useful in the development of the Control Proxy Functions that will be proposed for solving the co-design problem.

CHAPTER IV

Design for Ease of Control Using Control Proxy Functions

4.1 Introduction

In Chapter III, the issue of identifying coupling *a priori* in co-design problems was addressed. If coupling is not present, then a sequential solution strategy will produce a system-optimal solution. However, if coupling is present, this is not the case. A simultaneous formulation, if it can be solved, will produce system-optimal results, but this approach has some significant disadvantages due to computational and organizational complexity. An ideal approach would produce the same results as those found with the simultaneous formulation, but would exhibit the simplicity of the sequential formulation. Therefore, in this chapter a modified sequential solution strategy is proposed, in which the original artifact objective function, f_a, is augmented by a Control Proxy Function (CPF), representing the system's ease of control. The CPF, denoted as χ, is a function only of the artifact design variables $\boldsymbol{d}_a$ and not of the control design variables $\boldsymbol{d}_c$. The bi-objective artifact design problem with the two functions $f_a(\boldsymbol{d}_a)$ and $\chi(\boldsymbol{d}_a)$ may be solved in a variety of ways, as discussed in the multi-objective optimization literature [e.g., *Das and Dennis* (1997), *Messac and Puemi-Sukam* (2000), *Kitayama et al.* (2009), *Steuer* (1986)]. In this chapter, a weighted linear combination will be used to demonstrate the proposed method.

The modified sequential problem formulation, termed the CPF problem, is expressed

as

$$\min_{\boldsymbol{d}_a} f'_a(\boldsymbol{d}_a) = w_1 f_a(\boldsymbol{d}_a) + w_2 \chi(\boldsymbol{d}_a) \tag{4.1}$$

$$\text{subject to} \qquad \boldsymbol{g}_a(\boldsymbol{d}_a) \leq \boldsymbol{0} \tag{4.2}$$

$$\boldsymbol{h}_a(\boldsymbol{d}_a) = \boldsymbol{0} \tag{4.3}$$

followed by the control design problem

$$\min_{\boldsymbol{d}_c} f_c(\boldsymbol{d}^*_a, \boldsymbol{d}_c) \tag{4.4}$$

$$\text{subject to} \qquad \boldsymbol{g}_c(\boldsymbol{d}^*_a, \boldsymbol{d}_c) \leq \boldsymbol{0} \tag{4.5}$$

$$\boldsymbol{h}_c(\boldsymbol{d}^*_a, \boldsymbol{d}_c) = \boldsymbol{0} \tag{4.6}$$

where $\boldsymbol{d}^*_a = \text{argmin } f'_a(\boldsymbol{d}_a)$. The problem formulation can also be represented graphically, as in Fig. (4.1)

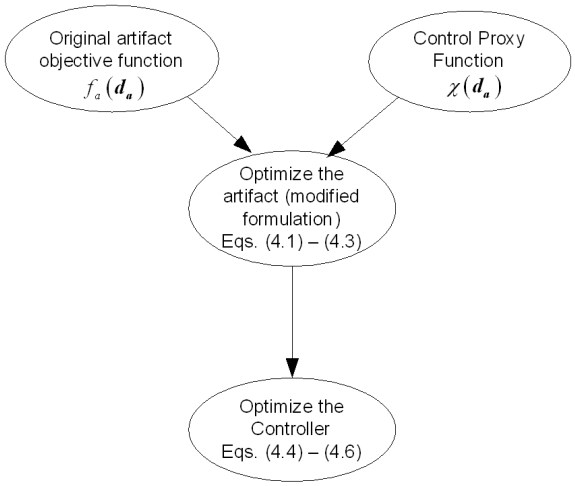

Figure 4.1: Control Proxy Function Problem Formulation

Of course, the goal in solving the modified sequential problem illustrated in Fig. 4.1

is to select the CPF, $\chi(\boldsymbol{d}_a)$, in such a way that the solution to this problem is 'close' to the system optimal solution that would be obtained by solving the original simultaneous problem in Eq. (1.9) - (1.13).

4.2 Characteristics of Effective Control Proxy Functions (CPFs)

The choice of an appropriate control proxy function (CPF), $\chi(\boldsymbol{d}_a)$, is critical in formulating the modified sequential optimization problem. A well-chosen CPF, which effectively captures the fundamental physical limitations of the system, will result in solutions that are close to the Pareto optimal points found by a simultaneous formulation, while a poorly chosen CPF will yield solutions that are far from system optimality. Clearly, the selected CPF must not require knowledge of the controller design.

This raises the questions of how to determine the 'closeness' of a CPF solution to the Pareto frontier, and how to formulate an appropriate CPF. The closeness of the CPF solution should be determined without solving the simultaneous formulation for Pareto optimal points, since the motivation for the CPF formulation is to eliminate the need to solve the simultaneous problem. A suitable measure of the CPF solution's closeness can be found by evaluating the angle ξ between two vectors that can be calculated at any point of the CPF solution set. The two vectors which define ξ are $\nabla\chi = \dfrac{\partial\chi}{\partial \boldsymbol{d}_a}$, the gradient of the CPF, and $\hat{\boldsymbol{\Gamma}}_v$, the estimate of the coupling vector. The equation for calculating $\hat{\boldsymbol{\Gamma}}_v$ is identical to that for $\boldsymbol{\Gamma}_v$; however, since the coupling vector is valid only at an optimal solution to the system, the vector found at a CPF point is an estimate. It is then shown that this measure of closeness to optimality can be used to justify two conditions that an effective CPF will satisfy. The issues of evaluating a CPF and of selecting an appropriate CPF are summarized in the four items listed below.

1. If $\boldsymbol{\Gamma}_v$ is parallel to $\nabla\chi$ at all points, then the CPF solution set will coincide with the Pareto frontier.

2. CPF solution points will approach the Pareto frontier as ξ, the angle between the estimate of the coupling vector $\hat{\boldsymbol{\Gamma}}_v$ and $\nabla\chi$ in the $\boldsymbol{d}_a$-space, approaches zero; i.e., CPF solution points will be close to the Pareto frontier when the angle ξ is small.

3. If the control objective function, $f_c(\boldsymbol{d}_a, \boldsymbol{d}_c)$, is monotonic with respect to some element of $\boldsymbol{d}_a$, then an effective CPF, $\chi(\boldsymbol{d}_a)$, will have the same coordinate-wise monotonicity as f_c with respect to that element of $\boldsymbol{d}_a$.

4. If the control objective function, $f_c(\boldsymbol{d}_a, \boldsymbol{d}_c)$, has an unconstrained minimum in the $\boldsymbol{d}_a$-space, then an effective CPF, $\chi(\boldsymbol{d}_a)$, will obtain its minimum close to it.

Each of these four items will be discussed in more detail in the following subsections, with mathematical examples given to illustrate the concepts. The items are stated as theorems; proof of each theorem is given in Appendix A.

4.2.1 Characterization of a Perfect CPF

A CPF will be described as 'perfect' if every solution of the CPF problem is also a solution to the simultaneous problem given in Eq. (1.9) - (1.13), i.e., every CPF point will coincide with the Pareto frontier. The condition which ensures that this will occur is stated as a theorem, followed by an example. The proof of the theorem is given in Appendix A.

THEOREM 4.1: If $\boldsymbol{\Gamma}_v \parallel \nabla\chi$ for all solutions to the CPF problem given in Eq. (4.1) - (4.3), then all solutions to the CPF problem will also be solutions to the simultaneous problem given in Eq. (1.9) - (1.13).

EXAMPLE: To illustrate the relationship between $\boldsymbol{\Gamma}_v$ and $\nabla\chi$, consider the following

coupled optimization problem:

$$\min w_a f_a(\boldsymbol{d}_a) + w_c f_c(\boldsymbol{d}_a, \boldsymbol{d}_c) \tag{4.7}$$

$$f_a(\boldsymbol{d}_a) = 0.5d_{a_1}^2 + d_{a_2}^2 - d_{a_1}d_{a_2} - 7d_{a_1} - 7d_{a_2} \tag{4.8}$$

$$f_c(\boldsymbol{d}_a, \boldsymbol{d}_c) = (d_{a_1} - d_{a_2})^2 + \frac{1}{9}(d_{a_1} + d_{a_2} + d_c - 10)^2 + (d_c - 5)^2 \tag{4.9}$$

$$\text{subject to } g_a(\boldsymbol{d}_a) = 4d_{a_1}^2 + d_{a_2}^2 - 900 \leq 0 \tag{4.10}$$

A CPF of

$$\chi(\boldsymbol{d}_a) = 11d_{a_1}^2 + 11d_{a_2}^2 - 18d_{a_1}d_{a_2} - 10d_{a_1} - 10d_{a_2} + 25 \tag{4.11}$$

is chosen, and the system is optimized both sequentially and simultaneously.

The coupling vector $\boldsymbol{\Gamma}_v$ is given by the relation

$$\boldsymbol{\Gamma}_v = \frac{2w_c}{9w_a} \left[\begin{array}{c} 10d_{a_1} - 8d_{a_2} + d_c - 10 \\ -8d_{a_1} + 10d_{a_2} + d_c - 10 \end{array} \right]^T \begin{array}{l} \boldsymbol{d}_a = \boldsymbol{d}_a^* \\ d_c = d_c^* \end{array} \tag{4.12}$$

and the CPF has the gradient

$$\nabla\chi = \left[\begin{array}{c} 22d_{a_1} - 18d_{a_2} - 10 \\ -18d_{a_1} + 22d_{a_2} - 10 \end{array} \right]^T \tag{4.13}$$

Since there are no controller constraints $\boldsymbol{g}_c(\boldsymbol{d}_a, \boldsymbol{d}_c)$ or $\boldsymbol{h}_c(\boldsymbol{d}_a, \boldsymbol{d}_c)$, $\dfrac{\partial f_c}{\partial d_c} = 0$, and therefore

$$d_c = 5.5 - 0.1d_{a_1} - 0.1d_{a_2}. \tag{4.14}$$

Substituting into Eq.(4.12),

$$\boldsymbol{\Gamma}_v = \frac{2w_c}{w_a} \begin{bmatrix} 1.1d_{a_1} - 0.9d_{a_2} - 0.5 \\ -0.9d_{a_1} + 1.1d_{a_2} - 0.5 \end{bmatrix}^T \begin{matrix} \boldsymbol{d}_a = \boldsymbol{d}_a^* \\ d_c = d_c^* \end{matrix} \tag{4.15}$$

It can be readily seen that, at any $\boldsymbol{d}_a$ that solves the simultaneous problem,

$$\boldsymbol{\Gamma}_v = 10\frac{w_c}{w_a}\nabla\chi \tag{4.16}$$

and therefore it is anticipated that the use of this CPF will duplicate the Pareto frontier. This is indeed the case, as shown by the numerical results in Fig. 4.2.

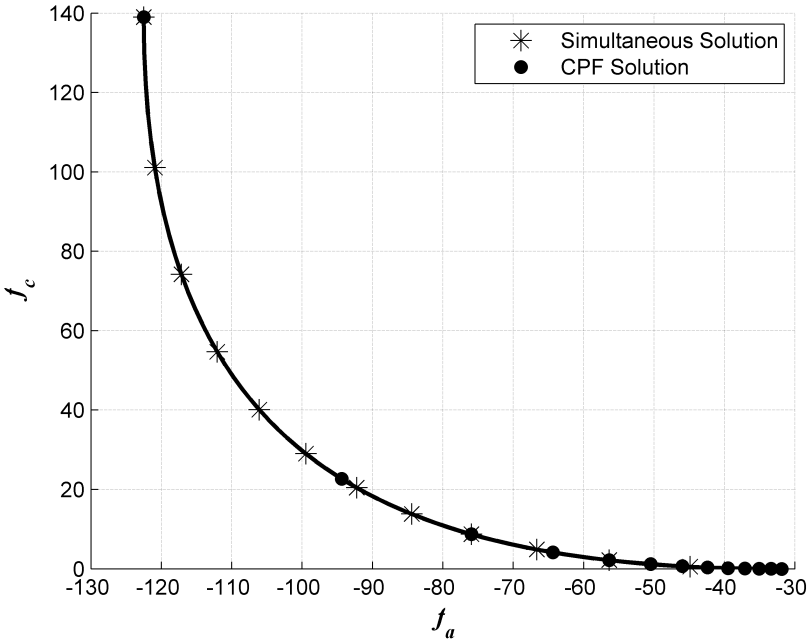

Figure 4.2: Comparison of Simultaneous and CPF Solutions for $\boldsymbol{\Gamma}_v \parallel \nabla\chi$

4.2.2 Quantification of the 'Closeness' of a CPF Point to the Pareto Frontier

As stated above, a perfect CPF is characterized by $\nabla\chi \parallel \mathbf{\Gamma}_v$, i.e., when the angle ξ between $\nabla\chi$ and $\mathbf{\Gamma}_v$ is zero. This suggests that ξ may serve as a means of evaluating the fidelity of a given CPF in modeling the behavior of f_c. If a CPF is not perfect, but it provides near-optimal results, then it can be useful when achieving true optimality would take significant additional computational effort. The condition which allows the use of ξ to characterize the closeness of a CPF is stated as a theorem, with the proof given in Appendix A. Note that the proof is valid only if no artifact constraints $\boldsymbol{g}_a(\boldsymbol{d}_a)$, $\boldsymbol{h}_a(\boldsymbol{d}_a)$ are active. However, it can be shown that the relation is true for some problems with active constraints on the artifact. Since constraints act to reduce the degrees of freedom present in an optimization problem, it is conjectured that, in the presence of constraints, the angle ξ will represent an upper bound on the 'distance' between a CPF point and the Pareto frontier. An example is given following the statement of the theorem.

THEOREM 4.2: If a co-design problem, as given in Eq. (1.9) - (1.13), is convex and no artifact constraints $\boldsymbol{g}_a(\boldsymbol{d}_a)$, $\boldsymbol{h}_a(\boldsymbol{d}_a)$ are active, then the angle ξ between $\nabla\chi$ and the estimated coupling vector $\hat{\mathbf{\Gamma}}_v$ at a CPF point will be monotonically related to ε, the distance between that CPF point and the nearest Pareto optimal point, measured in the $\boldsymbol{d}_a$-space.

EXAMPLE: Consider the following problem:

$$\min w_a f_a(\boldsymbol{d}_a) + w_c f_c(\boldsymbol{d}_a, \boldsymbol{d}_c) \tag{4.17}$$

$$f_a(\boldsymbol{d}_a) = 0.5d_{a_1}^2 + d_{a_2}^2 - d_{a_1}d_{a_2} - 7d_{a_1} - 7d_{a_2} \tag{4.18}$$

$$f_c(\boldsymbol{d}_a, \boldsymbol{d}_c) = (d_{a_1} - d_{a_2})^2 + \frac{1}{9}(d_{a_1} + d_{a_2} + d_c - 10)^2 + (d_c - 5)^2 \tag{4.19}$$

A CPF of

$$\chi_1(\boldsymbol{d}_a) = (d_{a_1} - 5)^2 + d_{a_2}^2 - 25 \tag{4.20}$$

is chosen, and the system is optimized both sequentially and simultaneously. The angle ξ is compared with the distance ε to the nearest point on the true Pareto frontier in Fig. (4.3), and it can be seen that, for this example, this angle is an effective measure of the distance to the frontier. Using this measure, the accuracy of a CPF can be evaluated without knowing the true Pareto frontier.

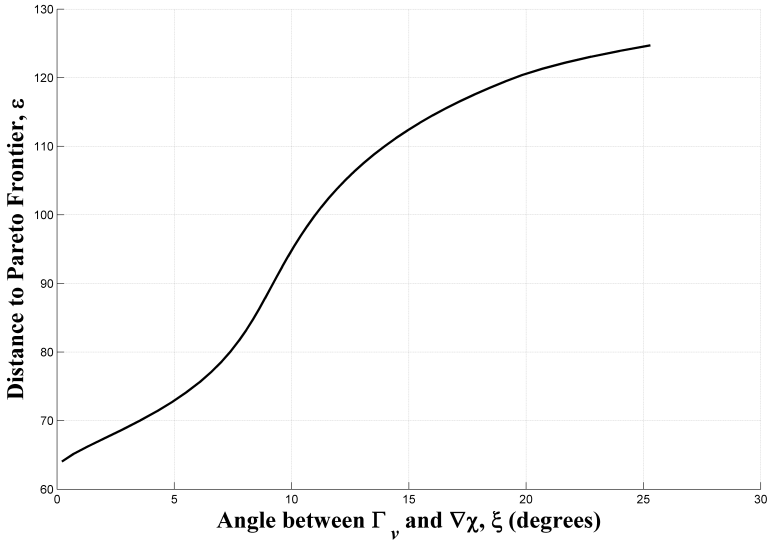

Figure 4.3: Comparison of angle ξ and distance ε

4.2.3 Monotonicity of Controller Objective and CPF

A function is said to be coordinate-wise monotonic if it is either always increasing or always decreasing with respect to a given variable, e.g., if the partial derivative of a continuous function does not change sign [*Papalambros and Wilde* (2000)]. Monotonicity analysis is a useful tool in optimization problems. For example, it can be used to determine constraint activity, to study the behavior of composite functions, and to give insight into the tradeoffs present in optimization problems [*Papalambros and Wilde* (2000)]. Here, we use monotonicity to characterize effective CPFs.

If a controller objective $f_c(\boldsymbol{d}_a, \boldsymbol{d}_c)$ is monotonic with respect to an element of $\boldsymbol{d}_a$, then

it seems logical that $\chi(\boldsymbol{d}_a)$ should have the same monotonicity with respect to that element of $\boldsymbol{d}_a$ in order to effectively model the behavior of f_c. This is the case, as stated in Theorem 4.3 below. An example follows the theorem, and the proof is given in Appendix A.

THEOREM 4.3: If $f_c(\boldsymbol{d}_a, \boldsymbol{d}_c)$ is monotonic with respect to some element of $\boldsymbol{d}_a$, and that element of $\boldsymbol{d}_a$ does not appear in any active constraint, then a CPF with the same monotonicity will produce closer solutions than a CPF with the opposite monotonicity.

EXAMPLE: Consider the following problem:

$$\min w_a f_a(\boldsymbol{d}_a) + w_c f_c(\boldsymbol{d}_a, d_c) \tag{4.21}$$

$$f_a(\boldsymbol{d}_a) = 0.5d_{a_1}^2 + d_{a_2}^2 - d_{a_1}d_{a_2} - 7d_{a_1} - 7d_{a_2} \tag{4.22}$$

$$f_c(\boldsymbol{d}_a, d_c) = d_{a_1} + d_{a_2} - d_c \tag{4.23}$$

subject to

$$g_a(\boldsymbol{d}_a) = 10 - d_{a_1} - d_{a_2} \leq 0 \tag{4.24}$$

$$g_c(\boldsymbol{d}_a, d_c) = \left(d_{a_2} - \frac{d_c}{2}\right)^2 - 25 \leq 0 \tag{4.25}$$

where $\boldsymbol{d}_a = \{\boldsymbol{d}_a : \boldsymbol{d}_a \geq \boldsymbol{0}\}$.

A CPF of

$$\chi(\boldsymbol{d}_a) = d_{a_1} + 0.25d_{a_2}^{0.5} \tag{4.26}$$

is chosen. It is evident that f_c and χ are both monotonically increasing with respect to d_{a_1} and d_{a_2}. Solving both the simultaneous optimization and the CPF problem, it can be seen in Fig. 4.4 that the CPF solution models the tradeoff between f_a and f_c, though imperfectly.

In contrast, consider a CPF of

$$\chi(\boldsymbol{d}_a) = -d_{a_1} + 0.25d_{a_2}^{0.5} \tag{4.27}$$

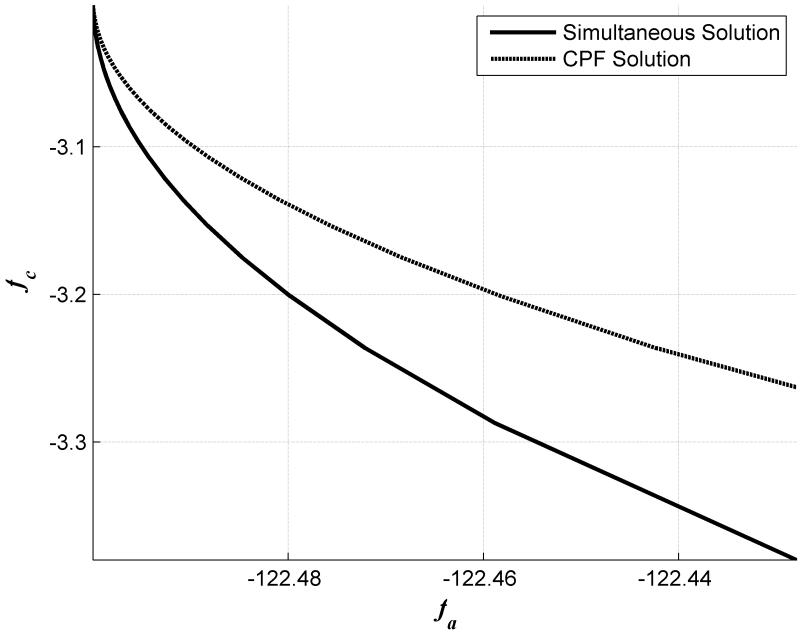

Figure 4.4: Comparison of Simultaneous and CPF Solutions for Appropriate Monotonicity

In this case, the monotonicity of χ and f_c with respect to d_{a_1} does not match. Solving the new CPF problem, it can be seen in Fig. 4.5 that this CPF does not model the tradeoff between f_a and f_c.

4.2.4 Locations of Unconstrained Minima of f_c and χ

In the previous section, f_c was assumed to be monotonic with respect to some element of $\boldsymbol{d}_a$. Here, we consider the case where f_c is not monotonic, but rather has an unconstrained minimum. Intuitively, it seems likely that the values taken by $\boldsymbol{d}_a$ at the minimum of f_c should also minimize χ, and that a CPF will become less effective if the minimum of χ is farther from the minimum of f_c in the $\boldsymbol{d}_a$-space. This can be proven for an unconstrained problem, and it is conjectured that it will also be true for constrained problems. This condition is stated as a theorem, with the proof given in Appendix A. The theorem is followed by an example.

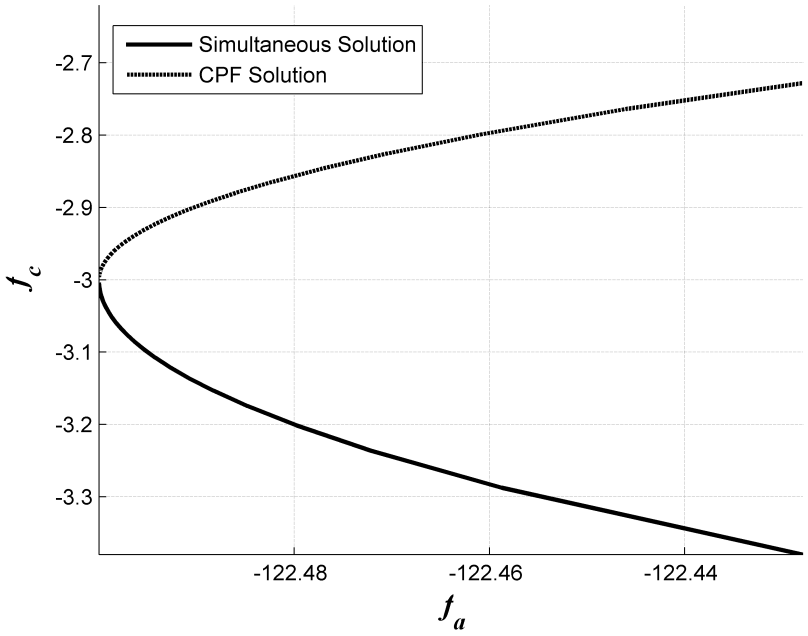

Figure 4.5: Comparison of Simultaneous and CPF Solutions for Inappropriate Monotonicity

THEOREM 4.4: Assume that $f_c(\boldsymbol{d}_a, \boldsymbol{d}_c)$ has an unconstrained minimum, and that $\chi(\boldsymbol{d}_a)$ is chosen such that it has an unconstrained minimum. Then, the distance between a CPF point and the Pareto frontier will increase as the distance increases between the minima of f_c and χ.

EXAMPLE: Consider the following problem:

$$\min w_a f_a(\boldsymbol{d}_a) + w_c f_c(\boldsymbol{d}_a, d_c) \tag{4.28}$$

$$f_a(\boldsymbol{d}_a) = 0.5d_{a_1}^2 + d_{a_2}^2 - d_{a_1}d_{a_2} - 7d_{a_1} - 7d_{a_2} \tag{4.29}$$

$$f_c(\boldsymbol{d}_a, d_c) = (d_{a_1} - d_{a_2})^2 + \frac{1}{9}(d_{a_1} + d_{a_2} + d_c - 10)^2 + (d_c - 5)^2 \tag{4.30}$$

subject to

$$g_a(\boldsymbol{d}_a) = 4d_{a_1}^2 + d_{a_2}^2 - 900 \leq 0 \tag{4.31}$$

$$g_c(\boldsymbol{d}_a, d_c) = \frac{1}{50}d_{a_1}^2 + \frac{1}{5}d_{a_2}^2 - 48 \leq 0 \tag{4.32}$$

Table 4.1: Comparison of Minima of Objective Functions and Control Proxy Functions

	d_{a_1}	d_{a_2}
f_a	21	14
f_c	2.5	2.5
χ_1	5	0
χ_2	1	-10

This problem is solved twice, with two different CPFs, which will then be compared.

$$\chi_1(\boldsymbol{d}_a) = (d_{a_1}-5)^2 + d_{a_2}^2 - 25 \tag{4.33}$$

$$\chi_2(\boldsymbol{d}_a) = (d_{a_1}-1)^2 + (d_{a_2}+10)^2 - 10 \tag{4.34}$$

The unconstrained minima of the functions f_a, f_c, χ_1, and χ_2 are given in Table 4.1. The solutions found by solving the two CPF sequential problems are shown in Fig. 4.6. It can be seen that χ_1, which obtains its minimum closer to that of f_c than does χ_2, produces a closer match to the simultaneous solution than χ_2.

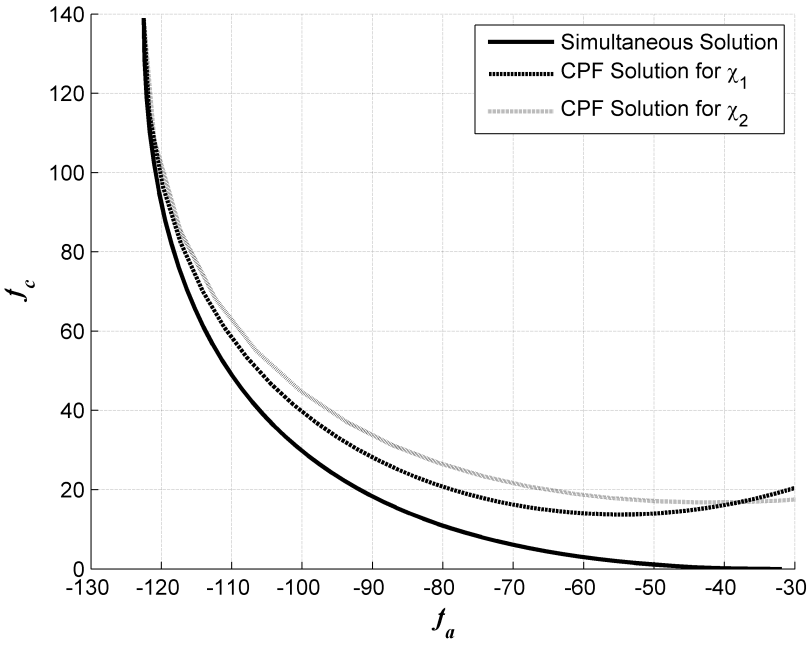

Figure 4.6: Comparison of Simultaneous and CPF Solutions for Two Choices of CPF

4.3 Control Proxy Functions for Specific Co-Design Problem Formulations

Given the characteristics of effective CPFs that have been developed in Section 4.2, we can formulate potential CPFs for specific problem formulations and evaluate them. In this section, we will show that a perfect CPF exists for each of several problem formulations. Of course, the formulations considered here are not exhaustive. There are many co-design problem formulations that are not considered here, and it is anticipated that future work will identify additional CPFs that would be useful for additional problem formulations.

The CPFs evaluated here will be based on either the natural frequency of the system or on the controllability Grammian matrix. The natural frequency is considered as the basis for a CPF because previous work has shown that, in some cases, it can be used as an effective proxy for a system's ease of control [e.g., *Peters et al.* (2008), *Hale et al.* (1985), *Khot and Abhyankar* (1993), *Bodden and Junkins* (1985), *Yee and Tsuei* (1991)]. The controllability Grammian matrix, $\boldsymbol{W}_c$, will be considered as the basis for a CPF because previous work, as described in Chapter III and in [*Peters et al.* (2010)], has shown that, for some problem formulations, there is a relationship between $\boldsymbol{W}_c$ and the coupling vector $\boldsymbol{\Gamma}_v$. Since there is also a relationship between $\boldsymbol{\Gamma}_v$ and an effective CPF, this suggests that a CPF based on $\boldsymbol{W}_c$ will be effective for some problems.

4.3.1 Natural Frequency as a Control Proxy Function

Since the natural frequency of a system depends only on the artifact and can be used, in some cases, to model the system's ease of control, there will be problems for which an effective control proxy function $\chi\left(\boldsymbol{d}_a\right)$ will be a function of the natural frequency. This raises the question of when a CPF of this type would be effective. There are several necessary conditions for a CPF based on natural frequency to be effective. Those that are common to all of the cases discussed in this section are listed below.

1. The co-design problem is formulated as in Eq. (1.9)-(1.13).

2. The system is linear and dominated by second-order dynamics. This system can be described, then, in the form

$$m\ddot{z} + b\dot{z} + kz = u(t) \tag{4.35}$$

where m, b, and k are functions of the design variables d_a, parameters, and constants. or alternatively in state-space form as

$$\dot{\boldsymbol{x}} = \boldsymbol{A}\boldsymbol{x} + \boldsymbol{B}u \tag{4.36}$$

where

$$\boldsymbol{A} = \begin{bmatrix} 0 & 1 \\ -\dfrac{k}{m} & -\dfrac{b}{m} \end{bmatrix} \tag{4.37}$$

$$\boldsymbol{B} = \begin{bmatrix} 0 \\ \dfrac{1}{m} \end{bmatrix} \tag{4.38}$$

$$\boldsymbol{x} = \begin{bmatrix} z \\ \dot{z} \end{bmatrix} \tag{4.39}$$

The open-loop system is underdamped, i.e., the open-loop eigenvalues are complex.

3. The matrix $\boldsymbol{B}$ is independent of the artifact design variables $\boldsymbol{d}_a$, i.e.,

$$\frac{\partial m}{\partial \boldsymbol{d}_a} = \boldsymbol{0}. \tag{4.40}$$

4. A state-feedback controller, possibly with a precompensator, is applied to the system, as shown in Fig. 2.3.

5. There are no active controller equality constraints $\boldsymbol{h}_c(\boldsymbol{d}_a, \boldsymbol{d}_c)$ or strongly active controller inequality constraints $\boldsymbol{g}_c(\boldsymbol{d}_a, \boldsymbol{d}_c)$ present. Weakly active controller inequality constraints may be present, where a weakly active constraint is one which is not satisfied as a strict equality but whose removal will affect the system optimum [*Pomrehn and Papalambros* (1994)].

In a second-order system, there are two eigenvalues, which are complex conjugates. These eigenvalues can be fully described by the frequency ω and damping coefficient ζ of the system.

$$\lambda_{1,2} = -\zeta\omega \pm \omega\sqrt{\zeta^2 - 1} \tag{4.41}$$

Here, we will denote the natural frequency, or frequency of the open-loop system, as ω_n and the damping coefficient of the open-loop system as ζ_n. The frequency of the controlled, or closed-loop, system will be denoted as ω_c and the damping coefficient of the closed-loop system will be denoted as ζ_c. The open-loop and closed-loop frequencies and damping coefficients for the second-order system subjected to state-feedback control are given by the following equations [*Franklin et al.* (1994)]:

$$\omega_n = \sqrt{\frac{k}{m}} \tag{4.42}$$

$$\zeta_n = \frac{b}{2\sqrt{mk}} \tag{4.43}$$

$$\omega_c = \sqrt{\frac{k+K_1}{m}} \tag{4.44}$$

$$\zeta_c = \frac{b+K_2}{2\sqrt{m(k+K_1)}} \tag{4.45}$$

These equations will be used to define three specific problem formulations where $\chi(\boldsymbol{d}_a) = \chi(\omega_n)$. In each case, additional necessary conditions are specified, relating to the damping of the system. These three problem formulations are stated and proved below using Theorem 4.1.

Control Objective Independent of Damping: If the control objective f_c is a function of the closed-loop frequency ω_c of the system but is independent of the closed-loop damping coefficient ζ_c, then the CPF $\chi = \chi(\omega_n)$ will yield system-optimal solutions to the simultaneous optimization problem. An example of this control objective is $f_c = t_r$, where $t_r = \dfrac{1.8}{\omega_c}$ is the rise time of the system [*Franklin et al.* (1994)].

(e.g., $f_c = t_r$, where t_r is the rise time of the system)

For a second-order system, ω_n is given by Eq. (4.42), and therefore the gradient of χ is given by

$$\nabla\chi = \frac{\partial\chi}{\partial\omega_n}\frac{\partial\omega_n}{\partial \boldsymbol{d}_a} = \frac{\partial\chi}{\partial\omega_n}\left(\frac{1}{2}\sqrt{\frac{1}{km}}\frac{\partial k}{\partial \boldsymbol{d}_a}\right) \tag{4.46}$$

where k is a function of $\boldsymbol{d}_a$. The closed-loop frequency of the system is given by Eq. (4.44). Using Eq. (1.14), the coupling is found to be

$$\boldsymbol{\Gamma}_v = \frac{w_2}{w_1}\frac{\partial f_c}{\partial\omega_c}\left(\frac{1}{2}\sqrt{\frac{1}{(k+K_1)m}}\frac{\partial k}{\partial \boldsymbol{d}_a}\right) \tag{4.47}$$

It is possible, then, to express the coupling vector $\boldsymbol{\Gamma}_v$ at the CPF solution as

$$\boldsymbol{\Gamma}_v = \frac{w_2}{w_1}\sqrt{\frac{k}{k+K_1}}\left(\frac{\partial f_c}{\partial\omega_c}\right) / \left(\frac{\partial\chi}{\partial\omega_n}\right)\nabla\chi \tag{4.48}$$

and it can be seen that the coupling vector at the CPF point must be parallel or anti-parallel to the gradient of the CPF, depending on the sign of the scalar term. If the CPF χ is selected such that $\operatorname{sgn}\left(\dfrac{\partial\chi}{\partial\omega_n}\right) = \operatorname{sgn}\left(\dfrac{\partial f_c}{\partial\omega_c}\right)$, then the two vectors will be parallel. From Theorem 4.1, then, the CPF points will be Pareto optimal for the co-design problem.

Control Objective Independent of Imaginary Component of Eigenvalues: If the control objective f_c is a function of the product $\omega_c\zeta_c$, i.e., of the real part of the closed-loop eigenvalues (e.g., $f_c = t_s$, where t_s is the settling time of the system), and the damping ratio ζ_n of the open-loop system is independent of $\boldsymbol{d}_a$, then the CPF $\chi = \chi(\omega_n)$ will yield

system-optimal solutions to the simultaneous optimization problem.

The condition that the damping ratio of the open-loop system is independent of $\boldsymbol{d}_a$ can be expressed mathematically as

$$\frac{\partial \zeta_n}{\partial \boldsymbol{d}_a} = \mathbf{0}. \tag{4.49}$$

The gradient $\nabla\chi$ is, once again, given by Eq. (4.46). Using Eq. (4.44) - (4.45), $\boldsymbol{\Gamma}_v$ is computed from Eq. (1.14) as

$$\boldsymbol{\Gamma}_v = \frac{w_2}{w_1}\frac{\partial f_c}{\partial\left(\omega_c\zeta_c\right)}\left(\zeta_c\frac{\partial \omega_c}{\partial \boldsymbol{d}_a} + \omega_c\frac{\partial \zeta_c}{\partial \boldsymbol{d}_a}\right) \tag{4.50}$$

By differentiating Eq. (4.43) and substituting Eq. (4.49), it is found that

$$\boldsymbol{\Gamma}_v = \frac{w_2}{w_1}\frac{\partial f_c}{\partial\left(\omega_c\zeta_c\right)}\frac{b}{4km}\frac{\partial k}{\partial \boldsymbol{d}_a} \tag{4.51}$$

and therefore the coupling vector can be expressed in terms of the gradient $\nabla\chi$ as

$$\boldsymbol{\Gamma}_v = \frac{w_2}{w_1}\frac{\partial f_c}{\partial\left(\omega_c\zeta_c\right)}\frac{b}{2\sqrt{km}}\left(1/\frac{\partial \chi}{\partial \omega_n}\right)\nabla\chi \tag{4.52}$$

and it can again be seen that the coupling vector at the CPF point must be parallel or anti-parallel to the gradient of the Control Proxy Function, depending on the sign of the scalar term. If the open-loop system is stable, $b > 0$, and the function χ should be chosen such that $\operatorname{sgn}\left(\frac{\partial \chi}{\partial \boldsymbol{d}_a}\right) = \operatorname{sgn}\left(\frac{\partial f_c}{\partial\left(\omega_c\zeta_c\right)}\right)$. If this condition is met, then the two vectors will be parallel. From Theorem 4.1, then, the CPF points will be Pareto optimal for the co-design problem.

Damping Term b Independent of $\boldsymbol{d}_a$: If the controller objective f_c is an arbitrary function of the closed-loop eigenvalues of the system, and the damping term b in the system

description is independent of $\boldsymbol{d}_a$, i.e.,

$$\frac{\partial b}{\partial \boldsymbol{d}_a} = \mathbf{0} \tag{4.53}$$

then the CPF $\chi = \chi(\omega_n)$ will yield system-optimal solutions to the simultaneous optimization problem.

The gradient $\nabla\chi$ is, once again, given by Eq. (4.46). Using Eq. (4.53), the coupling $\boldsymbol{\Gamma}_v$ can be computed from Eq. (1.14) as

$$\boldsymbol{\Gamma}_v = \frac{w_2}{w_1}\left(\frac{\partial f_c}{\partial \omega_c}\frac{\partial \omega_c}{\partial \boldsymbol{d}_a} + \frac{\partial f_c}{\partial \zeta_c}\frac{\partial \zeta_c}{\partial \boldsymbol{d}_a}\right) \tag{4.54}$$

Using the relations for ω_c and ζ_c given in Eqs. (4.44) and (4.45), respectively,

$$\boldsymbol{\Gamma}_v = \frac{w_2}{w_1}\frac{1}{\sqrt{m(k+K_1)}}\left(\frac{\partial f_c}{\partial \omega_c} - \frac{\partial f_c}{\partial \zeta_c}\frac{b+K_2}{2(k+K_1)}\right)\frac{\partial k}{\partial \boldsymbol{d}_a} \tag{4.55}$$

which can then be expressed in terms of $\nabla\chi$ as

$$\boldsymbol{\Gamma}_v = \frac{w_2}{w_1}\sqrt{\frac{k}{k+K_1}}\left(\frac{\partial f_c}{\partial \omega_c} - \frac{\partial f_c}{\partial \zeta_c}\frac{b+K_2}{2(k+K_1)}\right)\left(1/\frac{\partial \chi}{\partial \omega_n}\right)\nabla\chi \tag{4.56}$$

and it can be seen, yet again, that the coupling vector at the CPF point must be parallel or anti-parallel to the gradient of the Control Proxy Function, depending on the sign of the scalar term in parentheses. If the function $\chi(\boldsymbol{d}_a)$ is chosen such that the scalar term is positive, then the two vectors will be parallel. From Theorem 4.1, then, the CPF points will be Pareto optimal for the co-design problem.

In this section, it has been shown that there are at least three co-design problem formulations in which natural frequency will serve as an effective CPF. In each of these formulations, the system's damping coefficient either does not affect the controller objective function, or else it is subject to restrictions. It is anticipated that a CPF using both damping

of the open-loop system and the natural frequency would be effective in some additional cases, where these restrictions are not satisfied. Furthermore, all three of these problem formulations require the system to be modeled by second-order dynamics. It is expected that these results for a CPF using natural frequencies could be extended to systems of higher order. It is also conjectured that a CPF based on open-loop eigenvalues would be valid with some types of constraints, and it is anticipated that future research will develop such CPFs.

However, a CPF using open-loop eigenvalues will not be effective when the matrix $\boldsymbol{B}$ is sensitive to the artifact design variables $\boldsymbol{d}_a$, since open-loop eigenvalues cannot be used to model that system behavior. For problems of this type, the CPF must be based on some other fundamental metric of the system which is capable of modeling both the free and forced response characteristics of the system. The next section will evaluate the use of the controllability Grammian matrix $\boldsymbol{W}_c$, which depends on both the $\boldsymbol{A}$ and $\boldsymbol{B}$ matrices, for problems where the derivatives of the $\boldsymbol{B}$ matrix with respect to some components of $\boldsymbol{d}_a$, $\dfrac{\partial \boldsymbol{B}}{\partial d_{a_i}}$, are significant.

4.3.2 Control Proxy Functions Based on the Controllability Grammian

As shown in the previous section, a CPF based on natural frequency can be effective for problems in which the matrix $\boldsymbol{B}$ in Eq. (4.36) is not a function of the artifact design variables, $\boldsymbol{d}_a$. If $\boldsymbol{B}$ is a function of $\boldsymbol{d}_a$, then the CPF must incorporate $\boldsymbol{B}$ in some way. Since the controllability Grammian matrix $\boldsymbol{W}_c$ incorporates both the free and forced response characteristics of a system, it is logical to consider its use in a CPF. Furthermore, the physical meaning of the controllability Grammian matrix suggests that it might be effective as a CPF. The control effort required to move a system from one state to another is a function of the controllability Grammian matrix. If the determinant of the controllability Grammian matrices are compared for two systems, the system with the larger determinant will require less control effort for the same state transition; or, alternatively, the system with the larger determinant can be moved farther or faster with the same control effort. It

is therefore evident that the controllability Grammian matrix can be used to predispose a system to effective control, and may often be a good choice of CPF. This section will examine situations in which a CPF based on either the time-dependent controllability Grammian matrix, $\boldsymbol{W}_c\left(t_f\right)$, or the steady-state controllability Grammian matrix, $\boldsymbol{W}_c^{\infty}$, is perfect. In all cases, it is assumed that:

1. The co-design problem is formulated as in Eq. (1.9)-(1.13).

2. The system dynamics are linear and can be described in state-space form as in Eq. (4.36).

Control Proxy Function for the Case of Control Effort as Objective

Consider the case in which the control objective is to minimize control effort, as described in Eq. (3.9). If an optimal controller is chosen, then as stated in Chapter III, the control objective function f_c can be found from Eq. (3.10) to be

$$f_c = \boldsymbol{x}_f^T \boldsymbol{W}_c^{-1} \boldsymbol{x}_f. \tag{4.57}$$

This expression for f_c depends only on $\boldsymbol{d}_a$, and thus could serve as a CPF. Since the coupling vector $\boldsymbol{\Gamma}_v$ was calculated from this relation, as in Eq. (3.12), it can easily be seen that, for $\chi\left(\boldsymbol{d}_a\right) = \boldsymbol{x}_f^T \boldsymbol{W}_c^{-1} \boldsymbol{x}_f$,

$$\boldsymbol{\Gamma}_v = \frac{w_c}{w_a} \nabla \chi \tag{4.58}$$

and thus, the CPF is perfect.

There are situations, however, when a simpler CPF would suffice. In Case Ia, as detailed in Chapter III, the final state of the system, $\boldsymbol{x}_f$, is a parameter. Logically, one might expect that when this is the case, a CPF based only on $\boldsymbol{W}_c$ may be effective, and in at least two situations this is true, as shown below.

Consider first the case where the components of $\boldsymbol{x}_f$ are equal, i.e., $x_{f_q} = \alpha \ \forall \ q = 1, \ldots, p$. In this case, a CPF of

$$\chi(\boldsymbol{d}_a) = \sum_{q=1}^{p} \sum_{t=1}^{p} W_c^{-1}(q,t) \tag{4.59}$$

is chosen. It is shown here that this will be a perfect CPF.

The gradient of Eq. (4.59) is given by

$$\nabla\chi = \begin{bmatrix} \frac{\sum_{q=1}^{p}\sum_{t=1}^{p} \partial W_c^{-1}(q,t)}{\partial d_{a_1}} \\ \frac{\sum_{q=1}^{p}\sum_{t=1}^{p} \partial W_c^{-1}(q,t)}{\partial d_{a_2}} \\ \vdots \\ \frac{\sum_{q=1}^{p}\sum_{t=1}^{p} \partial W_c^{-1}(q,t)}{\partial d_{a_n}} \end{bmatrix}^T \tag{4.60}$$

The coupling vector $\boldsymbol{\Gamma}_v$ is found from Eq. (3.13):

$$\boldsymbol{\Gamma}_v = \frac{w_c}{w_a} \begin{bmatrix} \sum_{q=1}^{p}\sum_{t=1}^{p} x_{f_q} x_{f_t} \frac{\partial \boldsymbol{W}_c^{-1}(q,t)}{\partial d_{a_1}} \\ \sum_{q=1}^{p}\sum_{t=1}^{p} x_{f_q} x_{f_t} \frac{\partial \boldsymbol{W}_c^{-1}(q,t)}{\partial d_{a_2}} \\ \vdots \\ \sum_{q=1}^{p}\sum_{t=1}^{p} x_{f_q} x_{f_t} \frac{\partial \boldsymbol{W}_c^{-1}(q,t)}{\partial d_{a_n}} \end{bmatrix}^T \tag{4.61}$$

which can be re-written as

$$\boldsymbol{\Gamma}_v = \frac{w_c}{w_a} \begin{bmatrix} \alpha^2 \frac{\partial \sum_{q=1}^{p}\sum_{t=1}^{p} \boldsymbol{W}_c^{-1}(q,t)}{\partial d_{a_1}} \\ \alpha^2 \frac{\partial \sum_{q=1}^{p}\sum_{t=1}^{p} \boldsymbol{W}_c^{-1}(q,t)}{\partial d_{a_2}} \\ \vdots \\ \alpha^2 \frac{\partial \sum_{q=1}^{p}\sum_{t=1}^{p} \boldsymbol{W}_c^{-1}(q,t)}{\partial d_{a_n}} \end{bmatrix}^T \tag{4.62}$$

Thus,

$$\boldsymbol{\Gamma}_v = \frac{w_c}{w_a}\alpha^2 \nabla\chi \tag{4.63}$$

and, as stated, Eq. (4.59) will be a perfect CPF. Note that, if $\boldsymbol{W}_c\left(t_f\right)$ is diagonal, the CPF can be expressed as

$$\chi\left(\boldsymbol{d}_a\right) = \mathrm{tr}\left(\boldsymbol{W}_c^{-1}\right) = \frac{\mathrm{tr}\left(\boldsymbol{W}_c\right)}{\det\left(\boldsymbol{W}_c\right)} \tag{4.64}$$

In general, $\boldsymbol{W}_c\left(t_f\right)$ is not diagonal. However, if the system's balanced realization is used, then $\boldsymbol{W}_c\left(t_f\right)$ will be diagonal, regardless of the value of t_f [*Kailath* (1980)]. This is therefore recommended, as it simplifies the expression for χ.

In contrast, consider a situation in which the parameter $\boldsymbol{x}_f$ has as its only non-zero component the j^{th} element, i.e., $x_{f_j} \neq 0$, $x_{f_q} = 0 \;\forall\; q \neq j$; this situation corresponds to problems in which a system is to be moved to a final location where it is at rest. A CPF of

$$\chi = \boldsymbol{W}_{c_{jj}}^{-1}\left(t_f\right) = \frac{\boldsymbol{W}_{c_{jj}}^{*}\left(t_f\right)}{\det\left(\boldsymbol{W}_c\right)} \tag{4.65}$$

is chosen, where $\boldsymbol{W}_c^{*}\left(t_f\right)$ is the adjoint matrix of $\boldsymbol{W}_c\left(t_f\right)$, and $\boldsymbol{W}_{c_{jj}}^{*}\left(t_f\right)$ is the $(jj)^{th}$ element of $\boldsymbol{W}_c^{*}\left(t_f\right)$. Note that, if the $(jj)^{th}$ element of $\boldsymbol{W}_c^{*}\left(t_f\right)$ is not a function of $\boldsymbol{d}_a$, then this is equivalent to maximizing the determinant of $\boldsymbol{W}_c\left(t_f\right)$. It will be shown here that this is a perfect CPF.

The gradient of Eq. (4.59) is given by

$$\nabla\chi = \begin{bmatrix} \dfrac{\partial \boldsymbol{W}_{c_{jj}}^{-1}\left(t_f\right)}{\partial d_{a_1}} \\ \dfrac{\partial \boldsymbol{W}_{c_{jj}}^{-1}\left(t_f\right)}{\partial d_{a_2}} \\ \vdots \\ \dfrac{\partial \boldsymbol{W}_{c_{jj}}^{-1}\left(t_f\right)}{\partial d_{a_n}} \end{bmatrix}^T \tag{4.66}$$

The coupling vector $\boldsymbol{\Gamma}_v$ is found from Eq. (3.13):

$$\boldsymbol{\Gamma}_v = \frac{w_c}{w_a} \begin{bmatrix} x_{f_j}^2 \dfrac{\partial \boldsymbol{W}_{c_{jj}}^{-1}(t_f)}{\partial d_{a_1}} \\ x_{f_j}^2 \dfrac{\partial \boldsymbol{W}_{c_{jj}}^{-1}(t_f)}{\partial d_{a_2}} \\ \vdots \\ x_{f_j}^2 \dfrac{\partial \boldsymbol{W}_{c_{jj}}^{-1}(t_f)}{\partial d_{a_n}} \end{bmatrix}^T \tag{4.67}$$

which can be re-written as

$$\boldsymbol{\Gamma}_v = \frac{w_c}{w_a} x_{f_j}^2 \nabla \chi \tag{4.68}$$

Thus, as stated, Eq. (4.59) will be a perfect CPF for this situation.

In Chapter III, it was shown that the coupling vector was related to the controllability Grammian matrix for the case, denoted Case II, where the control objective function is the final time and a constraint on control effort is active. The coupling vector for that problem formulation was found to be parallel to the coupling vector found for Case I. Therefore, it can then be seen that the CPFs developed above will also apply to problems of Case II.

Control Proxy Function for the Case of Linear Quadratic Regulator (LQR):

As shown in Eq. (3.44), the coupling vector for the LQR problem can be related to the controllability Grammian for a specific choice of the state weighting matrix $\boldsymbol{Q} = \gamma \boldsymbol{B}\boldsymbol{B}^T$. In the most general LQR case discussed in Chapter III, the initial state $\boldsymbol{x}_0$, $\boldsymbol{W}_c^{\infty}$, and $\boldsymbol{A}$ all depend on $\boldsymbol{d}_a$, and a perfect CPF would take the form of

$$\chi(\boldsymbol{d}_a) = \boldsymbol{x}_0^T \boldsymbol{A}^{-T} \boldsymbol{A} \boldsymbol{W}_c^{\infty} \boldsymbol{x}_0. \tag{4.69}$$

As in previous cases, however, there are special circumstances where a simpler CPF may be chosen. This may be desirable in extremely large problems where computational demands must be minimized. Consider the situation in which the matrix $\boldsymbol{A}$ is not a function of $\boldsymbol{d}_a$

and the initial state $\boldsymbol{x}_0$ is a parameter with exactly one non-zero component, i.e., $x_{0_j} \neq 0$, $x_{0_q} = 0 \; \forall \; q \neq j, 0 \leq q \leq p$. Furthermore, the matrix $\boldsymbol{W}_c^{\infty}$ is diagonal, which will be the case when a balanced realization is utilized.

For the system described above, select a CPF of

$$\chi\left(\boldsymbol{d}_a\right) = \boldsymbol{W}_{c_{jj}}^{\infty}. \tag{4.70}$$

The gradient of Eq. 4.70 is given by

$$\nabla\chi = \begin{bmatrix} \dfrac{\partial \boldsymbol{W}_{c_{jj}}^{\infty}}{\partial d_{a_1}} \\ \dfrac{\partial \boldsymbol{W}_{c_{jj}}^{\infty}}{\partial d_{a_2}} \\ \vdots \\ \dfrac{\partial \boldsymbol{W}_{c_{jj}}^{\infty}}{\partial d_{a_n}} \end{bmatrix}^T \tag{4.71}$$

The coupling vector can be computed from Eq. (3.45) and is given by the relation

$$\boldsymbol{\Gamma}_v = \frac{w_c}{w_a}\gamma \begin{bmatrix} \dfrac{1}{\det \boldsymbol{A}} x_{0_j}^2 A_{jj}^2 \dfrac{\partial W_{c_{jj}}^{\infty}}{\partial d_{a_1}} \\ \dfrac{1}{\det \boldsymbol{A}} x_{0_j}^2 A_{jj}^2 \dfrac{\partial W_{c_{jj}}^{\infty}}{\partial d_{a_2}} \\ \vdots \\ \dfrac{1}{\det \boldsymbol{A}} x_{0_j}^2 A_{jj}^2 \dfrac{\partial W_{c_{jj}}^{\infty}}{\partial d_{a_n}} \end{bmatrix}^T \tag{4.72}$$

This leads to the relation

$$\boldsymbol{\Gamma}_v = \frac{w_c}{w_a}\frac{\gamma}{\det \boldsymbol{A}} x_{0_j}^2 A_{jj}^2 \nabla\chi \tag{4.73}$$

and therefore the CPF is perfect for this problem.

In this section, it has been shown that a CPF based on the controllability Grammian matrix, $\boldsymbol{W}_c\left(t_f\right)$, can be effective for many problems in which either f_c or an active constraint is dependent on control effort. This includes some problems in which the control objective,

f_c, is the response time of the system. For the specific problem formulations investigated here, a perfect CPF can be formulated based on either the the time-dependent or steady-state controllability Grammian matrix. As previously stated, these problem formulations are not exhaustive. It is anticipated that future work will show that a CPF based on the controllability Grammian matrix will be effective for additional co-design problem formulations, particularly those in which the objective function or constraints are dependent on control effort.

However, it may not always be possible to formulate a perfect CPF based on the control Grammian. For example, consider the case where f_c is the maximum control signal, rather than control effort. A control signal with a high peak that quickly decays may result in a lower control effort than a signal with a lower peak that does not decay as quickly. The relationship between the maximum control signal and control effort, and the choice of an appropriate CPF for problems in which the control objective, f_c, is based on the maximum control signal, requires further investigation. It is conjectured that a CPF based on the controllability Grammian will produce results that are near-optimal for a variety of problems, since it provides a measure of how easily a system is controlled.

4.4 Summary

In this chapter, a new method of solution for co-design problems was introduced, based upon a sequential optimization using a Control Proxy Function (CPF). The intent of the CPF method is to provide solutions that are identical with, or close to, the Pareto optimal solutions to the co-design problem, while allowing the problem to be decomposed into an artifact design problem and a control design problem. This decomposition allows the co-design problem to be more easily formulated and solved by experts in each of the functional areas of artifact design and control design. The key to the effectiveness of this method is the choice of the CPF. Therefore, guidelines to choose a CPF and a metric to evaluate the closeness of the solutions have been developed and presented in this chapter. Furthermore,

CPFs based on natural frequency and on the controllability Grammian matrix have been developed for specific problem formulations. These CPFs are all based on the assumption that the system of interest is linear and time-invariant. For a CPF based on natural frequency, the system is also assumed to be second-order, though this assumption does not apply to the use of the controllability Grammian matrix. The CPFs developed in this chapter are not exhaustive; it is possible to formulate and evaluate additional CPFs, based on open-loop eigenvalues, the controllability Grammian, and possibly other system metrics. CPFs for systems that are non-linear or which are not time-invariant could be developed, since the development of the mathematical basis for the use of a CPF did not require these assumptions. Of course, with a variety of possible CPFs, it is important to be able to determine easily which, if any, will be effective for a given system. If a CPF were found only by trial and error, or if the selection of a CPF were to require complex calculations, then the method would offer few advantages over other available solution techniques. In the next chapter, a set of tests will be given to determine whether a particular problem could be solved with a CPF, and if so, which CPF should be chosen. The selection of an appropriate CPF will be demonstrated by means of an example, and the computational effort required to solve the problem by the CPF method versus the simultaneous method will be discussed.

CHAPTER V

Application of the CPF Method

5.1 Introduction

In Chapter IV, the Control Proxy Function (CPF) method was developed and presented. This method allows a designer to perform sequential optimization of a coupled co-design problem, while producing optimal or near-optimal results. The CPF method offers several advantages over other methods of optimizing co-design problems, including reduced computational complexity and the ability to optimize the artifact before the controller configuration has been defined. However, in order to take advantage of the CPF method, it is necessary to easily identify or formulate an appropriate CPF. If it were intrinsically difficult to formulate the CPF problem, then it would not be useful in practice. Likewise, if the formulation of the CPF problem were to require highly specialized knowledge or expertise, its utility would be limited. Therefore, in this chapter we will present a simple procedure which a designer can use to determine whether she should consider using the CPF problem formulation, and if so, criteria to determine the type of CPF to be used.

An overview of the CPF selection process will be given in Section 5.2. In Section 5.3, the mathematical model of a MEMS actuator and its controller will be developed and presented. Two different co-design problems for the MEMS actuator will then be formulated and solved in Sections 5.4 and 5.5, using the approach presented in Section 5.2. In both cases, uni-directional coupling is found to be present, and an appropriate CPF will

be chosen for each case. In the first case, a suitable CPF can be formulated based on either the natural frequency or the controllability Grammian. However, for the second problem a CPF based on natural frequency is not suitable, while one based on the controllability Grammian is effective. The actuator model and control architecture will be identical in both cases, with changes made only to the objectives, constraints, and design variables.

5.2 Overview of Design Process Using a CPF

The process used to decide whether a CPF problem formulation is feasible for a given co-design problem, shown in Fig. 5.1, is performed as follows:

STEP 1: Problem Formulation

The process begins with the formulation of the co-design problem in the form of Eqs. (1.9)-(1.13). In this step, the artifact and control objectives, f_a and f_c, are chosen, the system model is developed, artifact and control design variables, $\boldsymbol{d}_a$ and $\boldsymbol{d}_c$, are chosen, and artifact and controller inequality and equality constraints, $\boldsymbol{g}_a$, $\boldsymbol{h}_a$, $\boldsymbol{g}_c$, and $\boldsymbol{h}_c$, are formulated.

STEP 2: Evaluation for Bi-Directional Coupling

After problem formulation, the designer evaluates the co-design problem to determine whether or not bi-directional coupling is present. If the artifact objective function, f_a, or any of the constraints, $\boldsymbol{g}_a$ and $\boldsymbol{h}_a$, are functions of any of the control design variables, $\boldsymbol{d}_c$, then bi-directional coupling exists, based on the definition given in Section 1.3.1. In this case, the CPF method does not apply, and the optimization should be performed using one of the methods discussed in Section 1.2.

STEP 3: Evaluation for Uni-Directional Coupling

If the co-design problem does not exhibit bi-directional coupling, then the designer

evaluates the problem to determine whether it exhibits uni-directional coupling. This evaluation is a two-step process; first, the control objective function, f_c, and constraints, $\boldsymbol{g}_c$ and $\boldsymbol{h}_c$, are examined to determine whether they are functions of any of the artifact design variables, $\boldsymbol{d}_a$. If they are not, i.e., if $f_c = f_c(\boldsymbol{d}_c)$, $\boldsymbol{g}_c = \boldsymbol{g}_c(\boldsymbol{d}_c)$, and $\boldsymbol{h}_c = \boldsymbol{h}_c(\boldsymbol{d}_c)$, then the problem is uncoupled, and should be solved with a simple sequential optimization.

If $f_c = f_c(\boldsymbol{d}_a, \boldsymbol{d}_c)$, $\boldsymbol{g}_c = \boldsymbol{g}_c(\boldsymbol{d}_a, \boldsymbol{d}_c)$, or $\boldsymbol{h}_c = \boldsymbol{h}_c(\boldsymbol{d}_a, \boldsymbol{d}_c)$, the problem may still decouple under certain conditions. In Chapter III, conditions were presented under which a co-design problem will decouple. It is, therefore, necessary to check the co-design problem to determine whether it satisfies any of these decoupling conditions, as discussed in Chapter III (see Eqs. (3.12), (3.30), (3.44)). If it does satisfy one of these conditions, then the coupling will vanish, and the problem can be solved using sequential optimization. If the problem does not satisfy any of the decoupling conditions, then it is considered to exhibit uni-directional coupling, and the CPF solution method can be considered.

STEP 4: Evaluation of Suitability of CPF Method

Any co-design problem with uni-directional coupling could be formulated as a CPF problem. However, in order to formulate a CPF problem that is effective at finding optimal (or near-optimal) solutions, one must be able to specify an appropriate CPF. This can be done in one of two ways, as indicated in Fig. 5.1. First, the problem may be of a type for which a CPF has already been developed. In this case, the designer simply has to determine that the problem is of the appropriate type, and she can use that CPF. The CPFs that were developed in Chapter IV are listed in Table 5.1, along with the conditions required to use them. These CPFs and their conditions for use are briefly re-stated in this section. Since this list is not exhaustive, it is anticipated that more CPFs will be developed, and the range of problems amenable to solution with existing CPFs will increase.

If a CPF, such as those listed in Table 5.1, has not been developed for a given problem, then the designer may consider formulating one. If the control objective function $f_c(\boldsymbol{d}_a, \boldsymbol{d}_c)$

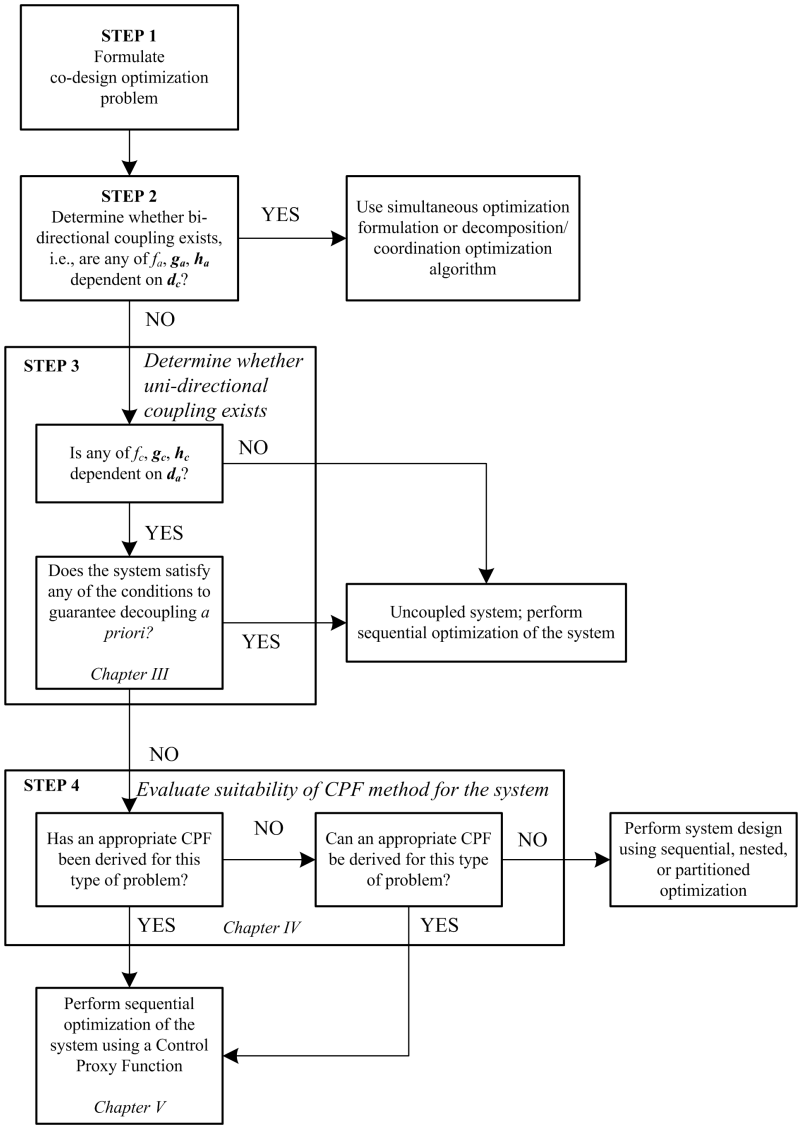

Figure 5.1: Choice of Solution Method for Co-Design Problems

is clearly monotonic, or is known to have an unconstrained minimum in the $\boldsymbol{d}_a$-space, then it may be possible to use this information to formulate a CPF for the problem based on Theorems 4.3 and 4.4.

As stated in Chapter IV, all of the CPFs that have been developed assume that the system dynamics can be modeled as linear and time-invariant. In the case of a CPF based on natural frequency, there is an additional assumption that system is second-order. This

Table 5.1: Control Proxy Functions (CPFs) and Conditions for Use (See Eqs. (4.38), (4.35), (4.44), (4.45), (4.43), (3.4), and (3.5) for the definitions of $\boldsymbol{B}$, b, ω_c, ζ_c, ζ_n, $\boldsymbol{W}_c\left(t_f\right)$, and $\boldsymbol{W}_c^{\infty}$, respectively.)

Control Proxy Function, χ	**Conditions for Use**
CPF Based on Natural Frequency (for second-order dynamics)	
$\chi = \dfrac{1}{\omega_n}$ or $\chi = -\omega_n$	$\dfrac{\partial \boldsymbol{B}}{\partial d_{a_i}} = \boldsymbol{0}\ \forall\ i = 1,\ldots,n$ $f_c = f_c\left(\omega_c\right)$
	$\dfrac{\partial \boldsymbol{B}}{\partial d_{a_i}} = \boldsymbol{0}\ \forall\ i = 1,\ldots,n$ $f_c = f_c\left(\omega_c \zeta_c\right)$ $\dfrac{\partial \zeta_n}{\partial \boldsymbol{d}_a} = \boldsymbol{0}$
	$\dfrac{\partial \boldsymbol{B}}{\partial d_{a_i}} = \boldsymbol{0}\ \forall\ i = 1,\ldots,n$ $\dfrac{\partial b}{\partial \boldsymbol{d}_a} = \boldsymbol{0}$
CPFs Based on Controllability Grammian Matrix	
$\chi = \dfrac{\mathrm{tr}\left(\boldsymbol{W}_c\left(t_f\right)\right)}{\det\left(\boldsymbol{W}_c\left(t_f\right)\right)}$	$f_c = \int_0^{t_f} \left(u\left(t\right)\right)^2 dt$, where t_f is a parameter $\boldsymbol{W}_c\left(t_f\right)$ is diagonal $x_{f_i} = \alpha\ \forall\ i = 1,\ldots,q$, where α is a parameter
	$f_c = t_f$ $g_c = \int_0^{t_f} \left(u\left(t\right)\right)^2 dt - E_{max} \leq 0$ $\boldsymbol{W}_c\left(t_f\right)$ is diagonal $x_{f_i} = \alpha\ \forall\ i = 1,\ldots,q$, where α is a parameter
$\chi = \dfrac{W_{c_{jj}}^{*}\left(t_f\right)}{\det\left(\boldsymbol{W}_c\left(t_f\right)\right)}$	$f_c = \int_0^{t_f} \left(u\left(t\right)\right)^2 dt$, where t_f is a parameter $\boldsymbol{W}_c\left(t_f\right)$ is diagonal $x_{f_i} = 0\ \forall\ i = 1,\ldots,q,\ i \neq j, x_{f_j} = \alpha$, where α is a parameter
	$f_c = t_f$ $g_c = \int_0^{t_f} \left(u\left(t\right)\right)^2 dt - E_{max} \leq 0$ $\boldsymbol{W}_c\left(t_f\right)$ is diagonal $x_{f_i} = 0\ \forall\ i = 1,\ldots,q,\ i \neq j, x_{f_j} = \alpha$, where α is a parameter
$\chi = \boldsymbol{W}_{c_{jj}}^{\infty}$	LQR control is to be applied $\boldsymbol{A} \neq \boldsymbol{A}\left(\boldsymbol{d}_a\right)$ $x_{0_i} = 0\ \forall\ i = 1,\ldots,q,\ i \neq j, x_{0_j} = \alpha$, where α is a parameter $\boldsymbol{W}_c^{\infty}$ is diagonal

assumption is not made for CPFs based on the controllability Grammian, which apply to systems of arbitrary order. The CPFs derived in Chapter IV and given in Table 5.1 are briefly summarized here.

CPF Based on Natural Frequency

As shown in Chapter IV, a CPF based on natural frequency can be effective in some cases. Here, three sets of conditions are presented in which this type of CPF is appropriate. If any of the three sets of conditions in Table 5.1 is satisfied, then a CPF of either $\chi = \frac{1}{\omega_n}$ or $\chi = -\omega_n$ will provide Pareto optimal solutions to the co-design problem. If any set of conditions is 'almost' satisfied, then a CPF based on natural frequency can be expected to yield solutions that are near-optimal.

The first set of conditions under which natural frequency is appropriate is the case where the matrix $\boldsymbol{B}$, as defined in Eq. (4.36), is invariant with respect to the design variables $\boldsymbol{d}_a$ and the control objective function depends only on the frequency of the controlled system, ω_c. In this situation, the free response of the system is dependent on $\boldsymbol{d}_a$, but the forced response is invariant with $\boldsymbol{d}_a$. One example of this type of objective would be the rise time of a system, which is given by the relation $t_r = \frac{1.8}{\omega_c}$.

In the second set of conditions under which natural frequency is appropriate, the matrix $\boldsymbol{B}$ and the damping of the uncontrolled system, ζ_n, are invariant with respect to the design variables $\boldsymbol{d}_a$, and the objective function f_c is a function of the real part of the eigenvalues of the controlled system. One example of this type of objective would be the settling time of a system, which is given by the relation $t_s = \frac{4}{\zeta_c \omega_c}$.

In the third set of conditions for the use of natural frequency as a CPF, the matrix $\boldsymbol{B}$ and the damping term b of the differential equation given by Eq. (4.35), are invariant with respect to the design variables $\boldsymbol{d}_a$. In this situation, the control objective can be an arbitrary function of the controlled system frequency and damping, ω_c and ζ_c.

CPF Based on Controllability Grammian Matrix

Three distinct CPFs are presented in Table 5.1 based on the controllability Grammian matrix. Two of those CPFs are valid for more than one set of conditions, while the third CPF is only valid for one set of conditions. They are briefly summarized here.

A CPF based on the trace and determinant of the time-dependent controllability matrix, $\chi = \dfrac{\text{tr}\left(\boldsymbol{W}_c\left(t_f\right)\right)}{\det\left(\boldsymbol{W}_c\left(t_f\right)\right)}$, can be used in either of two sets of conditions. In both sets of conditions, the matrix $\boldsymbol{W}_c\left(t_f\right)$ is diagonal, which will occur when the balanced realization is used. Also in both cases, the final state for the system is a parameter for which all of its components are equal. This can occur when the states comprising the vector $\boldsymbol{x}_f$ are all positions, and every component of the system is to be moved to the same position. The difference between the two sets of conditions for this CPF is seen in the role of the control effort; in one set of conditions, the control objective function is the control effort, while the other set of conditions is based on a constraint on the control effort. In that case, the control objective is the final time at which the system reaches the state $\boldsymbol{x}_f$.

A CPF based on a single value of the adjoint matrix, $\boldsymbol{W}_c^*\left(t_f\right)$, and on the determinant of the time-dependent controllability Grammian matrix, $\boldsymbol{W}_c\left(t_f\right)$, is formulated as $\chi = \dfrac{W_{c_{jj}}^*}{\det\left(\boldsymbol{W}_c\left(t_f\right)\right)}$. This CPF is also valid under two separate sets of circumstances. In both sets of conditions, the matrix $\boldsymbol{W}_c\left(t_f\right)$ is diagonal. Also in both cases, the final state of the system is a parameter, where only one component of $\boldsymbol{x}_f$ is non-zero. As an example of this situation, consider the case where a system is to be moved to a specified location, at which it is to be at rest. The location of the system is given by the non-zero component of $\boldsymbol{x}_f$, while the remaining components represent velocities, which must be zero. Again, the difference between the two sets of conditions for this CPF is seen in the role of the control effort; in one set of conditions, the control objective function is the control effort, while the other set of conditions is based on a constraint on the control effort. In that case, the control objective is the final time at which the system reaches the state $\boldsymbol{x}_f$.

The final CPF developed in Chapter IV and given in Table 5.1 is valid only under one

set of conditions, which includes the use of Linear Quadratic Regulator (LQR) control. This CPF, which depends on the steady-state controllability Grammian matrix, is given by $\chi = W_{c_{jj}}^{\infty}$. It is, again, required that the controllability Grammian matrix must be diagonal. In addition, it is required that the matrix $\boldsymbol{A}$ in Eq. (4.36) is invariant with respect to $\boldsymbol{d}_a$, and that only one component of the initial system state, $\boldsymbol{x}_0$, is non-zero. This state must also be a parameter. This would represent the situation where the forced response of the system is dependent on the artifact design variables, while the free response is invariant, and where the system starts at a given position at rest, and is to be brought to the zero position at rest.

Full details on the development of these CPFs were given in Section 4.3.

5.3 MEMS Actuator and Controller Case Study

The MEMS actuator considered in this case study was originally designed by Tung and Kurabayashi [*Tung and Kurabayashi* (2005)] and is shown in Fig. 5.2. The actuator utilizes four electrostatic comb-drive actuators to produce an out-of-plane displacement. The actuator can be used to produce an angular deflection of the platform as well, but here only the vertical displacement of the platform is considered. In order to produce this displacement, each of the four comb drives is excited with a voltage, V, resulting in horizontal (in-plane) movement (ΔX) of the silicon shuttles. The micro-hinges on the polydimethyl siloxane (PDMS) platform bend as shown in Fig. 5.3, and the platform moves vertically, or out-of-plane (ΔZ). The amount of movement resulting from the comb drives' actuation depends on both the applied voltage, V, and the physical dimensions of the actuator. Changing the actuator's dimensions results in a different output displacement for the same applied voltage.

The displacement of the actuator, ΔZ, is given by the equation

$$\Delta Z = (h_1 + h_2)(1 - \cos\Delta\theta) + (t + p)\sin\Delta\theta \tag{5.1}$$

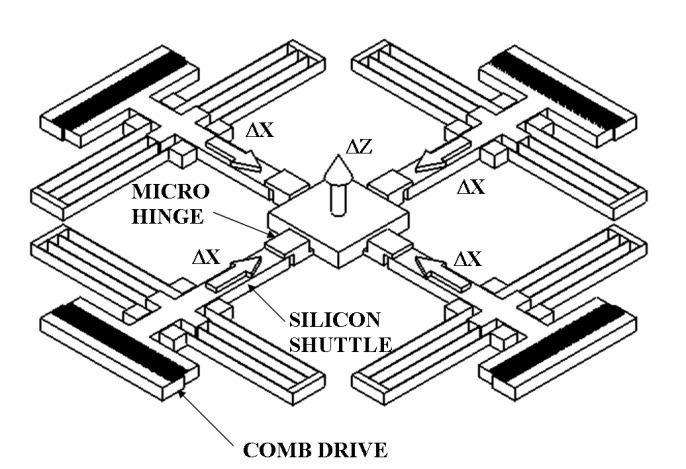

Figure 5.2: MEMS Actuator Configuration

where p, t, h_1, and h_2 are the hinge dimensions shown in Fig. 5.4, and $\Delta\theta$ is the angular displacement of the hinge. Eq. 5.1 is derived in Appendix B.

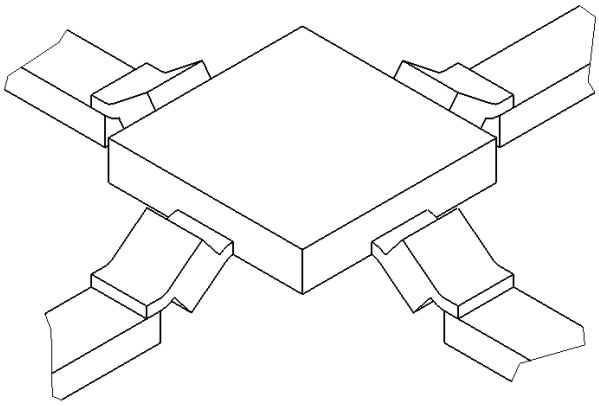

Figure 5.3: Hinge Actuation

The angular displacement $\Delta\theta$ can be found from the differential equation

$$M\Delta\ddot{\theta} + C\Delta\dot{\theta} + K\Delta\theta = A(\Delta\theta)V^2 \tag{5.2}$$

where M, C, K, and $A(\Delta\theta)$ are functions of the actuator geometry, as given in Eqs. (5.3) - (5.6) below. Derivations, and the equations for the masses and stiffnesses M_{Si}, M_{PDMS},

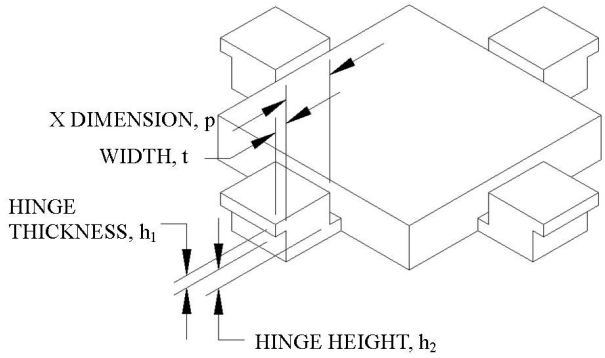

Figure 5.4: Micro-Hinge Structure

M_{hinge}, K_{Si}, and K_{PDMS}, are given in [*Tung and Kurabayashi* (2005)] and in Appendix B.

$$M = M_{Si}(h_1+h_2)^2 + M_{PDMS}(t+p)^2 + \frac{1}{3}M_{hinge}\left((h_1+h_2)^2+(t+p)^2\right) \quad (5.3)$$

$$C = 2\zeta\sqrt{\left(M_{Si}(h_1+h_2)^2 + M_{PDMS}(t+p)^2\right)\left(K_{Si}(h_1+h_2)^2 + 2K_{PDMS}\right)} \quad (5.4)$$

$$K = K_{Si}(h_1+h_2)^2 + 2K_{PDMS} \quad (5.5)$$

$$A(\Delta\theta) = \frac{n\varepsilon_o(h_1+h_2)}{d}\left((h_1+h_2)-(t+p)\Delta\theta\right) \quad (5.6)$$

where ζ is an experimentally determined parameter, n is the number of fingers in the comb drive, ε_o is the permittivity of vacuum, and d is the width of a finger, as shown in Fig. 5.5.

Alternatively, the system dynamics may be written in state-space form as

$$\begin{bmatrix} \Delta\dot{\theta} \\ \Delta\ddot{\theta} \end{bmatrix} = \begin{bmatrix} 0 & 1 \\ -K/M & -C/M \end{bmatrix}\begin{bmatrix} \Delta\theta \\ \Delta\dot{\theta} \end{bmatrix} + \begin{bmatrix} 0 \\ A(\Delta\theta)/M \end{bmatrix} V^2 \quad (5.7)$$

An integral controller with state feedback is applied to the system, as shown in Fig. 5.6. It is assumed that the angle $\Delta\theta$ and the angular velocity $\Delta\dot{\theta}$ can be measured, and that the angle $\Delta\theta$ is to be controlled. The dynamics of the closed-loop system can then be written

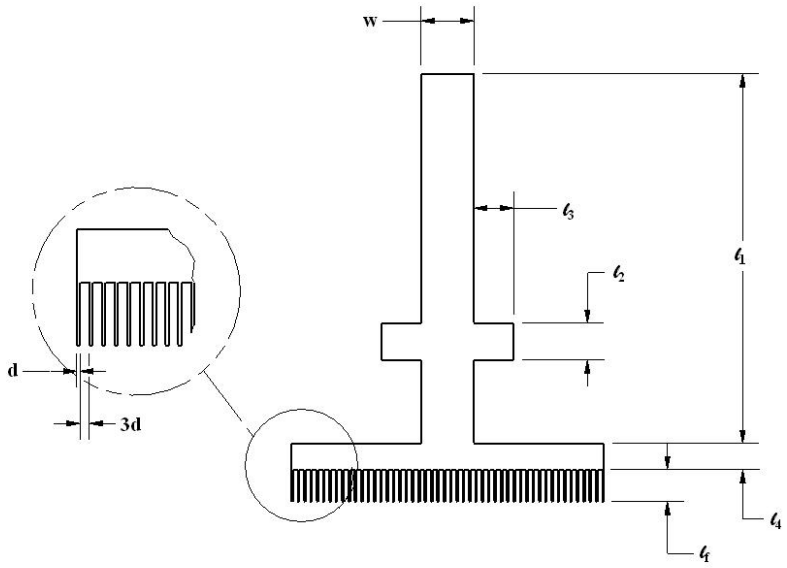

Figure 5.5: Plan View of Silicon Shuttle

as

$$M\Delta\ddot{\theta} + (C + K_2 A(\Delta\theta))\Delta\dot{\theta} + (K + K_1 A(\Delta\theta))\Delta\theta - K_i A(\Delta\theta)\int_0^t (\Delta\theta_r - \Delta\theta)\, d\tau \qquad (5.8)$$

Note that the controller output is $u = V^2$, and that the coefficient A in Eq. (5.2) is a function of $\Delta\theta$. Thus, the resulting controller design problem is non-linear.

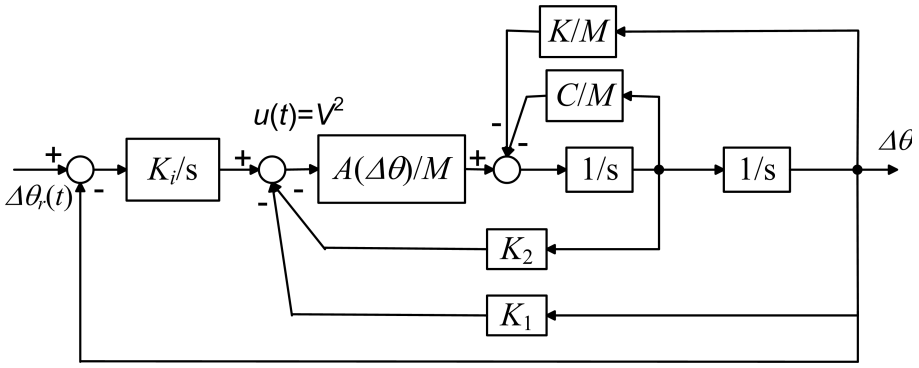

Figure 5.6: Control Architecture and System Dynamics

5.4 Co-Design of MEMS Actuator for Steady-State Displacement and Settling Time

Using the system described above, one can follow the procedure outlined in Fig. 5.1 to formulate a co-design optimization problem and choose an appropriate method of solution.

STEP 1: Problem Formulation

In this problem formulation, the goal is to maximize the steady-state displacement of the actuator, ΔZ_{ss}, and minimize the 1% settling time, t_s, as given in Eqs. (5.9) - (5.10). The artifact constraints, given by Eqs. (5.11) - (5.16), are based on manufacturability, stress, kinematics, and mechanical and electrical stability. Detailed derivations of the relevant equations are given in Appendix B. The control constraints, given by Eqs. (5.21) - (5.22), are formulated to limit the overshoot, M_p, and the maximum voltage, V_{max}. The control objective function and constraints are calculated by numerical integration and implemented in a Simulink model. The artifact design variables, $\boldsymbol{d}_a$, are selected to be the hinge dimensions p, t, h_1, and h_2, as shown in Fig. 5.4. These artifact design variables are given the bounds in Eqs. (5.17) - (5.20). The control design variables are the gains K_1, K_2, and K_i.

$$f_a = -\Delta Z_{ss} \tag{5.9}$$

$$f_c = t_s \tag{5.10}$$

$$g_{a_1} = t - 5h_1 \leq 0 \tag{5.11}$$

$$g_{a_2} = 910 - l_1 - \frac{l_p}{2} - 2t + \frac{\Delta X_{ss}}{2} \leq 0 \tag{5.12}$$

$$g_{a_3} = \frac{n\varepsilon_o (h_1 + h_2) V_{ss}^2}{d} - \frac{k_b \pi^2 E_{PDMS} w (2h_1 + h_2)^3}{12p^2} \leq 0 \tag{5.13}$$

$$g_{a_4} = \Delta X_{ss} - \left(\frac{l_{Si}}{\sqrt{2}} - \frac{l_{f_o}}{2} \right) \leq 0 \tag{5.14}$$

$$g_{a_5} = \frac{E_{PDMS} h_1 \Delta\theta_{ss}}{2p} - \sigma_{PDMS_{max}} \leq 0 \tag{5.15}$$

$$g_{a_6} = \frac{3\Delta X_{ss} E_{Si} b}{4 l_{Si}^2} - \sigma_{Si_{max}} \leq 0 \tag{5.16}$$

where l_p is the length of the platform, k_b is the beam end condition coefficient, E_{PDMS} is Young's modulus for PDMS, l_{Si} is the length of the silicon springs, l_{fo} is the initial finger engagement, E_{Si} is Young's modulus for silicon, and $\sigma_{PDMS_{max}}$ and $\sigma_{Si_{max}}$ are maximum allowable stresses in PDMS and silicon, respectively.

$$1\ \mu\text{m} \leq p \leq 1000\ \mu\text{m} \tag{5.17}$$

$$1\ \mu\text{m} \leq t \leq 1000\ \mu\text{m} \tag{5.18}$$

$$6\ \mu\text{m} \leq h_1 \leq 1000\ \mu\text{m} \tag{5.19}$$

$$6\ \mu\text{m} \leq h_2 \leq 1000\ \mu\text{m} \tag{5.20}$$

$$g_{c_1} = M_p - 0.05 \leq 0 \tag{5.21}$$

$$g_{c_2} = V_{max} - 25 \leq 0 \tag{5.22}$$

All other dimensions and physical properties of the actuator are parameters; in addition, the steady-state voltage, V_{ss}, is a parameter. Values of the parameters are given in Table 5.2.

STEP 2: Evaluation for Bi-Directional Coupling

The problem can be evaluated to determine whether bi-directional coupling is present. The functions f_a and $\boldsymbol{g}_a$ (see Eqs. (5.9) and (5.11) - (5.16)) are not dependent on the control design variables (i.e., K_1, K_2, K_i). Therefore, bi-directional coupling does not exist. Note,

Table 5.2: Parameter Values for MEMS Actuator

Parameter	**Value**
ε_o	8.854e-12 F/m
E_{PDMS}	750 KPa
E_{Si}	190 GPa
ρ_{PDMS}	1.05 g/cm^3
ρ_{Si}	2.44 g/cm^3
$\sigma_{Si_{max}}$	1.5 GPa
$\sigma_{PDMS_{max}}$	2.24 MPa
n	50
d	3 μm
b	3 μm
l_{Si}	500 μm
l_p	350 μm
l_f	50 μm
l_1	700 μm
l_2	70 μm
l_3	75 μm
l_4	50 μm
w	100 μm
ζ	0.1

Table 5.3: Original Design of MEMS Actuator [*Tung and Kurabayashi* (2005)]

Variable	Value (μm)
p	80
t	20
h_1	20
h_2	30

however, that an alternative problem formulation in which V_{ss} was not fixed as a parameter would exhibit bi-directional coupling.

STEP 3: Evaluation for Uni-Directional Coupling

Next, the problem is evaluated to determine whether uni-directional coupling exists. While explicit relations for f_c (see Eq. (5.10)) and $\boldsymbol{g}_c$ (see Eq. (5.21) - (5.22)) are not given, it is clear that the simulation which calculates them depends on M, C, K, and $A(\Delta\theta)$, and through them, on the artifact design variables, $\boldsymbol{d}_a$. Therefore, $f_c = f_c(\boldsymbol{d}_a, \boldsymbol{d}_c)$ and $\boldsymbol{g}_c = \boldsymbol{g}_c(\boldsymbol{d}_a, \boldsymbol{d}_c)$.

The problem is then examined to determine whether or not any of the decoupling conditions in Chapter III, as given by Eqs. (3.12), (3.30), and (3.44), are applicable. This problem formulation does not match the formulations in any of Cases I, II, or III, and therefore these conditions do not apply. Thus, the problem is presumed to exhibit uni-directional coupling, and is a candidate for solution with the CPF method.

STEP 4: Evaluation of Suitability of CPF Method

Now, consider whether one of the CPFs listed in Table 5.1 would be effective in solving this problem. Begin this evaluation by noting that the MEMS actuator is modeled as a second-order system. Since this is one of the necessary conditions for the use of natural frequency, one can consider whether natural frequency will be an effective CPF.

For this problem, the matrix $\boldsymbol{B}$ for the state-space formulation described in Eq. (4.36)

is given by

$$\boldsymbol{B} = \begin{bmatrix} 0 \\ A(\Delta\theta)/M \end{bmatrix} \tag{5.23}$$

and its derivatives relative to the artifact design variables are given by Eq. (5.24) - (5.27). These derivatives are evaluated at the values of p, t, h_1, and h_2 given in Table 5.3, corresponding to the original design [*Tung and Kurabayashi* (2005)]. This point is used because it is known to be a feasible design.

$$\frac{\partial \boldsymbol{B}}{\partial p} = \begin{bmatrix} 0 \\ 46 \end{bmatrix} \tag{5.24}$$

$$\frac{\partial \boldsymbol{B}}{\partial t} = \begin{bmatrix} 0 \\ 46 \end{bmatrix} \tag{5.25}$$

$$\frac{\partial \boldsymbol{B}}{\partial h_1} = \begin{bmatrix} 0 \\ -42 \end{bmatrix} \tag{5.26}$$

$$\frac{\partial \boldsymbol{B}}{\partial h_2} = \begin{bmatrix} 0 \\ 20 \end{bmatrix} \tag{5.27}$$

It is obvious that the values in Eqs. (5.24) - (5.27) are non-zero. However, if they are small, then it may be reasonable to regard them as negligible. This raises the question of what constitutes 'small' in a given problem. As an example, it is possible to change the values of these derivatives by orders of magnitude simply by scaling the problem. Therefore, some standard of comparison must be used to determine whether the derivatives of the matrix $\boldsymbol{B}$ are negligible. In order to determine whether they can be considered small, the derivatives of the matrix $\boldsymbol{A}$ are computed for the state-space formulation described in

Eq. (4.36), which is given by

$$\boldsymbol{A} = \begin{bmatrix} 0 & 1 \\ -K/M & -C/M \end{bmatrix} \tag{5.28}$$

These derivatives are also evaluated at the values in Table 5.3, and are given in Eqs. (5.29) - (5.32).

$$\frac{\partial \boldsymbol{A}}{\partial p} = \begin{bmatrix} 0 & 0 \\ 3.5e6 & 6.8e4 \end{bmatrix} \tag{5.29}$$

$$\frac{\partial \boldsymbol{A}}{\partial t} = \begin{bmatrix} 0 & 0 \\ 5.0e6 & 4.2e4 \end{bmatrix} \tag{5.30}$$

$$\frac{\partial \boldsymbol{A}}{\partial h_1} = \begin{bmatrix} 0 & 0 \\ -1.6e7 & 8.4e5 \end{bmatrix} \tag{5.31}$$

$$\frac{\partial \boldsymbol{A}}{\partial h_2} = \begin{bmatrix} 0 & 0 \\ -2.3e6 & 4.8e5 \end{bmatrix} \tag{5.32}$$

The values of $\frac{\partial \boldsymbol{B}}{\partial d_{a_i}}$ are several orders of magnitude smaller than $\frac{\partial \boldsymbol{A}}{\partial d_{a_i}}$. Therefore, it will be assumed that they are negligible, and the possible use of natural frequency as a CPF will be further evaluated.

The control objective function, $f_c = t_s = \frac{4.6}{\zeta_c \omega_c}$, as given in Eq. (5.10), is a function of the product $\zeta_c \omega_c$, which is among the second set of conditions for use of natural frequency as a CPF. Therefore, the derivatives of the open-loop damping are evaluated to determine whether or not this set of conditions is satisfied.

The derivatives of the open-loop damping coefficient, ζ_n, are calculated for each of the

artifact design variables, and found to be

$$\frac{\partial \zeta_n}{\partial p} = -1.3e-5 \tag{5.33}$$

$$\frac{\partial \zeta_n}{\partial t} = -7.0e-6 \tag{5.34}$$

$$\frac{\partial \zeta_n}{\partial h_1} = -2.3e-5 \tag{5.35}$$

$$\frac{\partial \zeta_n}{\partial h_2} = -8.0e-6 \tag{5.36}$$

where the artifact design variables p, t, h_1, and h_2 are measured in microns. The values of these derivatives may be considered negligible, and therefore the system closely approximates the second set of conditions for use of natural frequency as a CPF, as described in Table 5.1. Based on this analysis, then, the co-design problem will be formulated as a CPF problem utilizing the natural frequency of the system.

5.4.1 Optimization Using Natural Frequency

As stated in Section 4.1, there are a number of different ways to approach bi-objective optimization problems. One simple approach is to treat one objective as a constraint, exploring the trade-off by varying the constraint bound in a parametric study [*Papalambros and Wilde* (2000)]. This approach will be used to formulate the CPF problem, with the additional constraint given by

$$g_{a_7} = \omega_{min} - \omega_n \leq 0 \tag{5.37}$$

where

$$\omega_n = \sqrt{\frac{K}{M}} \tag{5.38}$$

and the minimum allowable frequency, ω_{min}, will be set based on an operating frequency, ω_o [*Peters et al.* (2008)].

$$\omega_{min} = 1.1\omega_o \tag{5.39}$$

Table 5.4: Sequential Optimization Results Using Natural Frequency

ω_o (rad/s)	p (μm)	t (μm)	h_1 (μm)	h_2 (μm)	K_1	K_2	K_i	ΔZ_{ss} (μm)	t_s (ms)
500	599	30	6	53	4.01e5	48.4	1.54e9	6.79	0.568
750	400	30	6	51	3.62e5	34.4	1.81e9	4.93	0.470
1000	296	30	6	51	3.02e5	23.7	1.87e9	3.84	0.387
1250	234	30	6	52	2.88e5	15.3	2.55e9	3.11	0.248
1500	189	30	6	52	3.12e5	13.4	3.39e9	2.57	0.201
1750	155	30	6	54	2.87e5	11.2	3.49e9	2.15	0.182
2000	126	30	6	54	2.53e5	9.10	3.40e9	1.80	0.166
2250	100	30	6	54	2.36e5	8.17	3.41e9	1.50	0.158
2500	73	30	6	53	2.17e5	6.76	3.46e9	1.23	0.142

Therefore, the CPF problem will be formulated as

$$\min_{p,t,h_1,h_2} \quad f_a \tag{5.40}$$

$$\text{subject to} \quad \boldsymbol{g}_a(p,t,h_1,h_2) \leq \mathbf{0} \tag{5.41}$$

where $f_a = -\Delta Z_{ss}$, as given by Eq. (5.9), and the constraints $\boldsymbol{g}_a$ are given by Eqs. (5.11) - (5.16) and (5.37); followed by

$$\min_{K_1,K_2,K_i} \quad f_c \tag{5.42}$$

$$\text{subject to} \quad \boldsymbol{g}_c \leq \mathbf{0} \tag{5.43}$$

where $f_c = t_s$, as given by Eq. (5.10), and the constraints $\boldsymbol{g}_c$ are given by Eqs. (5.21) - (5.22). The optimization is carried out for different values of the minimum frequency, ω_{min}, as presented in [*Peters et al.* (2008)]. The different designs produced by the optimization are given in Table 5.4.

Once these points have been generated for the CPF problem, it is possible to consider whether, as expected, they match the Pareto frontier of the co-design problem. The simultaneous problem was solved, as detailed in [*Peters et al.* (2008)]. The objectives f_a and f_c were combined using the exponential weighted criteria method, as shown in Eq. (5.44)

[*Athan* (1994)]. This method was used due to the non-convex nature of the Pareto frontier; as stated in Section 1.5.3, a linear combination of objectives is not appropriate in this case. However, as shown in Section 2.6.1, the relationships derived in Chapters III and IV are still valid.

$$f = (e^{w_1} - 1)\, e^{-\Delta Z_{ss}} + (e^{w_2} - 1)\, e^{t_s} \tag{5.44}$$

The results of the simultaneous optimization problem and of the CPF problem are compared in Fig. 5.7. It can be seen that the CPF problem produces results that are indistinguishable from the Pareto frontier, visualized from the Pareto points generated by simultaneous optimization.

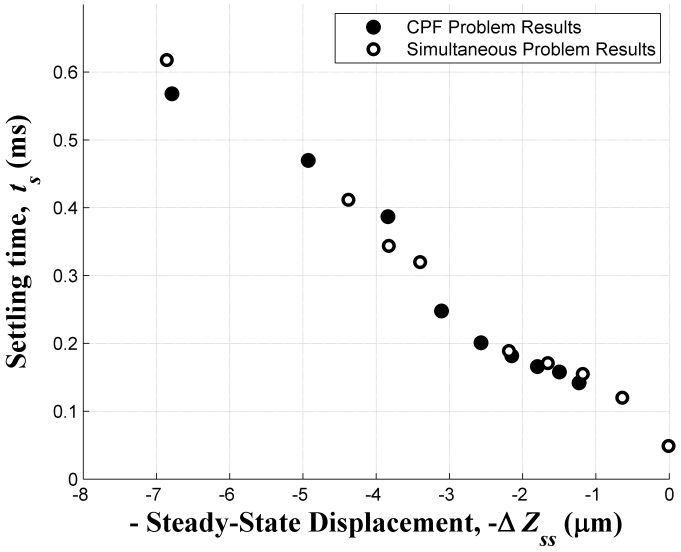

Figure 5.7: Comparison of CPF Points and Simultaneous Optimization Points for Frequency-Based CPF

Note that the CPF problem formulation is a less computationally intensive method to solve the problem. The computational cost of a simultaneous optimization formulation is typically higher than a sequential formulation [*Balling and Sobieszczanski-Sobieski* (1996)]. This problem provides an example of this. For a typical CPF point, 68 function

calls are required for the artifact optimization, and 59 function calls for the control optimization, with only the control optimization involving simulation. By contrast, generation of a typical point for the simultaneous optimization problem requires 137 function calls for both problems' functions, all of which require simulation [*Peters et al.* (2008)]. The CPF method, then, requires approximately half as many simulations as the simultaneous optimization, resulting in a more computationally efficient process.

5.4.2 Optimization Using Controllability Grammian

While the use of natural frequency was clearly effective in this problem, it is important to note that it is not necessarily the only possible CPF for the problem. Suppose that the control objective had not yet been formulated when the CPF was chosen, and therefore the CPF was chosen based only on the knowledge that the system would need to be controllable. Instead of constraining the natural frequency, consider the use of a constraint on the determinant of the steady-state controllability Grammian, i.e.,

$$g_{a_7} = D - \det \boldsymbol{W}_c^{\infty} \leq 0 \tag{5.45}$$

where the value of D is varied to produce a set of designs. Since there is no obvious means to determine the appropriate value of D, its initial value can be chosen by finding the controllability Grammian for the initial design, as given in Table 5.3. Then, D can be varied about that value. The CPF problem is then formulated as

$$\min_{p,t,h_1,h_2} \quad f_a \tag{5.46}$$

$$\text{subject to} \quad \boldsymbol{g}_a(p,t,h_1,h_2) \leq \boldsymbol{0} \tag{5.47}$$

where $f_a = -\Delta Z_{ss}$, as given by Eq. (5.9), and the constraints $\boldsymbol{g}_a$ are given by Eqs. (5.11) - (5.16) and (5.45); followed by

$$\min_{K_1,K_2,K_i} \quad f_c \tag{5.48}$$

$$\text{subject to} \quad \boldsymbol{g}_c \leq \mathbf{0} \tag{5.49}$$

where $f_c = t_s$, as given by Eq. (5.10), and the constraints $\boldsymbol{g}_c$ are given by Eqs. (5.21) - (5.22).

The results of this optimization are shown in Fig. 5.8. These CPF points are close to the Pareto frontier, though they do not all lie exactly on the frontier.

While Table 5.1 does not indicate that a CPF based on the controllability Grammian would be effective for this problem, its effectiveness could be predicted. Numerical simulations of the controlled system show that t_s is monotonic with respect to p, the variable which changes the most from one design to the next. Therefore, by Theorem 4.3, it can be predicted that a CPF with the same monotonicity with respect to p could be effective. The determinant of $\boldsymbol{W}_c^{\infty}$, which was chosen as the CPF for this problem, has the same monotonicity with respect to p as t_s exhibits, suggesting that it may be effective. The monotonicity of h_2 is more difficult to analyze, but simulations show that the effect of h_2 on both t_s and $\det \boldsymbol{W}_c^{\infty}$ is minimal. Therefore, this CPF would be expected to produce near-optimal results, as verified by the results in Fig. 5.8.

5.5 Co-Design of MEMS Actuator for Final Displacement and Control Effort

In this section, a new optimization problem for the same system is formulated, again following the procedure outlined in Fig. 5.1.

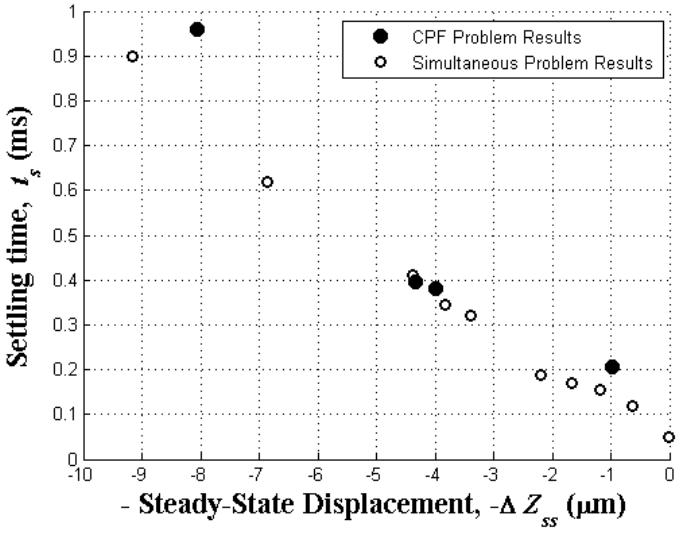

Figure 5.8: Comparison of CPF Points and Simultaneous Optimization Points for Controllability-Based CPF

STEP 1: Problem Formulation

In this problem formulation, the goal is to maximize the final displacement of the actuator, ΔZ_f, at a given time t_f, where ΔZ_f is the peak displacement and is 5% higher than the steady-state displacement, ΔZ_{ss}. We also wish to minimize the control effort used to achieve this. The artifact and control objective functions are given in Eqs. (5.50) - (5.51).

$$f_a = -\Delta Z_f = -1.05\Delta Z_{ss} \tag{5.50}$$

$$f_c = \int_0^{t_f} (u(t))^2 \, dt = \int_0^{t_f} (V(t))^4 \, dt \tag{5.51}$$

$$100\ \mu\text{m} \leq l_1 \leq 1000\ \mu\text{m} \tag{5.52}$$

where ΔZ_{ss} can be found from Eq. (5.1). The artifact constraints are identical to those for the problem formulated in Section 5.4, and are given by Eqs. (5.11) - (5.16). No control constraints are present. The artifact design variables, $\boldsymbol{d}_a$, are selected to be p, t, and l_1, and

are given the bounds in Eqs. (5.17), (5.18), and (5.52). The control design variables are, again, the gains K_1, K_2, and K_i. Note that the artifact design variable l_1 does not appear in either the artifact objective function, f_a, or in the artifact inequality constraints, $\boldsymbol{g}_a$. It is expected, therefore, that it will either be irrelevant to the co-design problem or will appear in the control objective function.

The parameters h_1 and h_2 are assigned the values of 20 μm and 30 μm, respectively, based on the original design in [*Tung and Kurabayashi* (2005)]. The final time, t_f, is a parameter and is given as $t_f = 0.25$ ms. This value is chosen based on the system responses seen in the first optimization. All other parameters have the values given in Table 5.2. Note that, in the first problem formulation, the primary concern was the speed of response. In this problem formulation, control effort is to be minimized.

STEP 2: Evaluation for Bi-Directional Coupling

The problem can then be evaluated to determine whether bi-directional coupling is present. The functions f_a and $\boldsymbol{g}_a$ are not dependent on the control design variables. Therefore, bi-directional coupling does not exist.

STEP 3: Evaluation for Uni-Directional Coupling

Next, the problem is evaluated to determine whether uni-directional coupling exists. While explicit relations for f_c and $\boldsymbol{g}_c$ are not given, the simulation which calculates them depends on M, C, K, and $A(\Delta\theta)$, and through them, on the artifact design variables, $\boldsymbol{d}_a$. Therefore, $f_c = f_c(\boldsymbol{d}_a, \boldsymbol{d}_c)$ and $\boldsymbol{g}_c = \boldsymbol{g}_c(\boldsymbol{d}_a, \boldsymbol{d}_c)$.

The problem is then evaluated to determine whether or not any of the decoupling conditions in Chapter III (i.e., Eqs. (3.12), (3.30), (3.44)) are applicable. In this case, the problem does match one of the formulations given in Chapter III, specifically the formulation denoted as Case I. Evaluation of Eq. (3.12) indicates that this co-design problem is coupled, since the coupling vector will not vanish for any feasible values of the artifact

design variables. Therefore, the problem exhibits uni-directional coupling.

STEP 4: Evaluation of Suitability of CPF Method

Now, consider whether one of the CPFs listed in Table 5.1 would be effective in solving this problem. While the $\boldsymbol{B}$ matrix is insensitive to the design variables, the remaining conditions are not met for the use of natural frequency as a CPF. The control objective function, f_c, is not a function of only ω_c, so the first set of conditions is not satisfied. The second set of conditions is not satisfied, since f_c is not a function of the product $\omega_c\zeta_c$. The third set of conditions is not satisfied, since $\dfrac{\partial b}{\partial \boldsymbol{d}_a} \neq \boldsymbol{0}$. Therefore, the natural frequency is not an appropriate choice of CPF for this problem.

The system does not satisfy the conditions for use of any of the controllability-based CPFs listed in Table 5.1. However, one can easily formulate an appropriate CPF for this problem. Since this problem matches Case I in Chapter III, we know that, for an optimal controller,

$$f_c = \boldsymbol{x}_f^T \boldsymbol{W}_c \left(t_f\right)^{-1} \boldsymbol{x}_f \tag{5.53}$$

which, for this problem, can be expressed as

$$f_c = \frac{\Delta Z_f^2 W_{c_{22}}\left(t_f\right)}{\det\left(\boldsymbol{W}_c\left(t_f\right)\right)}. \tag{5.54}$$

Therefore, the CPF χ_1 is chosen to be the control objective function, f_c, given by Eq. (5.54).

The characteristics of the Pareto frontier are not known prior to solution of the problem. Since the convexity of the Pareto frontier is not known, we will consider the possibility that it may be non-convex, and therefore the bi-objective optimization of f_a and χ is formulated with the exponential weighted criteria function [*Athan* (1994)]. The CPF problem is given by

Table 5.5: CPF Optimization Results Using χ_1

p (μm)	t (μm)	l_1 (μm)	K_1	K_2	K_i	ΔZ_f (μm)	E
162	25	523	5.72e5	28.2	6.47e9	2.08	22.82
176	25	509	6.60e5	32.4	7.40e9	2.26	25.71
188	25	497	7.43e5	36.3	8.28e9	2.42	29.11
199	25	486	8.27e5	40.2	9.17e9	2.57	33.17
211	25	475	9.14e5	44.3	1.01e10	2.71	38.10
222	25	463	1.01e6	48.7	1.11e10	2.85	44.22
233	25	452	1.11e6	53.5	1.22e10	3.00	51.00
246	25	439	1.22e6	59.0	1.34e10	3.15	59.59
259	25	426	1.36e6	65.4	1.49e10	3.32	72.33

$$\min_{p,t,l_1} \left(\left(e^{2w_1} - 1 \right) e^{2f_a} + \left(e^{2w_2} - 1 \right) e^{2\chi_1} \right) \tag{5.55}$$

subject to the constraints given in Eqs. (5.11) - (5.16), followed by

$$\min_{K_1,K_2,K_i} E \tag{5.56}$$

where

$$E = \int_0^{t_f} \left(V(t) \right)^4 dt. \tag{5.57}$$

Results are given in Table 5.5, and the optimal values of $-\Delta Z_f$ and E are shown in Fig. 5.9. At each of the points shown, the angle ξ is calculated in order to determine whether the point is optimal or near-optimal. For each point, $\xi = 0$, indicating that the CPF points are Pareto optimal, as anticipated.

Again, it should be noted that this CPF is not necessarily the only one that would be effective for this problem. Consider the case where we ignore the contribution of ΔZ_f to χ_1, and use the CPF

$$\chi_2 = \frac{W_{c_{22}}\left(t_f\right)}{\det\left(\boldsymbol{W}_c\left(t_f\right)\right)}. \tag{5.58}$$

The results of this optimization, as shown in Fig. 5.10, match the Pareto optimal set found

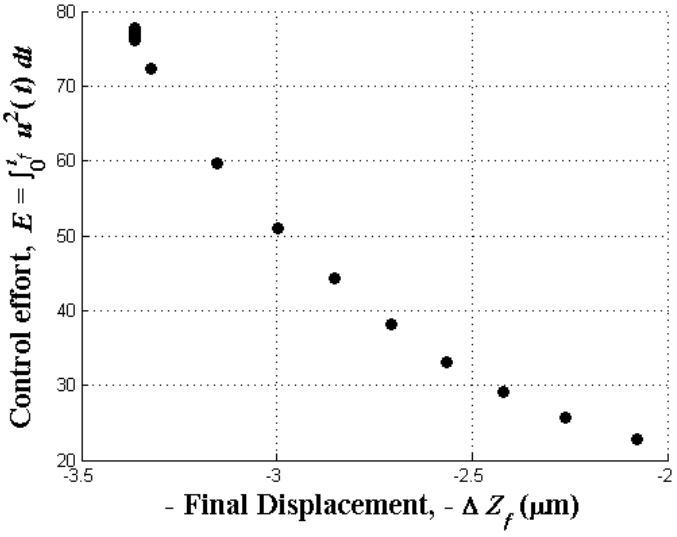

Figure 5.9: CPF Points for Optimization of MEMS Actuator

using χ_1 to formulate the CPF problem.

As previously mentioned, ΔZ_f is not a function of l_1. Therefore, since χ_1 is monotonic with respect to l_1, χ_2 must have the same monotonicity with respect to l_1. Furthermore, χ_1 and χ_2 each has an unconstrained minimum with respect to p, and these minima are relatively close to each other. Thus, it can be seen, based on Theorems 4.3 and 4.4, that this CPF is a reasonable choice, although this is not obvious at the outset.

5.6 Summary

In this chapter, a procedure for evaluating co-design problems based on the theory of the previous chapters was presented and demonstrated. This procedure was used to categorize co-design problems based on the type of coupling present. If the problem under consideration exhibits uni-directional coupling, then it can be further evaluated to determine whether an existing CPF would be effective.

The procedure was demonstrated using a MEMS actuator, with two co-design problem formulations. In each of the formulations, an effective CPF was derived, and optimal solu-

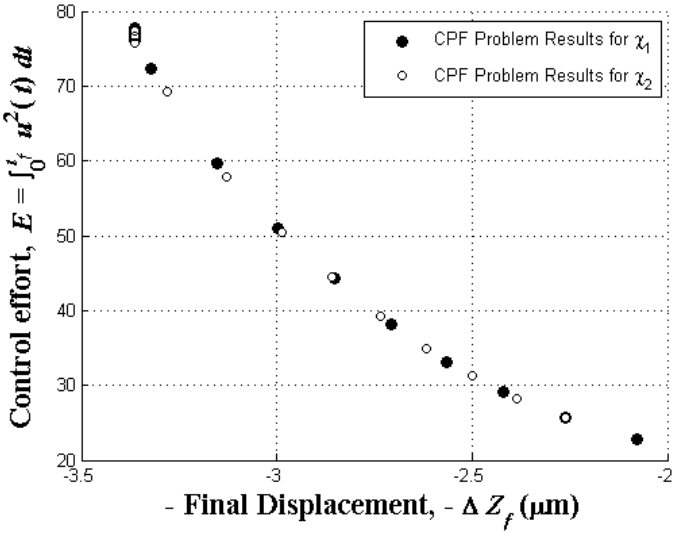

Figure 5.10: Comparison of CPF Points for Optimization with χ_1 and χ_2

tions were found with the chosen CPF formulation. It was also shown that in many cases there are alternative choices of a CPF that will produce optimal, or near-optimal, results. In the first example presented, one CPF was chosen from previously developed CPFs, as documented Table 5.1, while the other was justified based on Theorem 4.3. In the second example, one CPF was formulated by recognizing that the problem formulation matches one of the formulations considered in Chapter III, while the other was justified based on Theorems 4.3 and 4.4. In each case, the first CPF used to solve the problem could be seen as the 'obvious' or 'easy' choice, which could be chosen without extensive analysis of the system. Thus, it is seen that, in many cases, one can determine that the CPF problem formulation will be appropriate and choose an effective CPF function, thereby realizing its advantages of ease of solution and optimal or near-optimal results.

CHAPTER VI

Summary, Conclusions and Future Work

6.1 Summary

The dissertation addressed several open issues relating to the optimal design of an artifact and its controller in the presence of coupling. As described in Section 1.4, there are many examples of co-design problems in which coupling is significant, including many that exhibit uni-directional coupling. The dissertation focused specifically on those co-design problems which exhibit uni-directional coupling. Specifically, issues regarding coupling and controllability in co-design problems were studied. The issues addressed were the relationships between various coupling measures and their applicability to the co-design problem, the relationships between coupling and controllability, and the development of a new concept and solution strategy for co-design using the Control Proxy Function. The contributions promised in Section 1.7 are discussed further in Section 6.2.

6.2 Conclusions

This dissertation has made five key contributions to the co-design literature. These contributions are summarized here, and their significance and limitations are discussed.

6.2.1 Derivation of Relationships Between Coupling Measures and Extension of Coupling Vector to Bi-Directional Coupling

Previous contributions to the co-design and multi-disciplinary optimization literature have presented a variety of different metrics which can be used to characterize coupling in co-design problems. The previous literature has not fully addressed the relative advantages and disadvantages of these measures for the co-design problem. This dissertation has considered four measures of coupling and established previously unknown relationships between them. The four measures considered were the coupling vector, $\boldsymbol{\Gamma}_v$, the sensitivity of the control objective, normalized sensitivities, and the coupling matrix, $\boldsymbol{\Gamma}_m$. It has been shown that only two of the metrics considered, the coupling vector and the sensitivity of the sensitivity of the control objective, are commensurate. One measure, the coupling vector, $\boldsymbol{\Gamma}_v$, was chosen for this work, and its range of applicability was extended. In one extension, it was shown that it can be applied to problems in which the objective function is not a linear combination of the artifact and controller objectives. This extension is important since the linear combination of two objectives, while commonly used in many bi-objective optimization problems, is not applicable to all co-design problems. The second extension of the coupling vector was its formulation as a description of bi-directional coupling. While other measures exist that can be used for problems that exhibit bi-directional coupling, the bi-directional coupling vector is a simpler and more compact description. In addition, it may be useful in broadening the range of applicability of the work presented in this dissertation.

6.2.2 Derivation of Relationships Between Coupling and Controllability for Several Important Classical Control Problems

All of the coupling metrics studied in Chapter II are evaluated at a Pareto-optimal solution. In Chapter III, it was shown for the first time that it is sometimes possible to determine the existence and strength of coupling prior to the solution of a co-design problem. The controllability Grammian matrix, $\boldsymbol{W}_c$, is related to the fundamental control limitations of

a system, and can be used to determine the performance of an optimal controller, without knowledge of the controller architecture. This key observation was used to derive relationships between the controllability Grammian matrix and the coupling vector, $\boldsymbol{\Gamma}_v$, for three important classical control problems. These relationships between $\boldsymbol{W}_c$ and $\boldsymbol{\Gamma}_v$ can be used to determine whether or not a given artifact design variable participates in coupling. This insight can then be used to formulate the co-design problem and choose an appropriate solution method. It is important to note, however, that the relationships between $\boldsymbol{W}_c$ and $\boldsymbol{\Gamma}_v$ are only applicable for certain problems, those in which the control objective function or an active control constraint can be expressed in terms of the control effort. In the case of linear quadratic regulator (LQR) control, the relationship derived between $\boldsymbol{W}_c$ and $\boldsymbol{\Gamma}_v$ required the choice of specific weighting matrices.

6.2.3 Development of a Modified Sequential Method Using a Control Proxy Function (CPF) for Cases of Uni-directional Coupling

In Chapter IV, the Control Proxy Function (CPF) concept was introduced. The resulting method was designed to allow the problem to be solved sequentially by incorporating a measure of the system's ease of control into the artifact objective function. By solving the problem sequentially, it is possible to design the artifact prior to formulating the full control optimization problem. This facilitates the formulation of the individual artifact design and control design problems by experts in each discipline, thus alleviating the organizational challenges outlined in Section 1.2. Furthermore, the sequential formulation produces smaller problem sizes.

Conditions were derived which allow a CPF to be chosen in order to produce solutions that coincide with, or are close to, the Pareto frontier. Furthermore, a measure of how close a point is to the Pareto frontier was developed. This measure, the angle ξ between the gradient of the CPF, $\nabla\chi$, and the coupling vector, $\boldsymbol{\Gamma}_v$, is particularly useful because it can be calculated without the necessity of knowing any points on the Pareto frontier. The CPF-

based method, therefore, can be used to solve a co-design problem with uni-directional coupling sequentially, and to determine the closeness of the solutions to optimality.

These conditions were then utilized to formulate CPFs for problems that satisfied specific conditions. It was shown that, for certain types of problems, a CPF based on natural frequency will always be effective. In other types of problems, a CPF based on the controllability Grammian matrix will always be effective.

This method does have limitations. It has only been shown to be effective for co-design problems with uni-directional coupling, and cannot currently be applied to problems with bi-directional coupling. Constraint activity was severely restricted in the proof of the key theorems defining an effective CPF and the derivation of the relationship between ξ and the closeness to the Pareto frontier. Furthermore, the specific CPFs developed in this thesis are not exhaustive. While a CPF based on the controllability Grammian matrix will be effective for many problems, it is not guaranteed effective in all cases. In particular, if neither the control objective function nor an active control constraint is a function of control effort, then a CPF based on the controllability Grammian cannot be expected to produce Pareto optimal solutions, though it may produce near-optimal results since the controllability Grammian serves as a measure of the system's controllability.

6.2.4 Categorization of Problems According to Nature of Coupling and Appropriate Solution Methods

The dissertation presented a procedure for the analysis of a co-design problem in Chapter V. In this procedure, a co-design problem is analyzed to determine what form of coupling, if any, is present. If bi-directional coupling is present, then an appropriate solution method can be chosen. If uni-directional coupling is present, then the problem can be further analyzed to determine whether the CPF method is an appropriate technique, and what type of CPF might be most useful. This procedure was formulated to provide a rigorous approach to determine the solution method. Previously, solution methods were chosen pri-

marily based on the designer's experience with similar problems and intuition about the problem at hand.

One limitation of this procedure is that it does not currently provide a means to choose among the methods used for co-design problems with bi-directional coupling. The choice of a simultaneous formulation or a decomposition and coordination strategy is left to the designer, with no further guidance provided regarding which would be most efficient and effective for a particular problem.

6.2.5 Application of New Method to Case Studies

The application of the CPF-based method to case studies demonstrated its utility. In Chapter V, a MEMS actuator was used to demonstrate the CPF method. Two optimization problems were formulated for the actuator, and each was analyzed with the solution procedure presented in Section 5.2. This analysis, and the subsequent solution of the co-design problem using the CPF method, showed that the procedure can be applied to problems of interest. The use of this procedure can allow a designer to design an artifact effectively for ease of control, resulting in optimal or near-optimal solutions using the CPF method.

6.3 Future Work

As discussed in Section 6.2, the work presented in this dissertation is subject to certain limitations, which presents opportunities for future research. These opportunities are discussed in this section.

6.3.1 Further Investigation of Decoupling Conditions

In Chapter III, relationships between coupling and controllability were derived for three classical control problems. These relationships were used to define conditions when decoupling would occur. The physical significance of these relationships, however, has not been

fully defined. Research into the physical conditions under which these decoupling conditions occur can yield new insights into the tradeoffs present in co-design problems of the types discussed.

In addition, the classical control problems presented in Chapter III are not exhaustive. Additional problem formulations should be investigated in order to define appropriate relationships between coupling and controllability for other situations. It may also be possible to derive relationships between coupling and some other system metric representing ease of control, such as modal controllability, and this is also a subject for future research.

6.3.2 Further Development of Control Proxy Function (CPF) Method

In Chapter IV, the Control Proxy Function (CPF) concept was developed. While the CPF-based method can produce solutions that are optimal, or near-optimal, the robustness of the method to parametric uncertainty has not been investigated.

In addition, the CPFs developed in Chapter IV are not exhaustive. Additional CPFs should be developed for a variety of classical control problems, such as Linear Quadratic Gaussian (LQG) control, vehicle steering applications, trajectory control, sensor placement, and power management, in order to extend the range of applicability of the method. Additional CPFs based on the controllability Grammian should be investigated. Other system metrics, such as the observability Grammian matrix, could also be used to formulate CPFs for various co-design problems.

It may also be possible to extend the CPF method to co-design problems with bi-directional coupling, and this should be a subject of future research. Future work should determine whether there are cases in which the CPF method can be used to yield optimal, or near-optimal, solutions to co-design problems with bi-directional coupling.

6.3.3 Consideration of Observability

Given the duality between controllability and observability, and previous work using the observability Grammian matrix to locate sensors, it is reasonable to conjecture that an Observability Proxy Function could also be formulated [*Roh and Park* (1997), *Lim and Gawronski* (1993)]. Such a function could be used to determine optimal sensor configurations in the design of an artifact. By determining optimal sensor locations, it would be possible to address issues of state estimation, which are critical in the design of effective control systems. Thus, using both the controllability Grammian and observability Grammian matrices, this work could be extended to combined estimation and control.

6.3.4 Application of the CPF Method to Additional Case Studies

Given the range of co-design problems that have been identified, as discussed in Chapter I, future research should include the application of the CPF method to a variety of additional co-design problems. This research can focus both on further development of the CPF method and on the insights it can yield into the optimal design of the case studies that are carried out.

APPENDICES

APPENDIX A

Proofs for Theorems 4.1 – 4.4

Proof of Theorem 4.1

THEOREM 4.1: If $\Gamma_v \parallel \nabla\chi$ for all solutions to the CPF problem given in Eq. (4.1) - (4.3), then all solutions to the CPF problem will also be solutions to the simultaneous problem given in Eq. (1.9) - (1.13).

PROOF: For the simultaneous problem stated in Eq. (1.9) - (1.13), the Karush-Kuhn-Tucker (KKT) conditions can be stated as

$$\begin{bmatrix} \dfrac{\partial f_a}{\partial \boldsymbol{d}_a} + \dfrac{w_c}{w_a}\left(\dfrac{\partial f_c}{\partial \boldsymbol{d}_a} + \dfrac{\partial f_c}{\partial \boldsymbol{d}_c}\dfrac{\boldsymbol{d}_c}{\partial \boldsymbol{d}_a}\right) \\ \dfrac{w_c}{w_a}\dfrac{\partial f_c}{\partial \boldsymbol{d}_c} \end{bmatrix} + \boldsymbol{\lambda}^T \begin{bmatrix} \dfrac{\partial \boldsymbol{h}_a}{\partial \boldsymbol{d}_a} \\ \dfrac{\partial \boldsymbol{h}_c}{\partial \boldsymbol{d}_c} \end{bmatrix} + \boldsymbol{\mu}^T \begin{bmatrix} \dfrac{\partial \boldsymbol{g}_a}{\partial \boldsymbol{d}_a} \\ \dfrac{\partial \boldsymbol{g}_c}{\partial \boldsymbol{d}_c} \end{bmatrix} = \mathbf{0} \quad \text{(A.1)}$$

$$\boldsymbol{\mu}^T \begin{bmatrix} \boldsymbol{g}_a \\ \boldsymbol{g}_c \end{bmatrix} = \mathbf{0} \quad \text{(A.2)}$$

$$\boldsymbol{\lambda} \neq \mathbf{0} \quad \text{(A.3)}$$

$$\boldsymbol{\mu} \geq \mathbf{0} \quad \text{(A.4)}$$

and, for the CPF problem stated in Eq. (4.1) - (4.3), the KKT conditions are

$$\begin{bmatrix} \dfrac{\partial f_a}{\partial \boldsymbol{d}_a} + \dfrac{w_2}{w_1}\dfrac{\partial \chi}{\partial \boldsymbol{d}_a} \\ \dfrac{w_2}{w_1}\dfrac{\partial f_c}{\partial \boldsymbol{d}_c} \end{bmatrix} + \boldsymbol{\lambda}^T \begin{bmatrix} \dfrac{\partial \boldsymbol{h}_a}{\partial \boldsymbol{d}_a} \\ \dfrac{\partial \boldsymbol{h}_c}{\partial \boldsymbol{d}_c} \end{bmatrix} + \boldsymbol{\mu}^T \begin{bmatrix} \dfrac{\partial \boldsymbol{g}_a}{\partial \boldsymbol{d}_a} \\ \dfrac{\partial \boldsymbol{g}_c}{\partial \boldsymbol{d}_c} \end{bmatrix} = \mathbf{0} \tag{A.5}$$

$$\boldsymbol{\mu}^T \begin{bmatrix} \boldsymbol{g}_a \\ \boldsymbol{g}_c \end{bmatrix} = \mathbf{0} \tag{A.6}$$

$$\boldsymbol{\lambda} \neq \mathbf{0} \tag{A.7}$$

$$\boldsymbol{\mu} \geq \mathbf{0} \tag{A.8}$$

Assume that, for every set of weights w_a and w_c, there exists some set of weights w_1 and w_2 such that the two formulations will have identical solutions. Then

$$\frac{\partial f_a}{\partial \boldsymbol{d}_a} + \frac{w_c}{w_a}\left(\frac{\partial f_c}{\partial \boldsymbol{d}_a} + \frac{\partial f_c}{\partial \boldsymbol{d}_c}\frac{\partial \boldsymbol{d}_c}{\partial \boldsymbol{d}_a}\right) = \frac{\partial f_a}{\partial \boldsymbol{d}_a} + \boldsymbol{\Gamma}_v = \frac{\partial f_a}{\partial \boldsymbol{d}_a} + \frac{w_2}{w_1}\frac{\partial \chi}{\partial \boldsymbol{d}_a} \tag{A.9}$$

Thus,

$$\boldsymbol{\Gamma}_v = \frac{w_2}{w_1}\nabla\chi. \tag{A.10}$$

Such a set of weights will exist, and the modified sequential problem will produce the Pareto optimal solutions, when the gradient of the CPF, $\nabla\chi$, is parallel to the coupling vector $\boldsymbol{\Gamma}_v$. Thus, the theorem is proven. □

Proof of Theorem 4.2

THEOREM 4.2: If a co-design problem, as given in Eq. (1.9) - (1.13), is convex and no artifact constraints $\boldsymbol{g}_a(\boldsymbol{d}_a)$, $\boldsymbol{h}_a(\boldsymbol{d}_a)$ are active, then the angle ξ between $\nabla\chi$ and the estimated coupling vector $\hat{\boldsymbol{\Gamma}}_v$ at a CPF point will be monotonically related to ε, the distance between that CPF point and the nearest Pareto optimal point, measured in the $\boldsymbol{d}_a$-space.

PROOF: The distance from optimality has been defined mathematically in several different ways [*Papalambros and Wilde* (2000)]; in this case, it shall be defined as the distance between a given point, $\boldsymbol{d}_a$, and the nearest Pareto-optimal point, $\boldsymbol{d}_a^*$, in the $\boldsymbol{d}_a$-space.

$$\varepsilon = ||\boldsymbol{d}_a - \boldsymbol{d}_a^*||_2 \tag{A.11}$$

where $\boldsymbol{d}_a$ is the vector of design variables, and $\boldsymbol{d}_a^*$ denotes the vector of design variables at an optimal solution to the co-design problem.

It is possible to express the optimal control design variables $\boldsymbol{d}_c$ as a function of the artifact design variables, as follows,

$$\boldsymbol{d}_c^* = \boldsymbol{d}_c(\boldsymbol{d}_a^*), \tag{A.12}$$

which allows the control objective f_c to be transformed into a function only of $\boldsymbol{d}_a$. This shall be used later in the proof in order to find gradients of f_c in the $\boldsymbol{d}_a$-space. Note that it is possible to incorporate any active controller constraints $\boldsymbol{g}_c(\boldsymbol{d}_a, \boldsymbol{d}_c)$, $\boldsymbol{h}_c(\boldsymbol{d}_a, \boldsymbol{d}_c)$ into Eq. (A.12).

This co-design problem is also formulated as a CPF problem.

$$\min_{\boldsymbol{d}_a} w_1 f_a(\boldsymbol{d}_a) + w_2 \chi(\boldsymbol{d}_a), \tag{A.13}$$

followed by

$$\min_{\boldsymbol{d}_c} f_c(\boldsymbol{d}_c) \tag{A.14}$$

subject to

$$\boldsymbol{g}_c(\boldsymbol{d}_c) \leq \boldsymbol{0} \tag{A.15}$$

$$\boldsymbol{h}_c(\boldsymbol{d}_c) = \boldsymbol{0}. \tag{A.16}$$

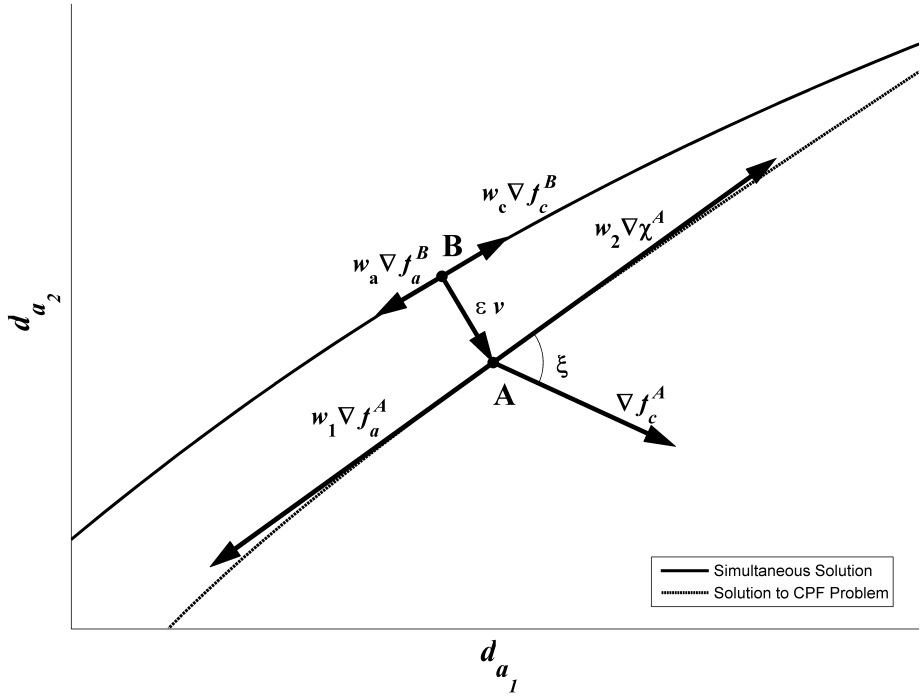

Figure A.1: Gradients at Points A and B

The functions $\chi(\boldsymbol{d}_a)$, $f_a(\boldsymbol{d}_a)$ and the reduced-space function $f_c(\boldsymbol{d}_a)$ are all assumed to be convex functions. Consider a point A which solves the CPF problem. At this point, with $\boldsymbol{d}_a = \boldsymbol{d}_a^A$,

$$w_1 \nabla f_a^A = -w_2 \nabla \chi^A. \tag{A.17}$$

The point B is chosen such that it is the nearest Pareto optimal solution to point A. Its location in the artifact design variable space therefore satisfies the relation $\boldsymbol{d}_a^A = \boldsymbol{d}_a^B + \varepsilon \boldsymbol{v}$, where $\boldsymbol{v}$ is a unit vector normal to ∇f_a^B and ε is the distance between A and B, as shown in Fig. A.1.

Using a Taylor series expansion about point B, the artifact and controller objective

functions at A can be expressed as

$$f_a^A = f_a^B + \nabla f_a^B \varepsilon \boldsymbol{v} + \frac{1}{2}\varepsilon^2 \boldsymbol{v}^T \nabla^2 f_a^B \boldsymbol{v} + \text{ higher order terms} \tag{A.18}$$

$$f_c^A = f_c^B + \nabla f_c^B \varepsilon \boldsymbol{v} + \frac{1}{2}\varepsilon^2 \boldsymbol{v}^T \nabla^2 f_c^B \boldsymbol{v} + \text{ higher order terms} \tag{A.19}$$

and therefore, neglecting higher-order terms, the gradients of f_a and f_c at A can be expressed in terms of the gradients at B as

$$\nabla f_a^A = \nabla f_a^B + \varepsilon \boldsymbol{v}^T \nabla^2 f_a^B \tag{A.20}$$

$$\nabla f_c^A = \nabla f_c^B + \varepsilon \boldsymbol{v}^T \nabla^2 f_c^B \tag{A.21}$$

The estimate of the coupling vector, computed from Eq. (1.14), is given by

$$\hat{\boldsymbol{\Gamma}}_v^A = \frac{w_2}{w_1} \nabla f_c^A \tag{A.22}$$

and the angle ξ can be found from the relation

$$\cos\xi = \frac{\boldsymbol{\Gamma}_v^A \bullet \nabla \chi^A}{\|\boldsymbol{\Gamma}_v^A\| \, \|\nabla \chi^A\|} = \frac{\nabla f_c^A \bullet \nabla \chi^A}{\|\nabla f_c^A\| \, \|\nabla \chi^A\|} \tag{A.23}$$

From optimality conditions, it is known that

$$w_a \nabla f_a^B = -w_c \nabla f_c^B \tag{A.24}$$

$$w_1 \nabla f_a^A = -w_2 \nabla \chi^A \tag{A.25}$$

Using Eq.(A.25), it is possible to re-write Eq.(A.23) as

$$\cos\xi = \frac{-\nabla f_c^A \bullet \nabla f_a^A}{\|\nabla f_c^A\| \, \|\nabla f_a^A\|} \tag{A.26}$$

Using Eq.(A.20), (A.21), and (A.24), this can be further re-written as

$$\begin{aligned}\cos\xi = &\left(\frac{w_c}{w_a}\nabla f_c^B - \varepsilon \boldsymbol{v}^T\nabla^2 f_a^B\right)\left(\nabla f_c^B + \varepsilon \boldsymbol{v}^T\nabla^2 f_c^B\right)^T \\ &/\left(\left(\frac{w_c}{w_a}\nabla f_c^B - \varepsilon \boldsymbol{v}^T\nabla^2 f_a^B\right)\left(\frac{w_c}{w_a}\nabla f_c^B - \varepsilon \boldsymbol{v}^T\nabla^2 f_a^B\right)^T\right)^{1/2} \\ &/\left(\left(\nabla f_c^B + \varepsilon \boldsymbol{v}^T\nabla^2 f_c^B\right)\left(\nabla f_c^B + \varepsilon \boldsymbol{v}^T\nabla^2 f_c^B\right)^T\right)^{1/2}\end{aligned} \tag{A.27}$$

Squaring both sides and cross-multiplying,

$$\begin{aligned}\cos^2\xi &\left(\frac{w_c}{w_a}\nabla f_c^{B^T} - \varepsilon\nabla^2 f_a^{B^T}\boldsymbol{v}\right)\left(\nabla f_c^B + \varepsilon \boldsymbol{v}^T\nabla^2 f_c^B\right) \\ &= \left(\nabla f_c^{B^T} + \varepsilon\nabla^2 f_c^{B^T}\boldsymbol{v}\right)\left(\frac{w_c}{w_a}\nabla f_c^B - \varepsilon \boldsymbol{v}^T\nabla^2 f_a^B\right)\end{aligned} \tag{A.28}$$

Expanding and post-multiplying by $\boldsymbol{v}$,

$$\begin{aligned}\cos^2\xi &\left(\frac{w_c}{w_a}\nabla f_c^{B^T}\nabla f_c^B\boldsymbol{v} + \frac{w_c}{w_a}\varepsilon\nabla f_c^{B^T}\boldsymbol{v}^T\nabla^2 f_c^B\boldsymbol{v} - \varepsilon\nabla^2 f_a^{B^T}\boldsymbol{v}\nabla f_c^B\boldsymbol{v} - \varepsilon^2\nabla^2 f_a^{B^T}\nabla^2 f_c^B\boldsymbol{v}\right) \\ &= \left(\frac{w_c}{w_a}\nabla f_c^{B^T} f_c^B\boldsymbol{v} - \varepsilon\nabla f_c^{B^T}\boldsymbol{v}^T\nabla^2 f_a^B\boldsymbol{v} + \frac{w_c}{w_a}\varepsilon\nabla^2 f_c^{B^T}\boldsymbol{v}\nabla f_c^B\boldsymbol{v} - \varepsilon^2\nabla^2 f_c^{B^T}\nabla^2 f_a^B\boldsymbol{v}\right)\end{aligned} \tag{A.29}$$

Because of the definition of point B, $\boldsymbol{v}$ is orthogonal to ∇f_c^B, and therefore the product of those two vectors will vanish.

$$\begin{aligned}\cos^2\xi &\left(\frac{w_c}{w_a}\nabla f_c^{B^T}\left(\boldsymbol{v}^T\nabla^2 f_c^B\boldsymbol{v}\right) - \varepsilon\nabla^2 f_a^{B^T}\boldsymbol{v}\left(\boldsymbol{v}^T\nabla^2 f_c^B\boldsymbol{v}\right)\right) \\ &= \left(-\nabla f_c^{B^T}\left(\boldsymbol{v}^T\nabla^2 f_a^B\boldsymbol{v}\right) - \varepsilon\nabla^2 f_c^{B^T}\boldsymbol{v}\left(\boldsymbol{v}^T\nabla^2 f_a^B\boldsymbol{v}\right)\right)\end{aligned} \tag{A.30}$$

Further re-arranging leads to the relation

$$\begin{aligned}\cos^2\xi &\left(\nabla^2 f_a^{B^T}\boldsymbol{v} - \frac{1}{\varepsilon}\frac{w_c}{w_a}\nabla f_c^{B^T}\right)\left(\boldsymbol{v}^T\nabla^2 f_c^B\boldsymbol{v}\right) \\ &= \left(\nabla^2 f_a^{B^T}\boldsymbol{v} - \frac{1}{\varepsilon}\nabla f_c^{B^T}\right)\left(\boldsymbol{v}^T\nabla^2 f_c^B\boldsymbol{v}\right)\end{aligned} \tag{A.31}$$

Since the functions have been specified as convex,

$$\boldsymbol{v}^T \nabla^2 f_c^B \boldsymbol{v} \geq 0 \tag{A.32}$$

$$\boldsymbol{v}^T \nabla^2 f_c^B \boldsymbol{v} \geq 0 \tag{A.33}$$

As the value of ε increases, then, it is evident that $\cos^2 \xi$ must decrease, and therefore ξ is increasing. Given that an increase in ξ corresponds to an increase in ε, then, the angle ξ is an appropriate measure of the distance between a CPF solution and the unknown Pareto frontier, and the theorem is proven. □

Proof of Theorem 4.3

THEOREM 4.3: If $f_c(\boldsymbol{d}_a, \boldsymbol{d}_c)$ is monotonic with respect to some element of $\boldsymbol{d}_a$, and that element of $\boldsymbol{d}_a$ does not appear in any constraint that is always active, then a CPF with the same monotonicity will produce closer solutions than a CPF with the opposite monotonicity.

PROOF: Assume that, in a co-design problem, the controller objective function $f_c(\boldsymbol{d}_a, \boldsymbol{d}_c)$ is monotonic with respect to the j^{th} component of the n-dimensional vector of artifact design variables $\boldsymbol{d}_a$. Two CPFs will be used to solve this problem, denoted as $\chi_1(\boldsymbol{d}_a)$ and $\chi_2(\boldsymbol{d}_a)$. $\chi_1(\boldsymbol{d}_a)$ and $\chi_2(\boldsymbol{d}_a)$ are selected such that:

$$\frac{\partial \chi_1}{\partial d_{a_i}} = \frac{\partial \chi_2}{\partial d_{a_i}} \; \forall \; \{i : i \neq j, 1 \leq i \leq n\} \tag{A.34}$$

$$\frac{\partial \chi_1}{\partial d_{a_j}} = -\frac{\partial \chi_2}{\partial d_{a_j}} \tag{A.35}$$

$$\operatorname{sgn}\left(\frac{\partial \chi_1}{\partial d_{a_j}}\right) = \operatorname{sgn}\left(\frac{\partial f_c}{\partial d_{a_j}}\right) \tag{A.36}$$

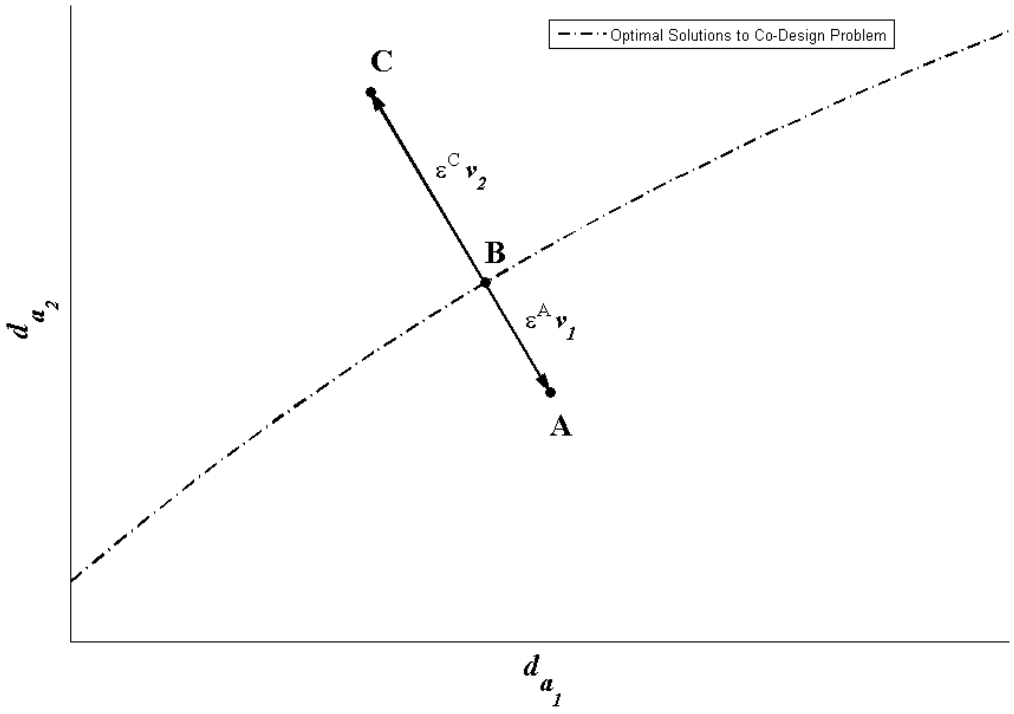

Figure A.2: Pareto-Optimal Point B and CPF Points A and C

Let the point A in the $\boldsymbol{d}_a$-space be a solution to the CPF problem using $\chi_1(\boldsymbol{d}_a)$, and let point B in the $\boldsymbol{d}_a$-space be the Pareto optimal solution to the co-design problem that is nearest to point A. Assume that, at point B, d_{a_j} does not appear in any active controller constraints $\boldsymbol{g}_c(\boldsymbol{d}_a, \boldsymbol{d}_c)$ or $\boldsymbol{h}_c(\boldsymbol{d}_a, \boldsymbol{d}_c)$. Choose point C such that it is a solution to the CPF problem using $\chi_2(\boldsymbol{d}_a)$ and such that point B is the Pareto optimal point nearest to it, as shown in Fig. (A.2).

If the distances from point B to points A and C, denoted as ε^A and ε^C, are sufficiently small, then the functions f_c, χ_1, and χ_2 can each be represented by first-order Taylor series

approximations. Expanding about the point B,

$$f_c^A = f_c^B + \varepsilon^A \nabla f_c^B \boldsymbol{v}_1 \tag{A.37}$$

$$f_c^C = f_c^B + \varepsilon^C \nabla f_c^B \boldsymbol{v}_2 \tag{A.38}$$

$$\chi_1^A = \chi_1^B + \varepsilon^A \nabla \chi_1^B \boldsymbol{v}_1 \tag{A.39}$$

$$\chi_2^C = \chi_2^B + \varepsilon^C \nabla \chi_2^B \boldsymbol{v}_1 \tag{A.40}$$

where $\boldsymbol{v}_1$ and $\boldsymbol{v}_2$ are unit vectors such that $\boldsymbol{v}_2 = \pm \boldsymbol{v}_1$.

By taking gradients of Eq. (A.37) and (A.38), we can state that

$$\nabla f_c^A = \nabla f_c^B \tag{A.41}$$

$$\nabla f_c^C = \nabla f_c^B \tag{A.42}$$

The coupling vector estimates at points A and C are given by the relations

$$\hat{\boldsymbol{\Gamma}}_v^A = \frac{w_2^A}{w_1^A} \nabla f_c^A \tag{A.43}$$

$$\hat{\boldsymbol{\Gamma}}_v^C = \frac{w_2^C}{w_1^C} \nabla f_c^A \tag{A.44}$$

where w_1^A, w_2^A are the weights which produce point A, and w_1^C, w_2^C are the weights which produce point C. Substituting Eq. (A.41) and (A.42) into Eq. (A.43) and (A.44),

$$\hat{\boldsymbol{\Gamma}}_v^A = \frac{w_2^A}{w_1^A} \nabla f_c^B \tag{A.45}$$

$$\hat{\boldsymbol{\Gamma}}_v^C = \frac{w_2^C}{w_1^C} \nabla f_c^B \tag{A.46}$$

The gradients $\nabla\chi_1^A$ and $\nabla\chi_2^C$ are given by the relations

$$\nabla\chi_1^A = \nabla\chi_1^B \tag{A.47}$$

$$\nabla\chi_2^C = \nabla\chi_2^B \tag{A.48}$$

Using Eq. (A.43) - (A.48), the angle ξ can be found for both points A and C, as follows:

$$\cos\xi^A = \frac{\hat{\mathbf{\Gamma}}_v^A \bullet \nabla\chi_1^A}{\left\|\hat{\mathbf{\Gamma}}_v^A\right\| \left\|\nabla\chi_1^A\right\|} \tag{A.49}$$

$$\cos\xi^A = \frac{\sum_{i=1}^{n}\left(\left(\frac{\partial f_c^B}{\partial d_{a_i}} + \frac{\partial f_c^B}{\partial \boldsymbol{d}_c}\frac{\partial \boldsymbol{d}_c}{\partial d_{a_i}}\right)\left(\frac{\partial \chi_1^B}{\partial d_{a_i}}\right)\right)}{\left(\sum_{i=1}^{n}\left(\frac{\partial f_c^B}{\partial d_{a_i}} + \frac{\partial f_c^B}{\partial \boldsymbol{d}_c}\frac{\partial \boldsymbol{d}_c}{\partial d_{a_i}}\right)^2\right)^{1/2}\left(\sum_{i=1}^{n}\left(\frac{\partial \chi_1^B}{\partial d_{a_i}}\right)^2\right)^{1/2}} \tag{A.50}$$

$$\begin{aligned}\cos\xi^A = &\frac{\sum_{i=1}^{j-1}\left(\left(\frac{\partial f_c^B}{\partial d_{a_i}} + \frac{\partial f_c^B}{\partial \boldsymbol{d}_c}\frac{\partial \boldsymbol{d}_c}{\partial d_{a_i}}\right)\left(\frac{\partial \chi_1^B}{\partial d_{a_i}}\right)\right) + \left(\frac{\partial f_c^B}{\partial d_{a_j}}\frac{\partial \chi_1^B}{\partial d_{a_j}}\right)}{\left(\sum_{i=1}^{n}\left(\frac{\partial f_c^B}{\partial d_{a_i}} + \frac{\partial f_c^B}{\partial \boldsymbol{d}_c}\frac{\partial \boldsymbol{d}_c}{\partial d_{a_i}}\right)^2\right)^{1/2}\left(\sum_{i=1}^{n}\left(\frac{\partial \chi_1^B}{\partial d_{a_i}}\right)^2\right)^{1/2}} \\ &+ \frac{\sum_{i=j+1}^{n}\left(\left(\frac{\partial f_c^B}{\partial d_{a_i}} + \frac{\partial f_c^B}{\partial \boldsymbol{d}_c}\frac{\partial \boldsymbol{d}_c}{\partial d_{a_i}}\right)\left(\frac{\partial \chi_1^B}{\partial d_{a_i}}\right)\right)}{\left(\sum_{i=1}^{n}\left(\frac{\partial f_c^B}{\partial d_{a_i}} + \frac{\partial f_c^B}{\partial \boldsymbol{d}_c}\frac{\partial \boldsymbol{d}_c}{\partial d_{a_i}}\right)^2\right)^{1/2}\left(\sum_{i=1}^{n}\left(\frac{\partial \chi_1^B}{\partial d_{a_i}}\right)^2\right)^{1/2}}\end{aligned} \tag{A.51}$$

$$\cos\xi^C = \frac{\hat{\mathbf{\Gamma}}_v^C \bullet \nabla\chi_2^A}{\left\|\hat{\mathbf{\Gamma}}_v^C\right\| \left\|\nabla\chi_2^C\right\|} \tag{A.52}$$

$$\cos\xi^C = \frac{\sum_{i=1}^{n}\left(\left(\frac{\partial f_c^B}{\partial d_{a_i}} + \frac{\partial f_c^B}{\partial \boldsymbol{d}_c}\frac{\partial \boldsymbol{d}_c}{\partial d_{a_i}}\right)\left(\frac{\partial \chi_2^B}{\partial d_{a_i}}\right)\right)}{\left(\sum_{i=1}^{n}\left(\frac{\partial f_c^B}{\partial d_{a_i}} + \frac{\partial f_c^B}{\partial \boldsymbol{d}_c}\frac{\partial \boldsymbol{d}_c}{\partial d_{a_i}}\right)^2\right)^{1/2}\left(\sum_{i=1}^{n}\left(\frac{\partial \chi_2^B}{\partial d_{a_i}}\right)^2\right)^{1/2}} \tag{A.53}$$

$$\cos\xi^C = \frac{\sum_{i=1}^{j-1}\left(\left(\frac{\partial f_c^B}{\partial d_{a_i}} + \frac{\partial f_c^B}{\partial \boldsymbol{d}_c}\frac{\partial \boldsymbol{d}_c}{\partial d_{a_i}}\right)\left(\frac{\partial \chi_2^B}{\partial d_{a_i}}\right)\right) + \left(\frac{\partial f_c^B}{\partial d_{a_j}}\frac{\partial \chi_2^B}{\partial d_{a_j}}\right)}{\left(\sum_{i=1}^{n}\left(\frac{\partial f_c^B}{\partial d_{a_i}} + \frac{\partial f_c^B}{\partial \boldsymbol{d}_c}\frac{\partial \boldsymbol{d}_c}{\partial d_{a_i}}\right)^2\right)^{1/2}\left(\sum_{i=1}^{n}\left(\frac{\partial \chi_2^B}{\partial d_{a_i}}\right)^2\right)^{1/2}} + \frac{\sum_{i=j+1}^{n}\left(\left(\frac{\partial f_c^B}{\partial d_{a_i}} + \frac{\partial f_c^B}{\partial \boldsymbol{d}_c}\frac{\partial \boldsymbol{d}_c}{\partial d_{a_i}}\right)\left(\frac{\partial \chi_2^B}{\partial d_{a_i}}\right)\right)}{\left(\sum_{i=1}^{n}\left(\frac{\partial f_c^B}{\partial d_{a_i}} + \frac{\partial f_c^B}{\partial \boldsymbol{d}_c}\frac{\partial \boldsymbol{d}_c}{\partial d_{a_i}}\right)^2\right)^{1/2}\left(\sum_{i=1}^{n}\left(\frac{\partial \chi_2^B}{\partial d_{a_i}}\right)^2\right)^{1/2}} \tag{A.54}$$

Substituting Eq. (A.34) and (A.35) into Eq. (A.54),

$$\cos\xi^C = \frac{\sum_{i=1}^{j-1}\left(\left(\frac{\partial f_c^B}{\partial d_{a_i}} + \frac{\partial f_c^B}{\partial \boldsymbol{d}_c}\frac{\partial \boldsymbol{d}_c}{\partial d_{a_i}}\right)\left(\frac{\partial \chi_1^B}{\partial d_{a_i}}\right)\right) - \left(\frac{\partial f_c^B}{\partial d_{a_j}}\frac{\partial \chi_1^B}{\partial d_{a_j}}\right)}{\left(\sum_{i=1}^{n}\left(\frac{\partial f_c^B}{\partial d_{a_i}} + \frac{\partial f_c^B}{\partial \boldsymbol{d}_c}\frac{\partial \boldsymbol{d}_c}{\partial d_{a_i}}\right)^2\right)^{1/2}\left(\sum_{i=1}^{n}\left(\frac{\partial \chi_1^B}{\partial d_{a_i}}\right)^2\right)^{1/2}} + \frac{\sum_{i=j+1}^{n}\left(\left(\frac{\partial f_c^B}{\partial d_{a_i}} + \frac{\partial f_c^B}{\partial \boldsymbol{d}_c}\frac{\partial \boldsymbol{d}_c}{\partial d_{a_i}}\right)\left(\frac{\partial \chi_1^B}{\partial d_{a_i}}\right)\right)}{\left(\sum_{i=1}^{n}\left(\frac{\partial f_c^B}{\partial d_{a_i}} + \frac{\partial f_c^B}{\partial \boldsymbol{d}_c}\frac{\partial \boldsymbol{d}_c}{\partial d_{a_i}}\right)^2\right)^{1/2}\left(\sum_{i=1}^{n}\left(\frac{\partial \chi_1^B}{\partial d_{a_i}}\right)^2\right)^{1/2}} \tag{A.55}$$

It is then possible to relate ξ^A and ξ^C.

$$\cos\xi^A = \cos\xi^C + \frac{2\frac{\partial f_c^B}{\partial d_{a_j}}\frac{\partial \chi_1^B}{\partial d_{a_j}}}{\left(\sum_{i=1}^{n}\left(\frac{\partial f_c^B}{\partial d_{a_i}} + \frac{\partial f_c^B}{\partial \boldsymbol{d}_c}\frac{\partial \boldsymbol{d}_c}{\partial d_{a_i}}\right)^2\right)^{1/2}\left(\sum_{i=1}^{n}\left(\frac{\partial \chi_1^B}{\partial d_{a_i}}\right)^2\right)^{1/2}} \tag{A.56}$$

From Eq. (A.36), we know that

$$\frac{2\dfrac{\partial f_c^B}{\partial d_{a_j}}\dfrac{\partial \chi_1^B}{\partial d_{a_j}}}{\left(\sum_{i=1}^{n}\left(\dfrac{\partial f_c^B}{\partial d_{a_i}}+\dfrac{\partial f_c^B}{\partial \boldsymbol{d}_c}\dfrac{\partial \boldsymbol{d}_c}{\partial d_{a_i}}\right)^2\right)^{1/2}\left(\sum_{i=1}^{n}\left(\dfrac{\partial \chi_1^B}{\partial d_{a_i}}\right)^2\right)^{1/2}} > 0 \tag{A.57}$$

and therefore,

$$\cos\xi^A > \cos\xi^C \tag{A.58}$$

leading to the conclusion that

$$\xi^A < \xi^C \tag{A.59}$$

Therefore, from Theorem 4.2, we know that $\chi_1(\boldsymbol{d}_a)$ will produce solutions closer to the Pareto optimal points than $\chi_2(\boldsymbol{d}_a)$ will. Since $\chi_1(\boldsymbol{d}_a)$ shares the same monotonicity as $f_c(\boldsymbol{d}_a, \boldsymbol{d}_c)$, the theorem is proven. □

Proof of Theorem 4.4

THEOREM 4.4: Assume that $f_c(\boldsymbol{d}_a, \boldsymbol{d}_c)$ has an unconstrained minimum, and that $\chi(\boldsymbol{d}_a)$ is chosen such that it has an unconstrained minimum. Then, the distance between a CPF point and the Pareto frontier will increase as the distance increases between the minima of f_c and χ.

PROOF: Assume that in a co-design problem the control objective function $f_c(\boldsymbol{d}_a, \boldsymbol{d}_c)$ has an unconstrained minimum in the $\boldsymbol{d}_a$-space, denoted as point D. The CPF $\chi(\boldsymbol{d}_a)$ is chosen such that it has an unconstrained minimum in the $\boldsymbol{d}_a$-space. The minimum of $\chi(\boldsymbol{d}_a)$, denoted as point C, is located at a distance δ from point D, as shown in Fig. (A.3).

Let point A be a solution to the CPF problem using $\chi(\boldsymbol{d}_a)$. The distance from point D

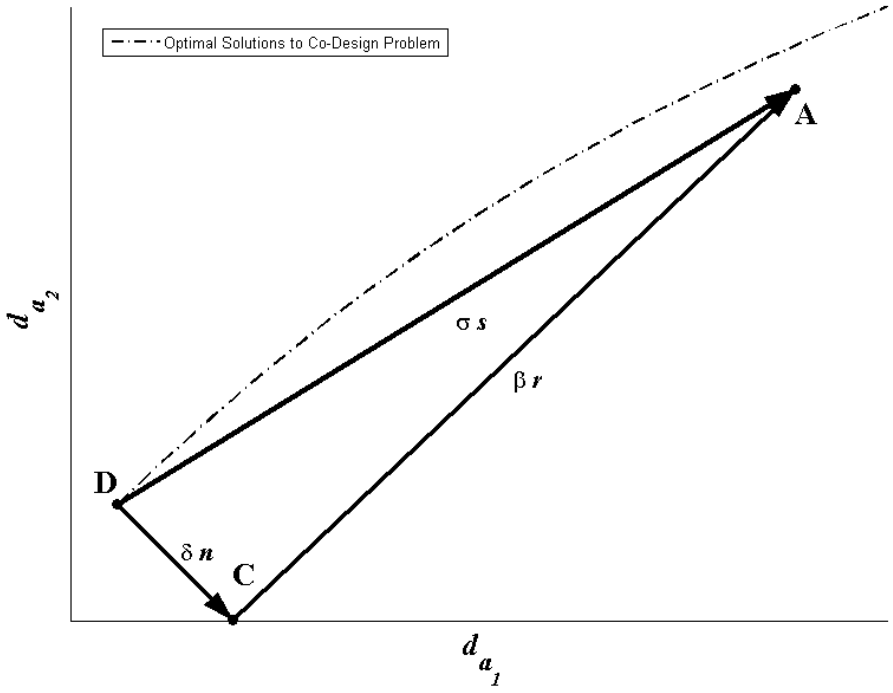

Figure A.3: Unconstrained Minima of f_c and χ

to point A is denoted as σ, and the distance from point C to point A is denoted as β. The vectors $\boldsymbol{n}$, $\boldsymbol{r}$, and $\boldsymbol{s}$ in Fig. (A.3) are unit vectors.

The function f_c evaluated at point A shall be represented by a second-order Taylor series expansion about its minimum, point D, as follows:

$$f_c^A = f_c^D + \frac{1}{2}\sigma^2 \boldsymbol{s}^T \nabla^2 f_c^D \boldsymbol{s}. \tag{A.60}$$

The function χ evaluated at point A shall be represented by a second-order Taylor series expansion about its minimum, point C, as follows:

$$\chi^A = \chi^C + \frac{1}{2}\beta^2 \boldsymbol{r}^T \nabla^2 \chi^C \boldsymbol{r}. \tag{A.61}$$

It is then possible to find the gradients of f_c and χ, evaluated at point A, in the $\boldsymbol{d}_a$-space.

$$\nabla f_c^A = \sigma \boldsymbol{s}^T \nabla^2 f_c^D \tag{A.62}$$

$$\nabla \chi^A = \beta \boldsymbol{r}^T \nabla^2 \chi^C \tag{A.63}$$

The unit vector $\boldsymbol{r}$ can be expressed as

$$\boldsymbol{r} = \frac{1}{\beta}(\sigma \boldsymbol{s} - \delta \boldsymbol{n}) \tag{A.64}$$

and therefore Eq. (A.63) can be re-written as

$$\nabla \chi^A = (\sigma \boldsymbol{s} - \delta \boldsymbol{n})^T \nabla^2 \chi^C. \tag{A.65}$$

From Eq. (A.23), it is known that

$$\cos \xi^A = \frac{\nabla \chi^A \bullet \nabla f_c^A}{\|\nabla \chi^A\| \, \|\nabla f_c^A\|} \tag{A.66}$$

which can be re-written as

$$\cos\xi^A = \frac{(\sigma\boldsymbol{s}-\delta\boldsymbol{n})^T\nabla^2\chi^A\nabla^2 f_c^{D^T}\boldsymbol{s}}{\left((\sigma\boldsymbol{s}-\delta\boldsymbol{n})^T\nabla^2\chi^C\nabla^2\chi^{C^T}(\sigma\boldsymbol{s}-\delta\boldsymbol{n})\right)^{1/2}\left(\boldsymbol{s}^T\nabla^2 f_c^D\nabla^2 f_c^{D^T}\boldsymbol{s}\right)^{1/2}} \tag{A.67}$$

The unit vector $\boldsymbol{s}$ can be expressed in terms of the unit vector $\boldsymbol{n}$ by means of a rotation matrix, R.

$$\boldsymbol{s} = \boldsymbol{R}\boldsymbol{n} \tag{A.68}$$

which can be substituted into Eq. (A.67). Thus, Eq. (A.67) can be re-written as

$$\cos\xi^A = \frac{\boldsymbol{n}^T\left(\sigma\boldsymbol{R}^T\nabla^2\chi^C\nabla^2 f_c^{D^T}\boldsymbol{R}-\delta\nabla^2\chi^C\nabla^2 f_c^{D^T}\boldsymbol{R}\right)\boldsymbol{n}}{T_1T_2} \tag{A.69}$$

where

$$T_1 = \left(\boldsymbol{n}\left(\sigma^2\boldsymbol{R}^T\nabla^2\chi^C\nabla^2\chi^{C^T}\boldsymbol{R}-2\sigma\delta\nabla^2\chi^C\nabla^2\chi^{C^T}\boldsymbol{R}+\delta^2\nabla^2\chi^C\nabla^2\chi^{C^T}\right)\boldsymbol{n}\right)^{1/2} \tag{A.70}$$

$$T_2 = \left(\boldsymbol{n}^T\left(\boldsymbol{R}^T\nabla^2 f_c^D\nabla^2 f_c^{D^T}\boldsymbol{R}\right)\boldsymbol{n}\right)^{1/2} \tag{A.71}$$

Note that, since $\chi(\boldsymbol{d}_a)$ achieves its minimum at point C, $\nabla^2\chi^C$ must be a positive definite matrix. Likewise, since f_c achieves its minimum at point D, $\nabla^2 f_c^D$ must also be positive definite. The matrix $\boldsymbol{R}$ must also be positive definite.

The monotonicity of $\cos\xi^A$ with respect to δ can now be established. If $\delta > 1$, then an increase in δ will result in a decrease of the numerator of Eq. (A.69). The denominator of Eq. (A.69) will increase, and therefore, $\cos\xi^A$ will decrease.

If $\delta > 1$, then an increase in δ will result in an increase in both the numerator and denominator of Eq. (A.69). However, the denominator will increase at a slower rate than the numerator due to the relative exponents, and therefore $\cos\xi^A$ will decrease. Since an increase in δ will always result in a decrease in $\cos\xi^A$, the function $\cos\xi^A$ is monotonically decreasing with respect to δ.

A decrease in $\cos \xi^A$ will result in an increase in ξ^A; thus, we see that an increase in the distance δ between the minima of f_c and χ will result in an increase in the angle ξ^A. From Theorem 4.2, we can then state that an increase in δ will result in CPF solutions that are farther from the Pareto optimal solutions to the co-design problem, and thus the theorem is proven. □

APPENDIX B

Derivation of Artifact and Control Objective and Constraints for MEMS Actuator

Formulation of Artifact Objective Function

The objective function chosen for the design problem was the negative of the vertical displacement of the actuator, ΔZ. The negative was chosen in order to formulate the problem as a minimization. From Eq. (4b) in Tung and Kurabayashi's paper [*Tung and Kurabayashi* (2005)], this is given by (see Fig. 5.2)

$$\Delta Z = l \sin \theta_o - l \sin (\theta_o - \Delta\theta) \tag{B.1}$$

where

$$l = \sqrt{(t+p)^2 + (h_1+h_2)^2} \tag{B.2}$$

$$\tan \theta_o = \frac{h_1+h_2}{t+p} \tag{B.3}$$

$$\Delta\theta_{ss} = \frac{A(\Delta\theta_{ss}) V_{ss}^2}{K} \tag{B.4}$$

$$A(\Delta\theta) = \frac{n\varepsilon_o hl}{d}(\sin\theta_o - \cos\theta_o\Delta\theta) \quad \text{(B.5)}$$

$$K = K_{Si}l^2\sin^2\theta_o + 2K_{PDMS} \quad \text{(B.6)}$$

$$K_{Si} = \frac{2E_{Si}hb^3}{l_{Si}^3} \quad \text{(B.7)}$$

$$K_{PDMS} = \frac{E_{PDMS}I}{p} \quad \text{(B.8)}$$

$$I = \frac{wh_1^3}{3} \quad \text{(B.9)}$$

$$h = h_1 + h_2 \quad \text{(B.10)}$$

The dimensions t, p, h_1, and h_2 are shown in Fig. 5.4. The kinematics of the hinge are modeled as though it were a link of length l, with an angle of θ_o when not actuated [*Tung and Kurabayashi* (2005)]. The change in the angle of the hinge is $\Delta\theta$. The variables K, C, and M represent the effective stiffness, damping, and mass of the entire system, respectively. The stiffness of the the silicon springs is denoted by K_{Si} and the stiffness of the PDMS hinge by K_{PDMS}. The constants E_{Si}, E_{PDMS}, and ε_o are Young's modulus for silicon, Young's modulus for PDMS, and the permittivity of vacuum, respectively. The dimensions d and w are shown in Fig. 5.5. The variables h, b, and n represent the overall height of the comb drive, the thickness of the silicon springs, and the number of fingers in the comb drive, respectively.

In the case of Eq. (B.9), the moment of inertia, I, was taken about the edge rather than the centroid of the cross-section due to the nature of the hinge. The upper edge is not restrained in the same way as the lower edge, which should have the result of shifting the neutral axis from the centroid.

Solving Eq. (B.4) and (B.5) for $\Delta\theta_{ss}$ yields Eq. (B.14), as shown below.

$$\Delta\theta_{ss} = \frac{A\left(\Delta\theta_{ss}\right)V_{ss}^2}{K} = \frac{V_{ss}^2}{K}\left(\frac{n\varepsilon_o hl}{d}\left(\sin\theta_o - \cos\theta_o \Delta\theta_{ss}\right)\right) \tag{B.11}$$

$$\Delta\theta_{ss}\left(1 + \frac{V_{ss}^2 n\varepsilon_o hl}{Kd}\cos\theta_o\right) = \frac{V_{ss}^2 n\varepsilon_o hl}{Kd}\sin\theta_o \tag{B.12}$$

$$\Delta\theta_{ss}\left(Kd + V_{ss}^2 n\varepsilon_o hl\cos\theta_o\right) = V_{ss}^2 n\varepsilon_o hl\sin\theta_o \tag{B.13}$$

$$\Delta\theta_{ss} = \frac{V_{ss}^2 n\varepsilon_o hl\sin\theta_o}{Kd + V_{ss}^2 n\varepsilon_o hl\cos\theta_o} \tag{B.14}$$

Substituting Eqs. (B.2), (B.3), and (B.6) - (B.10) into Eq. (B.1) and Eq. (B.14) yields equations involving only $\Delta\theta$, ΔZ, the design variables t, p, h_1, and h_2, and the constants and parameters of the problem.

$$\Delta\theta_{ss} = \frac{V_{ss}^2 n\varepsilon_o \left(h_1+h_2\right)^2}{Kd + V_{ss}^2 n\varepsilon_o \left(h_1+h_2\right)\left(t+p\right)} \tag{B.15}$$

$$\Delta\theta_{ss} = \frac{V_{ss}^2 n\varepsilon_o \left(h_1+h_2\right)^2}{\left(K_{Si} l^2 \sin^2\theta_o + 2K_{PDMS}\right)d + V_{ss}^2 n\varepsilon_o \left(h_1+h_2\right)\left(t+p\right)} \tag{B.16}$$

$$\Delta\theta_{ss} = \frac{V_{ss}^2 n\varepsilon_o \left(h_1+h_2\right)^2}{\left(K_{Si}\left(h_1+h_2\right)^2 + 2K_{PDMS}\right)d + V_{ss}^2 n\varepsilon_o \left(h_1+h_2\right)\left(t+p\right)} \tag{B.17}$$

Substituting Eqs. (B.7) - (B.8),

$$\Delta\theta_{ss} = \frac{V_{ss}^2 n\varepsilon_o \left(h_1+h_2\right)^2}{\left(\left(\frac{E_{Si}b^3}{l_{Si}^3}\right)\left(h_1+h_2\right)^3 + \left(\frac{E_{PDMS}I}{p}\right)\right)2d + V_{ss}^2 n\varepsilon_o \left(h_1+h_2\right)\left(t+p\right)} \tag{B.18}$$

$$\Delta\theta_{ss} = \frac{V_{ss}^2 n\varepsilon_o \left(h_1+h_2\right)^2}{\left(\left(\frac{E_{Si}b^3}{l_{Si}^3}\right)\left(h_1+h_2\right)^3 + \frac{E_{PDMS}wh_1^3}{3p}\right)2d + V_{ss}^2 n\varepsilon_o \left(h_1+h_2\right)\left(t+p\right)} \tag{B.19}$$

$$\Delta Z_{ss} = l\sin\theta_o - l\sin(\theta_o - \Delta\theta_{ss}) \tag{B.20}$$

$$\Delta Z_{ss} = l(\sin\theta_o - \sin\theta_o\cos\Delta\theta_{ss} + \cos\theta_o\sin\Delta\theta_{ss}) \tag{B.21}$$

$$\Delta Z_{ss} = l\left(\left(\frac{h_1+h_2}{l}\right) - \left(\frac{h_1+h_2}{l}\right)\cos\Delta\theta_{ss} + \left(\frac{t+p}{l}\right)\sin\Delta\theta_{ss}\right) \tag{B.22}$$

$$\Delta Z_{ss} = (h_1+h_2)(1-\cos\Delta\theta_{ss}) + (t+p)\sin\Delta\theta_{ss} \tag{B.23}$$

The coefficients M, C, and K which appear in the state-space representation of the system dynamics in Eq. (5.7) were given in [*Tung and Kurabayashi* (2005)]. The expressions for C and K are used in this work, without modification; however, in this problem formulation, an additional term was incorporated in M. The development of M in [*Tung and Kurabayashi* (2005)] was based on the assumption that the mass of the hinge was small compared to the mass of the silicon shuttle and the PDMS platform, but as the design variables change, this may not always be the case; therefore the mathematical model was modified to include this effect. The given expression for M was

$$M = M_{Si}l^2\sin^2\theta_o + M_{PDMS}l^2\cos^2\theta_o. \tag{B.24}$$

The contribution of the hinge is found following a similar procedure to that used in for the contributions of the platform and shuttle [*Tung and Kurabayashi* (2005)]. The kinetic energy of the moving hinge is given by

$$T_{hinge} = \frac{1}{2}M_{hinge}v_{cg_{hinge}}^2 + \frac{1}{2}I_{hinge}\Delta\dot{\theta}^2. \tag{B.25}$$

Assuming that the hinge is long and thin, it can be modeled as a rod, and its inertia is given by

$$I_{hinge} = \frac{1}{12}M_{hinge}l^2. \tag{B.26}$$

The velocity of the center of gravity of the hinge satisfies the equation

$$v_{cg_{hinge}}^2 = v_{cg_x}^2 + v_{cg_y}^2 \tag{B.27}$$

$$v_{cg_{hinge}}^2 = \left(\Delta\dot{X} - \frac{l}{2}\Delta\dot{\theta}\sin(\theta_o - \Delta\theta)\right)^2 + \left(\frac{l}{2}\Delta\dot{\theta}\cos(\theta_o - \Delta\theta)\right)^2 \tag{B.28}$$

Since ΔX is given by

$$\Delta X = l\cos(\theta_o - \Delta\theta) - l\cos\theta_o, \tag{B.29}$$

its time derivative $\Delta\dot{X}$ is found to be

$$\Delta\dot{X} = l\sin(\theta_o - \Delta\theta)\Delta\dot{\theta} \tag{B.30}$$

and therefore the kinetic energy of the hinge can be expressed as follows:

$$\begin{aligned} T_{hinge} =& \frac{1}{2}M_{hinge}\left(\left(\frac{l}{2}\sin(\theta_o - \Delta\theta)\Delta\dot{\theta}\right)^2 + \left(\frac{l}{2}\cos(\theta_o - \Delta\theta)\Delta\dot{\theta}\right)^2\right) \\ &+ \frac{1}{2}\left(\frac{1}{12}M_{hinge}l^2\right)\Delta\dot{\theta}^2 \end{aligned} \tag{B.31}$$

$$T_{hinge} = \frac{1}{2}M_{hinge}\Delta\dot{\theta}^2\left(\frac{l^2}{4}\left(\sin^2(\theta_o - \Delta\theta) + \cos^2(\theta_o - \Delta\theta)\right) + \frac{l^2}{12}\right) \tag{B.32}$$

$$T_{hinge} = \frac{1}{6}M_{hinge}l^2\Delta\dot{\theta}^2 \tag{B.33}$$

The equation of motion was found by using the Lagrangian, as detailed in Eq. (14) of [*Tung and Kurabayashi* (2005)]. The additional term in the system differential equation is given by

$$\frac{d}{dt}\left(\frac{\partial T_{hinge}}{\partial\Delta\dot{\theta}}\right) = \frac{d}{dt}\left(\frac{1}{3}M_{hinge}l^2\Delta\dot{\theta}\right) = \frac{1}{3}M_{hinge}l^2\Delta\ddot{\theta} \tag{B.34}$$

and therefore, for the mathematical model used in this work,

$$M = M_{Si} l^2 \sin^2 \theta_o + M_{PDMS} l^2 \cos^2 \theta_o + \frac{1}{3} M_{hinge} l^2. \tag{B.35}$$

The mass terms in Eq. (B.35) are as follows:

$$M_{Si} = \rho_{Si} (h_1 + h_2) \left(0.5 (w l_1 + 2 l_2 l_3 + l_4 (nd + (n-1) 3d)) + n d l_f\right) \tag{B.36}$$

$$M_{PDMS} = \frac{1}{4} \rho_{PDMS} l_p^2 (2h_1 + h_2) \tag{B.37}$$

$$M_{hinge} = \rho_{PDMS} w (2h_1 t + p (2h_1 + h_2)) \tag{B.38}$$

The dimensions used in Eq. (B.36) - (B.38) are shown in Fig. 5.4.

Note that, in the derivation of these equations, it is assumed that the device remains small. If the optimization results were to indicate that the size of the actuator was substantially larger than the original design, then then model developed here would no longer be valid.

Formulation of Artifact Constraints

The stresses in the actuator are found from the theory of a beam under concentrated end loading. For purposes of this analysis, it was assumed that the weight of the actuator is much less than the externally applied forces. The maximum stress in the silicon spring is given by [*Bao* (2005)]

$$\sigma_{Si_{max}} = \frac{6 M_o g l_{Si}}{h b^2} \tag{B.39}$$

where M_o is the moment in the spring, and g is the acceleration due to gravity. The moment in the spring, M_o, is related to the deflection, ΔX, by

$$\frac{\Delta X}{2} = \frac{4 M_o g l_{Si}^3}{E_{Si} h b^3}, \tag{B.40}$$

yielding

$$\sigma_{Si_{max}} = \frac{3E_{Si}b\Delta X}{4l_{Si}^2}. \tag{B.41}$$

The maximum stress in the PDMS micro-hinge is given by [*Bao* (2005)],

$$\sigma_{PDMS_{max}} = \frac{Fth_1}{2I}, \tag{B.42}$$

where the force F in the hinge, under static conditions, is given by [*Tung and Kurabayashi* (2005)]

$$Ft = \frac{E_{PDMS}I\Delta\theta_{ss}}{p}. \tag{B.43}$$

This yields a relation for the maximum steady-state stress in the hinge of

$$\sigma_{PDMS_{max}} = \frac{E_{PDMS}h_1\Delta\theta_{ss}}{2p}. \tag{B.44}$$

BIBLIOGRAPHY

BIBLIOGRAPHY

Abdalla, M., C. Reddy, W. Faris, and Z. Gurdal (2005), Optimal design of an electrostatically actuated microbeam for maximum pull-in voltage, *Computers & Structures*, *83*, 1320–1329.

Allison, J., M. Kokkolaras, and P. Papalambros (2005), On the impact of coupling strength on complex system optimization for single-level formulations, in *ASME 2005 International Design Engineering Technical Conferences & Computers and Information in Engineering Conference*, ASME, Long Beach, CA, paper number DETC2005-84790.

Alyaqout, S. (2006), A Multi-System Optimization Approach to Coupling in Robust Design and Control, PhD Thesis, University of Michigan, Ann Arbor, MI.

Alyaqout, S. F., P. Y. Papalambros, and A. G. Ulsoy (2005), Quantification and use of system coupling in decomposed design optimization problems, in *Proceedings of the ASME IMECE 2005*, pp. 95–103, ASME, Orlando, FL, paper number IMECE2005-81364.

Athan, T. (1994), A quasi-Monte Carlo method for multicriteria optimization, PhD Thesis, University of Michigan, Ann Arbor, MI.

Athan, T., and P. Y. Papalambros (1996), A note on weighted criteria methods for compromise solution in multi-objective optimization, *Engineering Optimization*, *27*, 155–176.

Balling, R., and J. Sobieszczanski-Sobieski (1996), Optimization of coupled systems: A critical overview of approaches, *AIAA Journal*, *34*, 6–17.

Bao, M. (2005), *Analysis and Design Principles of MEMS Devices*, Elsevier, San Diego, CA.

Belvin, W., and K. Park (1990), Structural tailoring and feedback control synthesis: An interdisciplinary approach, *Journal of Guidance, Control, and Dynamics*, *13*, 424–428.

Bloebaum, C. (1995), Coupling strength-based system reduction for complex engineering design, *Structural Optimization*, *10*, 113–121.

Bodden, D., and J. Junkins (1985), Eigenvalue optimization algorithms for structure/controller design iterations, *Journal of Guidance, Control, and Dynamics*, *8*, 697–706.

Brown, R. G. (1966), Not just observable, but how observable?, *Proceedings of the 1966 National Electronic Conference*, *22*, 709–714.

Brusher, G., P. Kabamba, and A. G. Ulsoy (1997a), Trade-offs between performance specifications, uncertainty and admissible models, in *Proceedings of the American Control Conference*, pp. 3646–3651, ACC, Albuquerque, NM.

Brusher, G., P. Kabamba, and A. G. Ulsoy (1997b), Coupling between the modeling and controller-design problems - part II: Design, *Journal of Dynamic Systems, Measurement, and Control*, *119*, 278–283.

Bryson, A., and Y. Ho (1975), *Applied Optimal Control*, Hemisphere Publishing Corporation, New York, NY.

Carley, L., G. Ganger, D. Guillou, and D. Nagle (2001), System design considerations for MEMS-actuated magnetic-probe-based mass storage, *IEEE Transactions on Magnetics*, *37*, 657–662.

Chen, C., and C. Cheng (2005), Integrated design for a mechatronic feed drive system of machine tools, in *IEEE/ASME International Conference on Advanced Intelligent Mechatronics*, Monterey, CA.

Chen, C., and C. Cheng (2006), 3D model-based design for control of a mechatronic machine tools system, *Materials Science Forum*, *505*, 967–972.

Chu, P., et al. (2005), Design and nonlinear servo control of MEMS mirrors and their performance in a large port-count optical switch, *Journal of Microelectromechanical Systems*, *14*, 261–273.

Das, I. (1999), On characterizing the "knee" of the Pareto curve based on normal-boundary intersection, *Structural and Multidisciplinary Optimization*, *18*(2), 107–115.

Das, I., and J. Dennis (1997), A closer look at drawbacks of minimizing weighted sums of objectives for Pareto set generation in multicriteria optimization problems, *Structural Optimization*, *14*, 63–69.

Eastep, F., N. Khot, and R. Grandhi (1987), Improving the active vibrational control of large space structures through structural modifications, *Acta Astronautica*, *15*, 383–389.

Fathy, H. (2003), Combined Plant and Control Optimization: Theory, Strategies and Applications, PhD Thesis, University of Michigan, Ann Arbor, MI.

Fathy, H., S. Bortoff, G. Copeland, P. Y. Papalambros, and A. G. Ulsoy (2002), Nested optimization of an elevator and its gain-scheduled LQG controller, in *Proceedings of the ASME IMECE 2002*, pp. 119–126, ASME, New Orleans, LA, iMECE2002-34273.

Fathy, H., D. Hrovat, P. Y. Papalambros, and A. G. Ulsoy (2003), Nested plant/controller optimization and its application to combined passive/active automotive suspensions, in *Proceedings of the American Control Conference*, pp. 3375–3380, IEEE, Denver, CO.

Fathy, H., P. Y. Papalambros, and A. G. Ulsoy (2004), On combined plant and control optimization, in *8th Cairo University International Conference on Mechanical Design and Production*, Cairo University, Cairo, Egypt.

Franklin, G., J. Powell, and A. Emami-Naeini (1994), *Feedback Control of Dynamic Systems*, Addison-Wesley Publishing Company, Reading, MA.

Frischknecht, B., D. L. Peters, and P. Y. Papalambros (2009), Pareto set analysis: Local measures of objective coupling in multi-objective design optimization, in *Proceedings of the 8th World Congress on Structural and Multidisciplinary Optimization*, Lisbon, Portugal.

Grigoriadis, K., and R. Skelton (1998), Integrated structural and control design for vector second-order systems via LMIs, in *Proceedings of the American Control Conference*, pp. 1625–1629, IEEE, Philadelphia, PA.

Haftka, R. (1990), Integrated structure/control optimization of space structures, in *Proceedings of the AIAA Dynamics Specialists Conference*, pp. 1–9, AIAA, Long Beach, CA.

Haftka, R., Z. Martinovic, W. H. Jr., and G. Schamel (1986), An analytical and experimental study of a control system's sensitivity to structural modifications, *AIAA Journal*, *25*, 310–315.

Hale, A., R. Lisowski, and W. Dahl (1985), Optimal simultaneous structural and control design of maneuvering flexible spacecraft, *Journal of Guidance, Control, and Dynamics*, *8*, 86–93.

Ionescu, V., C. Oara, and M. Weiss (1999), *Generalized Riccati Theory and Robust Control*, John Wiley & Sons Ltd., West Sussex, England.

Isermann, R. (1996a), Modeling and design methodology for mechatronic systems, *IEEE/ASME Transactions on Mechatronics*, *1*, 16–28.

Isermann, R. (1996b), On the design and control of mechatronic systems - a survey, *IEEE Transactions on Industrial Electronics*, *43*, 4–15.

Junkins, J., and Y. Kim (1993), *Introduction to Dynamics and Control of Flexible Structures*, American Institute of Aeronautics and Astronautics, Inc., Washington, D.C.

Kailath, T. (1980), *Linear Systems*, Prentice-Hall, Inc., Englewood Cliffs, NJ.

Kajiwara, I., and R. Haftka (2000), Integrated design of aerodynamics and control system for micro air vehicles, *JSME International Journal*, *43*, 684–690.

Khot, N., and N. Abhyankar (1993), Integrated optimum structural and control design, in *Structural Optimization: Status and Promise*, edited by M. P. Kamat, Washington, D.C.

Kitayama, S., K. Yamazaki, M. Arakawa, and H. Yamakawa (2009), Quantitative trade-off analysis and its application to the compromise solution in the multi-objective design optimization, in *Proceedings of the 8th World Congress on Structural and Multidisciplinary Optimization*, WCSMO, Lisbon, Portugal.

Kosut, R., G. Kabuli, S. Morrison, and Y. Harn (1990), Simultaneous control and structure design for large space structures, in *Proceedings of the American Control Conference*, pp. 860–865, IEEE, San Diego, CA.

Kuhn, H. W., and A. W. Tucker (1950), Nonlinear programming, in *Proceedings of the Second Berkeley Symposium on Mathematical Statistics and Probability*, pp. 481–492, University of California, Berkeley, CA.

Legtenberg, R., A. Groeneveld, and M. Elwenspoek (1996), Comb-drive actuators for large displacements, *Journal of Micromechanical Microengineering*, *6*, 320–329.

Li, Q., W. Zhang, and L. Guo (1999), Integrated design and control for a programmable four-bar linkage, in *Proceedings of the ASME Design Engineering Technical Conference*, ASME, Las Vegas, NV, paper number DAC99/DAC8663.

Li, Q., W. Zhang, and L. Chen (2001), Design for control - a concurrent engineering approach for mechatronic systems design, *IEEE/ASME Transactions on Mechatronics*, *6*, 161–169.

Lim, K., and W. Gawronski (1993), Modal Grammian approach to actuator and sensor placement for flexible structures, *AIAA Journal*, *31*, 674–684.

Maghami, P., S. Gupta, K. Elliott, and S. Joshi (1996), Experimental validation of an integrated controls-structures design methodology, *Journal of Guidance, Control, and Dynamics*, *19*, 324–333.

Messac, A. (1998), Control-structure integrated design with closed-form design metrics using physical programming, *AIAA Journal*, *36*, 855–864.

Messac, A., and C. Puemi-Sukam (2000), Aggregate objective functions and Pareto frontiers: Required relationships and practical implications, *Optimization and Engineering*, *1*, 171–188.

Milman, M., M. Salama, R. Scheid, R. Bruno, and J. Gibson (1991), Combined control-structural optimization, *Computational Mechanics*, *8*, 1–18.

Muller, P. C., and H. I. Weber (1972), Analysis and optimization of certain qualities of controllability and observability for linear dynamical systems, *Automatica*, *8*, 237–246.

Oldham, K., X. Huang, A. Chahwan, and R. Horowitz (2005), Design, fabrication and control of a high-aspect ratio microactuator for vibration suppression in a hard disk drive, in *Proceedings of the IFAC World Congress*, Prague.

Onoda, J., and N. Watanabe (1989), Integrated direct optimization of structure/regulator/observer for large flexible spacecraft, *AIAA Journal*, *27*, 1336–1344.

Ou, J., and N. Kikuchi (1996), Integrated optimal structural and vibration control design, *Structural Optimization*, *12*, 209–216.

Ouyang, P., W. Zhang, and F. Wu (2002), Nonlinear PD control for trajectory tracking with consideration of the design for control methodology, in *Proceedings of the IEEE International Conference on Robotics & Automation*, pp. 4126–4131, IEEE, Washington, D.C.

Papalambros, P., and D. Wilde (2000), *Principles of Optimal Design: Modeling and Computation*, Cambridge University Press, Cambridge, NY.

Park, J., and H. Asada (1992), Integrated structure/control design of a two-link nonrigid robot arm for high speed positioning, in *Proceedings of the IEEE International Conference on Robotics & Automation*, IEEE, Nice, France.

Park, S., and R. Horowitz (2003), Adaptive control for the conventional mode of operation of MEMS gyroscopes, *Journal of Microelectromechanical Systems*, *12*, 101–108.

Peters, D. L., K. Kurabayashi, P. Y. Papalambros, and A. G. Ulsoy (2008), Co-design of a MEMS actuator and its controller using frequency constraints, in *Proceedings of the ASME Dynamic Systems and Control Conferences*, ASME, Ann Arbor, MI, paper number DSCC 2008-2212.

Peters, D. L., P. Y. Papalambros, and A. G. Ulsoy (2009), On measures of coupling between the artifact and controller optimal design problems, in *Proceedings of the ASME Design Engineering Technical Conference & Computers in Engineering Conference*, ASME, San Diego, CA, paper number DETC 2009-86868.

Peters, D. L., P. Y. Papalambros, and A. G. Ulsoy (2010), Relationship between coupling and the controllability Grammian in co-design problems, in *Proceedings of the American Control Conference*, ASME, Baltimore, MD, (submitted).

Pil, A., and H. Asada (1996), Integrated structure/control design of mechatronic systems using a recursive experimental optimization method, *IEEE/ASME Transactions on Mechatronics*, *1*, 191–203.

Pomrehn, L., and P. Papalambros (1994), Global and discrete constraint activity, *Journal of Mechanical Design*, *116*, 745–748.

Rao, S., and T. Pan (1990), Modeling, control, and design of flexible structures: A survey, *Applied Mechanics Review*, *43*, 99–117.

Ravichandran, T., D. Wang, and G. Heppler (2006), Simultaneous plant-controller design optimization of a two-link planar manipulator, *Mechatronics*, *16*, 233–242.

Reyer, J. (2000), Combined Embodiment Design and Control Optimization: Effects of Cross-Disciplinary Coupling, PhD Thesis, University of Michigan, Ann Arbor, MI.

Roh, H., and Y. Park (1997), Actuator and exciter placement for flexible structures, *Journal of Guidance, Control, and Dynamics*, *20*, 850–856.

Shabde, V. S., and K. A. Hoo (2008), Optimum controller design for a spray drying process, *Control Engineering Practice*, *16*(5), 541–552.

Skogestad, S., and I. Postlethwaite (2005), *Multivariable Feedback Control: Analysis and Design*, John Wiley and Sons, Ltd., West Sussex, UK.

Sobieszczanski-Sobieski, J., and R. Haftka (1997), Multidisciplinary aerospace design optimization: Survey of recent developments, *Structural Optimization*, *14*, 1–23.

Steuer, R. E. (1986), *Multiple Criteria Optimization: Theory, Computation, and Application*, John Wiley and Sons, Inc., New York, NY.

Tilbury, D., and S. Kota (1999), Integrated machine and control design for reconfigurable machine tools, in *Proceedings of the IEEE/ASME International Conference on Advanced Intelligent Mechatronics*, IEEE/ASME, Atlanta, GA.

Tung, Y., and K. Kurabayashi (2005), A single-layer PDMS-on-silicon hybrid microactuator with multi-axis out-of-plane motion capabilities - part I: Design and analysis, *Journal of Microelectromechanical Systems*, *14*, 548–557.

Wan, J., Q. Li, and F. Wu (2002), Integrated design and control of a closed-chain mechanism, in *Proceedings of the Seventh International Conference on Control, Automation, Robotics and Vision*, pp. 1349–1353, IEEE, Singapore.

Wolfram, H., R. Schmiedel, K. Hiller, T. Aurich, W. Gunther, S. Kurth, J. Mehner, W. Dotzel, and T. Gebner (2005), Model building, control design and practical implementation of a high precision, high dynamical MEMS acceleration sensor, in *Society of Photo-Optical Instrumentation Engineers*, pp. 1–15, SPIE, Sevilla, Spain.

Yee, E., and Y. Tsuei (1991), Method for shifting natural frequencies of damped mechanical systems, *AIAA Journal*, *29*, 1973–1977.

Youcef-Toumi, K. (1996), Modeling, design, and control integration: A necessary step in mechatronics, *IEEE/ASME Transactions on Mechatronics*, *1*, 29–38.

Zhang, J., M. Wiecek, and W. Chen (1999), Local approximation of the efficient frontier in robust design, in *Proceedings of the ASME Design Engineering Technical Conferences*, ASME, Las Vegas, NV, paper number DETC99/DAC-8566.

Zhu, Y., J. Qiu, and J. Tani (2001), Simultaneous optimization of a two-link flexible robot arm, *Journal of Robotic Systems*, *18*, 29–38.